

## Doping on Demand

### Permanent electrochemical doping of colloidal quantum dots and organic semiconductors

Gudjónsdóttir, S.

#### DOI

[10.4233/uuid:f4b5a89a-4466-40aa-b28a-ee26e5906696](https://doi.org/10.4233/uuid:f4b5a89a-4466-40aa-b28a-ee26e5906696)

#### Publication date

2020

#### Document Version

Final published version

#### Citation (APA)

Gudjónsdóttir, S. (2020). *Doping on Demand: Permanent electrochemical doping of colloidal quantum dots and organic semiconductors*. [Dissertation (TU Delft), Delft University of Technology].  
<https://doi.org/10.4233/uuid:f4b5a89a-4466-40aa-b28a-ee26e5906696>

#### Important note

To cite this publication, please use the final published version (if applicable).  
Please check the document version above.

#### Copyright

Other than for strictly personal use, it is not permitted to download, forward or distribute the text or part of it, without the consent of the author(s) and/or copyright holder(s), unless the work is under an open content license such as Creative Commons.

#### Takedown policy

Please contact us and provide details if you believe this document breaches copyrights.  
We will remove access to the work immediately and investigate your claim.

**Doping on Demand:**  
**Permanent electrochemical doping of colloidal quantum**  
**dots and organic semiconductors**

**Sólrún Guðjónsdóttir**



# Doping on Demand: Permanent electrochemical doping of colloidal quantum dots and organic semiconductors

Dissertation

for the purpose of obtaining the degree of doctor  
at Delft University of Technology  
by the authority of the Rector Magnificus *Prof. dr. ir. T. H. J. J. van der Hagen*  
chair of the Board for Doctorates,

to be defended publicly on  
Monday 8th of October 2020 at 15:00 o'clock

by  
*Sólrún GUÐJÓNSDÓTTIR*

*Chemical engineer*  
*Delft University of Technology, Netherlands*  
*born in Reykjavík, Iceland*

This dissertation has been approved by the promotor.

Prof. dr. A. J. Houtepen	Delft University of Technology, promotor
Dr. ir. T. J. Savenije	Delft University of Technology, promotor

Composition of the doctoral committee:

Rector Magnificus,	chairperson
Prof. dr. A. J. Houtepen	Delft University of Technology, promotor
Dr. ir. T. J. Savenije	Delft University of Technology, promotor

Independent members:

Prof. dr. D. R. Gamelin	University of Washington, United States of America
Prof. dr. D. A. M. Vanmaekelbergh	Utrecht University
Dr. W. A. Smith	University of Colorado Boulder, United States of America
Prof. dr. F. M. Mulder	Delft University of Technology

Other members:

Dr. W. van der Stam	Utrecht University
---------------------	--------------------

This work received financial support from the European Research Council Horizon 2020 ERC Grant Agreement No. 678004 (Doping on Demand).



**European Research Council**

Established by the European Commission

ISBN: 978-94-6332-667-4

Copyright © 2020 Sólrún Guðjónsdóttir

Printed by GVO drukkers & vormgevers B.V.

An electronic version of this thesis is freely available at

<http://repository.tudelft.nl>





# Table of Contents

---

<b>Chapter 1 - Electrochemical doping</b>	<b>1</b>
<b>Chapter 2 - The role of dopant ions on charge injection and transport in electrochemically doped quantum dot films</b>	<b>19</b>
<b>Chapter 3 - On the stability of permanent electrochemical doping of quantum dot, fullerene and conductive polymer films in frozen electrolytes</b>	<b>47</b>
<b>Chapter 4 - Enhancing the stability of the electron density in electrochemically doped ZnO quantum dots</b>	<b>73</b>
<b>Chapter 5 - Permanent electrochemical doping of semiconductor films using frozen electrolyte solvents at room temperature</b>	<b>91</b>
<b>Summary and outlook</b>	<b>119</b>
<b>Samenvatting en vooruitzichten</b>	<b>125</b>
<b>Acknowledgements</b>	<b>131</b>
<b>List of publications</b>	<b>135</b>
<b>Curriculum vitae</b>	<b>139</b>



# 1



## Electrochemical doping

---

Eitt bros getur dimmu í dagsljós breytt  
Einræður Starkaðar – Einar Benediktsson (1864-1940)

A single smile can turn darkness into daylight.  
From the poem Einræður Starkaðar by Einar Benediktsson (1864-1940)

## 1.1 Introduction

Throughout the last decades semiconductors have become an irreplaceable part of our lives, as integrated parts of electronic technologies we use every day. Usually, the first group of semiconductor technology that pops into people minds are consumer electronics such as phones, computers and televisions, but semiconductors can be found in many other applications. Semiconductors are for example used in ATMs, trains, self-driven cars, washing machines and as temperature sensors in air conditioners. In fact, anything that is computerized or uses radio waves depends on semiconductors.<sup>1</sup>

Semiconductors are also a crucial part of optoelectronics. Optoelectronics are electronic devices which can either convert electrical energy into light, or light into energy. Examples of optoelectronics and their applications are for example photodiodes, laser diodes, light emitting diodes (LEDs), solar cells, cameras, medical instruments, telecommunications, CD players, watches, surgical equipment and many other consumer electronics.<sup>2</sup> This is only a short list of all the applications surrounding us that include semiconductors (Figure 1.1) and it is safe to say that most of us could not imagine a life without them.

Semiconductors themselves are very interesting materials, with properties in between conductors and insulators. Many metals, such as copper, are common conductors, as they have “free electrons”. These free electrons can move easily between atoms, and as electricity involves a flow of electrons a metal such as copper has a high conductivity. Therefore, copper is commonly used in electrical cords and cables. On the other hand,

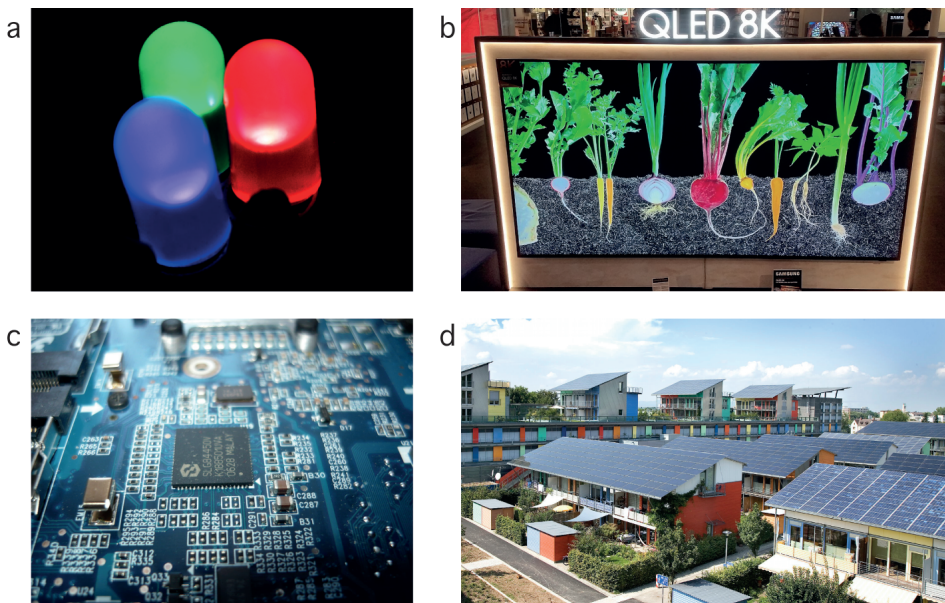


**Figure 1.1 Various semiconductor devices.** (a) Light-emitting diodes, LEDs. Image by Piccolo Namek.<sup>3</sup> (b) Television made out of semiconductor quantum dots. Image by Bretwa.<sup>4</sup> (c) Circuit board. d) Solar cells on rooftops. Image by Andrew Glaser.<sup>5</sup>

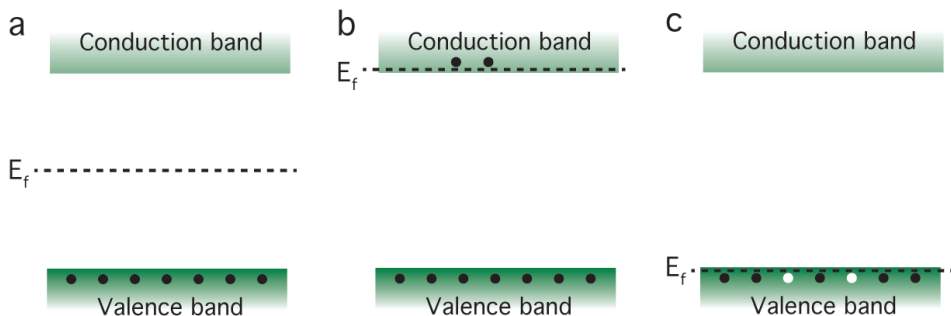


**Figure 1.2 Doping of semiconductors.** a) Intrinsic semiconductor, b) n-type semiconductor and c) p-type semiconductor.  $E_f$  is the Fermi level.

insulators, such as glass, do not have free electrons and are therefore poor conductors. As an example, glass was widely used as an insulator in early history of electrical power industry. Semiconductors, do not have many free electrons, and their conductivity is in between of an insulator and a conductor. Interestingly, the conductivity of a semiconductor can be very sensitive towards properties such as temperature, magnetic field, light illumination and minute amounts of impurity atoms. This can be seen for the most common semiconductor material silicon. A pure silicon crystal has a very low conductivity and behaves almost like an insulator. However, by the use of electronic doping, the conductivity of the silicon crystal increases and it starts behaving more like a conductor.<sup>6</sup> Electronic doping can be used to tune the charge carrier density, and therefore the conductivity of semiconductors. This doping phenomenon is discussed in more detail in the following sections.

## 1.2 Electronic doping of semiconductors

As stated above, the conductivity of semiconductors can be increased by doping. Figure 1.2a shows an undoped semiconductor, which is often called an intrinsic semiconductor. In an intrinsic semiconductor the number of electrons is equal to the number of holes (lack of an electron). Additionally, at 0 K the electrons fully occupy the valence band, VB, while the conduction band, CB, is empty. When a semiconductor is doped, electrons are either introduced to the CB or extracted from the VB (see Figure 1.2b,c) of the semiconductor. In the former case, the semiconductor has more free electrons than holes. As the majority of carriers have a negative charge, it is called n-type. In the latter case, the semiconductor contains more holes than electrons. Consequently, the semiconductor is p-type, as the majority carriers have a positive charge.<sup>7</sup>

Figure 1.2 also shows how the position of the Fermi level,  $E_f$ , changes by doping. The Fermi level is seen in the Fermi-Dirac distribution for electrons in equation 1.1:

$$f(E) = \frac{1}{1 + \exp\left(\frac{E - E_f}{kT}\right)} \quad 1.1$$

Here,  $f(E)$  is the probability of a state with energy  $E$  to be occupied,  $k$  is the Boltzmann constant and  $T$  is the temperature. When  $E$  is equal to  $E_F$  the Fermi distribution is  $\frac{1}{2}$ , that is the probability of an energy state positioned at the Fermi level being occupied is  $\frac{1}{2}$ . When  $E < E_F$  the Fermi distribution approaches 1, that is energy states below the Fermi level are likely to be populated. In contrast, when  $E > E_F$  the Fermi distribution decreases exponentially, that is energy states higher than the Fermi level are less likely to be filled. Therefore, for an intrinsic semiconductor, the Fermi level is near the middle of the bandgap. For an n-type semiconductor, additional electrons are in the CB which will shift the Fermi level to a higher energy. On the other hand, when the semiconductor is p-type, electron vacancies are in the VB which will shift the Fermi level to lower energies.<sup>8</sup> This can also be seen in the relation between the electron density  $n_0$  and the Fermi-level:

$$n_0 = N_c \exp \left[ \frac{-(E_c - E_F)}{kT} \right] \quad 1.2$$

Here  $N_c$  is the effective density of states function in the conduction band,  $E_c$  is the energy at the bottom edge of the conduction band,  $k$  is the Boltzmann constant and  $T$  is the temperature. Equation 1.2 shows that the higher the Fermi-level is, the higher the electron density. In deriving Equation 1.2 it is assumed that the Fermi energy is within the bandgap of the semiconductor, that is, the semiconductor is not degenerately doped. By doing so, the Boltzmann approximation can be used.<sup>9</sup>

### 1.2.1 Why do we dope semiconductors?

As was explained above, the number of free carriers is increased in the semiconductor by the use of doping. The connection between the charge carrier density,  $n$ , and the conductivity,  $\sigma$ , is shown in the following equation:

$$\sigma = e \times n \times \mu \quad 1.3$$

Where,  $e$  is the elementary charge and  $\mu$  is the mobility. Equation 1.3 shows that the conductivity increases linearly with the charge carrier density. As the charge carrier density is controlled by doping, the conductivity of a doped semiconductor can often be tuned over a great range. As an example, the conductivity of a silicon crystal can be increased by a factor 106 by doping, and the conductivity of CdSe QD films can be increased by 12 orders of magnitude.<sup>10-11</sup>

Even if n and p-type semiconductors are very interesting themselves, the combination of them is even more impressive. The simplest combination is a p-n junction which forms a diode. A p-n junction is the interface between a p and an n-type semiconductor (see Figure 1.3a). Since there are few electrons in the p-type region and few holes in the n-type region, a concentration gradient exists. Due to the concentration gradient, electrons from the n-type region diffuse to the p-type region and recombine with holes. Similarly, holes diffuse from the p-type to the n-type region where they recombine with electrons. A region is formed which is depleted of any mobile charge, which is either called the space charge region or the depletion region. An equilibrium of the junction is reached when diffusion, due to the concentration gradient, is just cancelled by drift, due to the induced

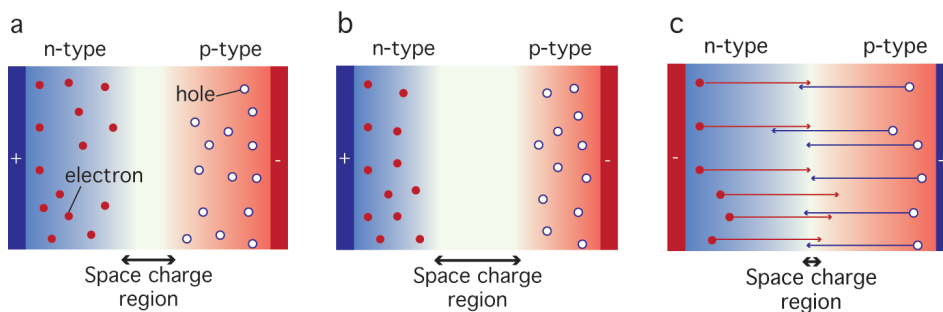


**Figure 1.3 p-n junction** under a) zero bias, b) reverse bias and c) forward bias.

electric field.<sup>12</sup>

When a reverse bias is applied to the p-n junction, the n-type side is connected to a positive terminal, while the p-type side is connected to a negative terminal. As the electrons are attracted to the positive side and the holes to the negative side, very little current flows across the junction. This will lead to an increased width of the space charge region (Figure 1.3b). On the other hand, in a forward bias mode the n-type side is connected to a negative terminal while the p-type side is connected to a positive terminal, so the electrons start to flow toward the positive terminal while the holes to the negative terminal. When the space charge region has been neutralized, charge starts to flow across the junction (Figure 1.3c). Therefore, due to the p-n junction, current can only flow in one direction through the material, that is a switch has been made.<sup>13</sup>

A p-n junction is not the only combination of n and p-type semiconductors. For example, transistors are made of at least three doped regions, which allows them to act as a switch or an amplifier. Due to the control over the magnitude and the direction of current, both diodes and transistors are key component in electronic devices.<sup>12</sup> Therefore, understanding of doping procedures of semiconductors is crucial for semiconductor devices.

### 1.3 Doping methods

Overall, there are two different methods to control the charge carrier densities of semiconductor materials, internal and external doping (or remote doping). In internal doping the dopants are placed inside the semiconductor material, as is the case for impurity doping, where impurity atoms are introduced into the semiconductor crystal structure to introduce extra charge carriers. On the other hand, in external doping the dopants are placed outside of the semiconductor material as is the case for both chemical and electrochemical doping.

#### 1.3.1 Impurity doping

The most common way of doping bulk semiconductor materials is by impurity doping. As stated above, impurity doping is performed by introducing impurity atoms into the crystal lattice of the semiconductor material. These impurity atoms are either donor impurities or acceptor impurities. The donor impurities introduce an extra electron to

the semiconductor conduction band to make it n-type, while the acceptor impurities introduce an extra hole to the semiconductor valence band to make it p-type. Impurity doping is very well known for silicon. In a pure silicon crystal, each silicon atom contains four valence electrons which form a covalent bond with four other silicon atoms to form a crystal lattice. If one silicon atom is replaced by phosphor which has five valence electrons, the fifth valence electron becomes a free electron and the silicon is n-doped. On the other hand, if a silicon atom is replaced by boron which has only three valence electrons, an additional hole is made and the silicon is p-doped.<sup>7</sup>

It is also possible to dope semiconductors based on charge balance perspective. That is the entire material must be charge neutral, otherwise, the cumulative repulsion of all charges will lead to diverging energy of the system. So net positive dopants add electrons and net negative dopants add holes. Therefore, if silicon is replaced by a negatively charged boron,  $B^-$ , (compared to a neutral one described before) it also leads to p-doping. Furthermore, a positively charged phosphor,  $P^+$ , leads to n doping. The doping becomes even more complicated when a compound semiconductor is used (a semiconductor that consist of two or more elements), where the same dopant atom can act as an acceptor, donor or neutral specie depending on which lattice atom it replaces.

Nowadays, there are two commercial ways of impurity doping for semiconductor wafers; thermal diffusion and ion implantation. Thermal diffusion is performed in two steps. In step one, the dopant source is introduced to the wafer, while in step two, the dopants diffuse into the wafer. As the doping process is governed by dopant diffusion, a concentration gradient is obtained where the highest concentration of dopant is at the surface of the semiconductor material. The used dopant source in the procedure can be gas, solid or a liquid (carrier gas is used to carry the liquid). The diffusion coefficient of the dopant needs to be high enough for the dopants to diffuse through the material on a reasonable timescale. Since the diffusion coefficient increases strongly with temperature, diffusion doping takes place at high temperature. For example when boron tribromide solution is used as the dopant source for boron in silicon the doping takes place at 1200 °C, when boron can diffuse into and inside the silicon wafer (diffusion coefficient in the order of  $10^{-11} \text{ cm}^2/\text{s}$ ).<sup>14</sup> In order to stop the doping process the temperature is lowered, and at room temperature the diffusion of the dopant atom is minimum.<sup>15</sup>

In contrast to thermal diffusion, ion plantation takes place at room temperature. In this process the impurity atoms are accelerated by an electric field and irradiated onto the wafer. As the doping is performed at room temperature, diffusion of dopant ions out of the wafer does not take place. In this process, the dopants are slowed down by collision with the crystal lattice. This means that majority of them are placed in interstitial states, additionally, due to the collisions the crystal lattice is often heavily damaged. This can lead to high resistivity of the semiconductor as the electrical behaviour is dominated by deep-level electron and hole traps. Therefore, an extra annealing step is performed at about 1000 °C to recover the crystal lattice and to move the dopants into the crystal lattice. This step is also called an activation step. At 1000 °C, dopants might diffuse out of the crystal lattice, therefore this activation step needs to be very short. Compared to thermal diffusion, ion implantation is more expensive, but it offers higher control of the doping

process.<sup>15</sup>

These two doping methods are most commonly used for silicon wafers, but have also been implemented for other semiconductors such as germanium, III-V and II-VI semiconductors.<sup>16-19</sup> Unfortunately, some semiconductors don't survive these high temperatures. Therefore, there are also cases when the impurities are placed into the semiconductor material during synthesis.<sup>11</sup> Even with this protocol, impurity doping does not work well for some semiconductors such as organic semiconductors and quantum dots, QDs (inorganic semiconductor nanocrystals). For organic semiconductors the dopant atom, such as halides or alkali metals, tends to diffuse as it is not covalently bound to the host.<sup>20-21</sup> For QDs, the dopant ions rarely introduce extra charges to the semiconductor due to charge compensation by surface charges.<sup>22-23</sup> Additionally, by adding only a single impurity atom to a QD, it will lead to high doping densities which can cause a disruption to the crystal lattice, alter the density of states and the electronic properties of the QD.<sup>24</sup> Therefore, other doping techniques have been more successful for these semiconductor systems.

### 1.3.2 External doping

When external doping is used as a doping method, the semiconductor is not doped by the introduction of impurity atoms into the crystal lattice of the semiconductor, where their valence electrons lead to doping. Instead, external dopants are introduced to the semiconductor. Therefore, no disruption of the semiconductor crystal lattice or molecular structure should take place. Additionally, it is less likely that the dopant will introduce additional states in the band gap of the semiconductor which serve as recombination centres for electrons and holes, as can be the case in substitutional impurity doping. External doping can be split up into two groups, chemical doping and electrochemical doping.

#### 1.3.2.1 Chemical doping

In chemical doping a charge transfer takes place between a dopant and a semiconductor for the generation of mobile carriers. As for impurity doping, the dopant can either be a donor (reducing agent) or an acceptor (oxidizing agent). For a donor dopant, the standard reduction potential of the dopant needs to be above the LUMO level of the semiconductor, which results in n-type doping. On the other hand, when an acceptor dopant is used, its standard reduction potential should be below the HOMO level of the semiconductor, and p-type doping takes place.

Chemical doping is widely used for organic semiconductors, and is often called molecular doping. There, large organic molecules are used either as the donor or the acceptors to either inject or extract electrons from the organic semiconductor. In many cases this is a reasonable model for the doping process, but in some cases it is more complicated. For many small molecule organic semiconductors and oligomers, electronic interactions between the dopant ion and the semiconductor takes place where a locally bound charge transfer complex is formed. This charge transfer complex is analogous to a covalent bond formed by the linear combination of molecular orbitals. Therefore, a new local HOMO (highest occupied molecular orbital) and LUMO (lowest unoccupied molecular orbital)

is formed.<sup>21, 25</sup>

Unfortunately, the possible formation of charge transfer complexes is not the only complication in doping organic semiconductors. Organic semiconductors do not follow the standard theory of doping in inorganic semiconductors where the conductivity increases with the amount of dopant. It is often seen for organic semiconductors that the conductivity initially decreases by the addition of dopants up to a certain threshold, where it starts to increase. This might be due to increased disorder or a higher density of trap states in organic semiconductors upon doping. Additionally the dopants can interact very strongly with charge carriers due to the low dielectric constant of organic semiconductors.<sup>20-21, 25-26</sup>

Even with all the aforementioned complications, the conductivity for various organic semiconductors can now be tuned by several orders of magnitude by the use of molecular doping. Many questions are still unanswered, and therefore controlled doping of organic semiconductors and the process behind it is still a hot topic in research today.<sup>20-21, 25-26</sup>

Chemical doping has also been used for quantum dots, QDs. Early investigation of Henglein et. al showed electron injection into ZnO QDs by the use of  $\text{CH}_2\text{OH}$  radicals. Since then numerous studies have been performed where various QDs were doped by either reducing agents or photochemical doping. In the case of photochemical doping, electrons are excited from the valence band to the conduction band by light and the hole is extracted from the valence band by a hole scavenger. This leaves a free electron in the conduction band.<sup>23, 27-34</sup> Even though some control has been gained over chemical doping for QDs, in many cases the stability of the doped system is not high. Additionally, in most cases when a doped system is introduced to ambient conditions, the QDs lose their introduced charges and become undoped.<sup>23</sup>

### 1.3.2.2 Electrochemical doping

In electrochemical doping, electrons are either injected or extracted from semiconductor materials by the use of a potentiostat. That is, the desired charge carrier density can be obtained by changing one button on the potentiostat. Therefore, it is a very controlled way to dope semiconductors. Electrochemical doping will be explained in more detail in the next section.

## 1.4 Electrochemical doping

### 1.4.1 Electrochemical cell

Electrochemical doping is performed in an electrochemical cell, which most often contains three different electrodes. These electrodes are the working electrode, WE, counter electrode, CE, and the reference electrode, RE. The observed electrochemical reaction, or doping, takes place at the WE. That is, the WE can either inject or extract electrons into/from the material of interest, by changing its potential vs. a RE. Therefore, the RE has to have a stable and known potential. The potential of the RE is controlled by a well-known redox couple of known concentrations, which do not change significantly during the measurement. At last, the CE acts as an electron sink, as it passes the needed current to balance the current observed at the WE.

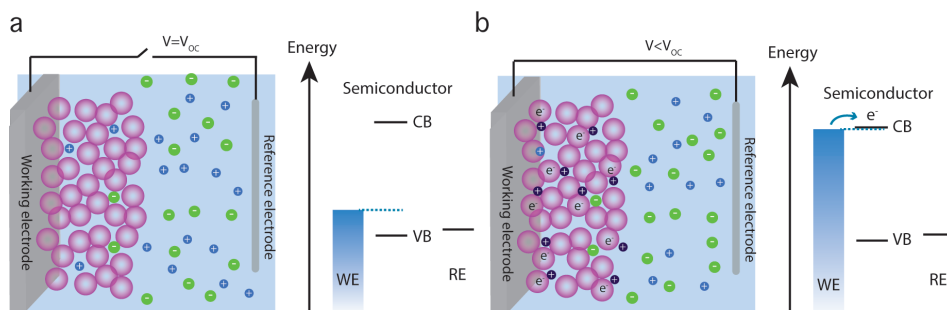


**Figure 1.4 Schematic of electrochemical doping of a semiconductor film.** a) When no potential is applied the Fermi level is inside the bandgap of the semiconductor film. b) When a negative enough potential is applied to the WE, the Fermi level moves to the conduction band of the semiconductor which will lead to electron injection. To neutralize injected electrons in the conduction band, electrolyte cations diffuse into the voids of the film. Image from Chapter 3.<sup>37</sup>

In an electrochemical measurement these three electrodes are immersed in an electrolyte solution. The electrolyte is dissolved into cations and anions in a polar solution, which makes the solution electrically conducting. Therefore, the electrolyte solution closes the circuit between the WE and the CE. The last part of the electrochemical cell is the analyte, that is the material under observation. Firstly, the analyte can be dissociated in the electrolyte solution. When the analyte diffuses close enough to the WE, electron transfer can occur.<sup>35</sup> The analyte can also be deposited or bound to the WE, to form a film. When that is the case, electrons can be injected or extracted from the semiconductor film at the interface of the electrode. If the semiconductor film contains more than a monolayer, electron transfer needs to occur between semiconductor molecules. As an example, semiconductor QDs can be “bound” together with cross-linking ligands to form a film. The cross-linking ligands are short enough for electrons to transfer (tunnel) between the QDs.<sup>36</sup>

If the semiconductor material is supposed to be implemented in devices, a semiconductor film is more useful than an analyte in solution. If the doping proves to be stable, the film can be implemented in the desired device. In this thesis we want to investigate charge transport and doping in semiconductor films, that hopefully can be used in devices. The next section explains the process where a semiconductor film is doped by the use of electrochemistry.<sup>35</sup>

### 1.4.2 Electrochemical doping of porous semiconductor films

Figure 1.4 shows an example of electrochemical doping of a semiconductor film. The semiconductor film is deposited on the WE, and is immersed in a solvent containing electrolyte cations and anions. By applying a negative enough potential to the film vs. the RE, electrons can be injected into the conduction band of the semiconductor film. In order to neutralize the injected charge, electrolyte cations diffuse into the voids of the film. When a positive enough potential is applied to the film, electrons are extracted from the valence band and electrolyte anions diffuse into the film. In contrast to the other

doping methods discussed above, electrochemical doping thus starts with the injection of the free charge carriers, which subsequently attract “dopant ions” to achieve charge neutrality. These electrolyte cations and anions can be seen as external dopants. As the ions are external dopants, they do not lead to distortion of the crystal lattice as happens in impurity doping. Additionally, they do not introduce extra energy states in the middle of the bandgap which can act as recombination centres for electrons and holes.

In order to use electrochemical doping on a semiconductor film, it needs to fulfil two requirements. Firstly, the semiconductor needs to withstand the applied potential. It can occur that the semiconductor material itself is either reduced or oxidized instead of being doped.<sup>38-39</sup> If that is the case, it is most likely not possible to dope the semiconductor to the same degree with another doping method, as the Fermi level decides if the introduced electrons/holes are stable or react, irrespective of the doping method. Secondly, if a semiconductor film is used, it needs to be porous. If the film is not porous, electrolyte cations and anions are not able to diffuse into the voids of the film, and a space charge region is formed. Changes in the charge carrier density will only occur in this space charge region, which is usually 10-1000 nm.<sup>40</sup> On the other hand, if the film is nano-porous, electrolyte ions can penetrate the whole film to neutralize the injected charge. That is, during the doping process the overall film remains neutral, no space charge region forms and the semiconductor film is doped uniformly.<sup>41</sup>

Examples of porous semiconductor films are organic semiconductors, such as conjugated polymers and fullerenes, and QDs. As stated above, for QDs and organic semiconductors impurity doping often does not introduce free charge carriers in these systems. On the other hand electrochemical doping has been performed for a variety of both organic semiconductors and QDs with good effect.<sup>36, 42-48</sup> In many of these experiments, electrochemistry is combined with spectroscopy such as absorbance or photoluminescence and is called spectro-electrochemistry. In the majority of the measurements electrochemistry is used as an analytical method. (Spectro)-electrochemical measurements have been able to show positions of electron bands, placement of trap states and the effect of charge injection on blinking in quantum dots.<sup>36, 45, 49-51</sup> It has also been shown that by using electrochemical doping the conductivity of QD films can be increased by 12 orders of magnitude.<sup>11</sup> That is, the doping density can be tuned over 12 orders of magnitude, by only applying different potentials.

### 1.4.3 Electrochemical measurements

As was stated above, electrochemistry is a powerful analytical tool. It has a wide selection of measurements which are documented in numerous books. One of the more common electrochemical measurement is cyclic voltammetry (CV), where the potential of the WE is scanned while the current is measured. If a redox reaction takes place an increase in current is seen, as current ( $i$ ) is the flow of electrical charge,  $q$ , over time,  $t$ :

$$i = dq/dt \quad 1.4$$

If electrons move from the WE to the system, a negative current is measured (following the IUPAC definition<sup>52</sup>). In contrast, if electrons move from the system to the WE, a positive

current is detected. From the area of the measured current, the injected/extracted charge can be calculated with the following equation:

$$q = (\sum(i \times dE)) / v \quad 1.5$$

Where  $dE$  is the potential step and  $v$  is the scan rate. If the injected charge is equal to the extracted charge, the reaction is chemically reversible.<sup>35</sup>

By performing CV measurements a great amount of information can be gained about the observed electron transfer to the analyte. The shape of the CV itself can show if the reaction is reversible, if adsorption of species takes place and if multiple redox reactions occur. By performing CVs at different scan rates in a well-known system, the diffusion coefficient of either the analyte or the electrolyte cations can be calculated.<sup>46</sup> And finally, the combination of a CV with a light source can give information such as energy band placement and trap states.<sup>53-54</sup> This list contains only a few examples about information that can be gained from a CV, which shows how remarkable the measurement technique can be.

A CV is a powerful analytical technique, but it doesn't give information about the conductivity of a doped semiconductor film. In order to measure the conductivity, it is necessary to add an additional working electrode. By applying a potential difference between the two working electrodes,  $dV$ , the conductance,  $G$ , can be calculated with equation 1.6:

$$G = dI/dV \quad 1.6$$

Where  $dI$  is the measured current. The conductivity,  $\sigma$ , can be connected to the conductance by the following equation:

$$\sigma = (G \times w) / (l \times h) \quad 1.7$$

Where  $w$  is the distance between the two working electrodes,  $l$  is the gap length and  $h$  is the height of the film. In our conductivity measurements we use home-built interdigitated electrodes which contain four working electrodes (see Figure 1.5a). Each WE pair has a different gap length, which gives different sensitivities. Therefore, one gold electrode has 5 different sensitivities for conductivity measurements. The gold electrode also contains an optical mesh and a solid gold square for absorbance and reflectance measurements, respectively.

By performing conductivity measurements on semiconductor systems, it is possible to see if electrochemical doping is successful. An example of a conductivity measurement performed on a ZnO QD film in 0.1 M  $\text{LiClO}_4$  is given in Figure 1.5b. In this measurement the potential of one working electrode (the source) is scanned around the fixed potential of the other working electrode (the drain). The conductance is then calculated from the slope of the measured source-drain current (equation 1.6). By repeating the measurement at different potentials, the conductivity can be obtained for a wide range of potentials.

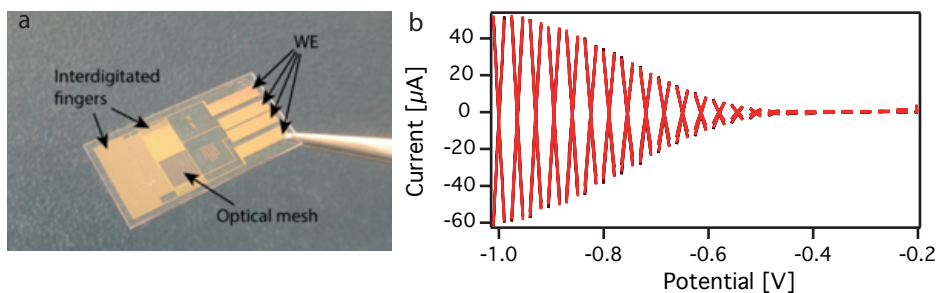


**Figure 1.5** a) Home-built interdigitated gold electrode. It contains four working electrodes with different sensitivities. It additionally contains an optical mesh for absorbance measurements. b) Conductivity measurements for a ZnO QD film in 0.1 M  $\text{LiClO}_4$  acetonitrile solution. The source-drain bias is  $\pm 10$  mV

#### 1.4.4 Stability of electrochemically doped semiconductor films

In an ideal world, we would dope our semiconductor film to the desired charge carrier density by the use of electrochemistry, disconnect it and implement it in a device of choice. Unfortunately, when the semiconductor film is disconnected from the potentiostat, injected charges leave the film.<sup>22, 39</sup> The only cases of stable electrochemical doped films have been at low temperatures (200 K and lower).<sup>50-51, 55-56</sup> At these low temperatures, both redox active impurities and electrolyte ions are immobilized. If the electrolyte ions can't move out of the voids of the semiconductor film, injected charge should stay inside the semiconductor to keep a neutralized system. Additionally, at very low temperatures, the rate of electrochemical side reactions, which could decrease the free carrier density, is decreased immensely.<sup>35</sup>

The goal of this thesis is to understand better electrochemical doping and why injected charges leave the semiconductor film. At last we want to produce stable electrochemically doped films, which can be used in semiconductor devices. It is important to keep in mind that when the doped films are implemented into devices, they have to withstand an external electric field. If the electrolyte ions are not immobilized in the voids of the semiconductor film, they will move in the presence of this electric field. When the ions move, the injected charge will disappear leading to a decrease in the charge carrier density. Therefore, it is necessary to immobilize the electrolyte ions. We are going to do so by freezing the electrolyte solvent. Clearly, it is not suitable to keep films at cryogenic temperature in devices, therefore we are going to look at solvents with melting points above room temperature. Therefore, at room temperature the solvent should be frozen, and hopefully the injected charge will not disappear.

When electrolyte solvents with melting points above room temperature are used, the electrochemical doping is performed when the solvent is liquid and the electrolyte ions can freely diffuse in the system. When the desired charge carrier density is reached, the temperature is decreased to room temperature. If the solvent is frozen in the voids of the

semiconductor film, diffusion of the electrolyte ions is minimized, and as stated above the charge carrier density should be stable. This approach is similar to thermal diffusion in impurity doping. There, the doping process takes place at high temperature when the dopant is able to diffuse inside the semiconductor wafer. When the doping process is finished, the temperature is decreased to room temperature. Therefore, in both doping processes, the dopant diffusion needs to be minimized.

### 1.5 Outline of this thesis

This thesis presents a variety of electrochemical measurements performed on porous semiconductor materials. The role of these electrochemical measurements is to gain further insight into the doping mechanism itself and the doping stability.

In electrochemical doping of a porous semiconductor film, electrolyte cations and anions serve as external dopants. The exact role of these external dopants is not known. In **Chapter 2**, various electrolyte cations were investigated in electrochemical doping of ZnO QDs. We show, in fact that the choice of the electrolyte cation is very important, as electron charge injection into ZnO QD films is limited by the diffusion of the cation. Additionally, the concentration and the size of the cation can greatly affect both the rate of charge injection and onset potential, as small ions can intercalate into the ZnO crystal lattice. On the other hand, the size of the cation does not affect the conductivity and the mobility of electrons in the ZnO QD film.

In **Chapter 3**, the electrochemical doping stability of various porous semiconductor films is investigated. The reason for charge disappearance is threefold. Impurities can extract the injected charge, internal electrochemical reactions of the semiconductor itself can take place, and if any external field is applied electrolyte ions will start moving. In order to increase the doping stability of the semiconductor films, measurements were performed where the electrolyte solvent is frozen. When the solvent is frozen, both electrolyte and impurities should be immobilized in the pores of the film. In order to gain electrochemically doped films at room temperature, the chosen electrolyte solvents have melting points above room temperature. Complete doping stability was obtained by using succinonitrile (melting point is 57 °C) at -75 °C.

As stated here above, one of the reasons for the disappearance of injected charge is impurities such as oxygen, which can react with the injected charge. In **Chapter 4** the role of impurities is investigated in the disappearance of injected electrons in ZnO QD films. Two different ways are used to reduce the effect of impurities toward the QD film. In the first one, solvent impurities were reduced before charge injection into the film takes place and in the second one a diffusion barrier is used to prevent impurity diffusion.

When succinonitrile was used as an electrolyte solvent, a stable electrochemically doped film was gained at -75 °C. Even if the melting point is 57 °C, injected charge leaves various porous semiconductor films at room temperature. Therefore, solvents with even higher melting points are needed. In **Chapter 5**, various nitriles with melting points ranging between 75 and 165 °C were used as the electrolyte solvents. Cyanoacetamide (mp: 120 °C) gave the best results, as no electrons leave the conduction band of a ZnO QD film for

over 20 hours and even on a time scale of 10 days 80% of the conductivity is retained. It is shown that this method also works for p doping of P3DT and for n doping of PbS QDs films, with even better stability.

Overall the results of this thesis show that it is possible to use electrochemical doping on a very wide range of porous semiconductors and that the doping density can be stabilized by using solvents that are frozen at RT. It is expected that the application of a proper gas diffusion barrier, such as  $\text{Al}_2\text{O}_3$  could stabilize the charge density completely so that such electrothermally doped systems could indeed be used in devices.

## References

1. BRAIN, M. How Semiconductors Work. <https://electronics.howstuffworks.com/diode.htm> (accessed 14 April).
2. Types of Optoelectronics Devices with Applications. <https://www.elprocus.com/optoelectronics-devices-with-their-applications/> (accessed 17th April).
3. Namek, P. <https://commons.wikimedia.org/wiki/File:RBG-LED.jpg>.
4. Bretwa [https://commons.wikimedia.org/wiki/File:Samsung\\_QLED\\_TV\\_8K\\_-\\_75\\_inches\\_-\\_2018-11-02.jpg](https://commons.wikimedia.org/wiki/File:Samsung_QLED_TV_8K_-_75_inches_-_2018-11-02.jpg).
5. Glaser, A. [https://commons.wikimedia.org/wiki/File:SoSie%2BSoSchiff\\_Ansicht.jpg](https://commons.wikimedia.org/wiki/File:SoSie%2BSoSchiff_Ansicht.jpg)
6. Augustyn, A.; Bauer, P.; Duignan, B.; Eldridge, A.; Gregersen, E.; McKenna, A.; Petruzzello, M.; Rafferty, J. P.; Ray, M.; Rogers, K.; Tikkanen, A.; Wallenfeldt, J.; Zeidan, A.; Zelazko, A. Semiconductor. <https://www.britannica.com/science/semiconductor> (accessed April 17).
7. Nanostructured Semiconductor Oxides for the Next Generation of Electronics and Functional Devices. Woodhead publishing: UK, 2014; Vol. 53, p 466.
8. Schubert, E. F., Doping in III-V semiconductors. Cambridge University Press: 1993.
9. Neamen, D. A., Semiconductor physics and devices: Basic principles. 4th ed.; McGraw-Hill Education: New York, United States, 2012.
10. Laube, P. Semiconductor Technology from A to Z. <https://www.halbleiter.org/en/fundamentals/doping/> (accessed April 17).
11. Norris, D. J.; Efros, A. L.; Erwin, S. C., Doped Nanocrystals. *Science* 2008, 319, 1776-1779.
12. The Mechatronics Handbook. CRC press: Boca Raton, 2002.
13. Atkins, P.; Paula, J. d., Atkins' Physical Chemistry. 10th ed.; Oxford University Press: United Kingdom, 2014.
14. Fuller, C. S.; Ditzenberger, J. A., Diffusion of Boron and Phosphorus into Silicon. *J. Appl. Phys.* 1954, 25 (11), 1439-1440.
15. Laube, P. Semiconductor Technology from A to Z. <https://www.halbleiter.org/en/waferfabrication/doping/> (accessed April 19).
16. Shaw, D., Diffusion in semiconductors. In *Springer Handbook of electronic and photonic materials*. Springer, Cham: 2017.
17. Sgourou, E. N.; Panayiotatos, Y.; Vovk, R. V.; Kuganathan, N.; Chroneos, A., Diffusion and Dopant Activation in Germanium: Insights from Recent Experimental and Theoretical Results. *Applied Sciences* 2019, 9 (12).
18. E.M.Hunta; J.M.Hampikian, Ion implantation-induced nanoscale particle

- formation in Al<sub>2</sub>O<sub>3</sub> and SiO<sub>2</sub> via reduction. *Acta Mater.* 1999, 47 (5), 1497-1511.
19. Ion implantation. Science and technology. 2nd ed.; Academic Press, Inc: United Kingdom, 1988.
  20. Lüssem, B.; Riede, M.; Leo, K., Doping of organic semiconductors. *physica status solidi (a)* 2013, 210 (1), 9-43.
  21. Salzmann, I.; Heimel, G.; Oehzelt, M.; Winkler, S.; Koch, N., Molecular Electrical Doping of Organic Semiconductors: Fundamental Mechanisms and Emerging Dopant Design Rules. *Acc. Chem. Res.* 2016, 49 (3), 370-8.
  22. Shim, M.; Wang, C.; Norris, D. J.; Guyot-Sionnest, P., Doping and Charging in Colloidal Semiconductor Nanocrystals. *MRS Bull.* 2001, 26 (12), 1005-1008.
  23. Schimpf, A. M.; Knowles, K. E.; Carroll, G. M.; Gamelin, D. R., Electronic doping and redox-potential tuning in colloidal semiconductor nanocrystals. *Acc. Chem. Res.* 2015, 48 (7), 1929-37.
  24. Mocatta, D.; Cohen, G.; Schattner, J.; Millo, O.; Rabani, E.; Banin, U., Heavily Doped Semiconductor Nanocrystal Quantum Dots. *Science* 2011, 332, 77-81.
  25. Jacobs, I. E.; Moule, A. J., Controlling Molecular Doping in Organic Semiconductors. *Adv. Mater.* 2017, 29 (42).
  26. Liu, H.; Liu, Y.; Zhu, D., Chemical doping of graphene. *J. Mater. Chem.* 2011, 21 (10), 3335-3345.
  27. Shim, M.; Wang, C.; Guyot-Sionnest, P., Charge-Tunable Optical Properties in Colloidal Semiconductor Nanocrystals. *J. Phys. Chem. B* 2001, (105), 2369-2373.
  28. Palomaki, P. K.; Miller, E. M.; Neale, N. R., Control of plasmonic and interband transitions in colloidal indium nitride nanocrystals. *J. Am. Chem. Soc.* 2013, 135 (38), 14142-50.
  29. Schimpf, A. M.; Gunthardt, C. E.; Rinehart, J. D.; Mayer, J. M.; Gamelin, D. R., Controlling carrier densities in photochemically reduced colloidal ZnO nanocrystals: size dependence and role of the hole quencher. *J. Am. Chem. Soc.* 2013, 135 (44), 16569-77.
  30. Rinehart, J. D.; Schimpf, A. M.; Weaver, A. L.; Cohn, A. W.; Gamelin, D. R., Photochemical electronic doping of colloidal CdSe nanocrystals. *J. Am. Chem. Soc.* 2013, 135 (50), 18782-5.
  31. Valdez, C. N.; Schimpf, A. M.; Gamelin, D. R.; Mayer, J. M., Proton-Controlled Reduction of ZnO Nanocrystals: Effects of Molecular Reductants, Cations, and Thermodynamic Limitations. *J. Am. Chem. Soc.* 2016, 138 (4), 1377-1385.
  32. Schimpf, A. M.; Lounis, S. D.; Runnerstrom, E. L.; Milliron, D. J.; Gamelin, D. R., Redox chemistries and plasmon energies of photodoped In<sub>2</sub>O<sub>3</sub> and Sn-doped In<sub>2</sub>O<sub>3</sub> (ITO) nanocrystals. *J. Am. Chem. Soc.* 2015, 137 (1), 518-24.
  33. Koh, W. K.; Kaposov, A. Y.; Stewart, J. T.; Pal, B. N.; Robel, I.; Pietryga, J. M.; Klimov, V. I., Heavily doped n-type PbSe and PbS nanocrystals using ground-state charge transfer from cobaltocene. *Sci. Rep.* 2013, 3, 2004.
  34. Jeong, K. S.; Deng, Z.; Keuleyan, S.; Liu, H.; Guyot-Sionnest, P., Air-Stable n-Doped Colloidal HgS Quantum Dots. *J. Phys. Chem. Lett.* 2014, 5 (7), 1139-1143.
  35. Bard, A. J.; Faulkner, L. R., *Electrochemical methods. Fundamentals and applications.* 2nd ed.; John Wiley & sons, INC.: New York, United states of America, 2001.
  36. Boehme, S. C.; Wang, H.; Siebbeles, L. D. A.; Vanmaekelbergh, D.; Houtepen, A.

- J., Electrochemical charging of CdSe quantum dot films: Dependence on voids size and counterion proximity. *ACS Nano* 2013, 7 (3), 2500-2508.
37. Gudjonsdottir, S.; Stam, W. v. d.; Koopman, C.; Kwakkenbos, B.; Evers, W. H.; Houtepen, A. J., On the Stability of Permanent Electrochemical Doping of Quantum Dot, Fullerene, and Conductive Polymer Films in Frozen Electrolytes for Use in Semiconductor Devices. *ACS Applied Nano Materials* 2019.
38. du Fossé, I.; ten Brinck, S.; Infante, I.; Houtepen, A. J., Role of Surface Reduction in the Formation of Traps in n-Doped II–VI Semiconductor Nanocrystals: How to Charge without Reducing the Surface. *Chem. Mater.* 2019.
39. Guyot-Sionnest, P., Charging colloidal quantum dots by electrochemistry. *Microchim. Acta* 2008, 160 (3), 309-314.
40. Krishnan, R., Fundamentals of Semiconductor. Electrochemistry and Photoelectrochemistry. Wiley-VCH Verlag GmbH & Co. KGaA: 2007.
41. Vanmaekelbergh, D.; Houtepen, A. J.; Kelly, J. J., Electrochemical gating: A method to tune and monitor the (opto)electronic properties of functional materials. *Electrochim. Acta* 2007, 53 (3), 1140-1149.
42. Shimotani, H.; Diguët, G.; Iwasa, Y., Direct comparison of field-effect and electrochemical doping in regioregular poly(3-hexylthiophene). *Appl. Phys. Lett.* 2005, 86 (2), 022104.
43. ECHEGOYEN, L.; ECHEGOYEN, L. E., Electrochemistry of Fullerenes and Their Derivatives. *Acc. Chem. Res.* 1998, 31, 593-601.
44. Braunger, M. L.; Barros, A.; Ferreira, M.; Olivati, C. A., Electrical and electrochemical measurements in nanostructured films of polythiophene derivatives. *Electrochim. Acta* 2015, 165.
45. Boehme, S. C.; Azpiroz, J. M.; Aulin, Y. V.; Grozema, F. C.; Vanmaekelbergh, D.; Siebbeles, L. D.; Infante, I.; Houtepen, A. J., Density of Trap States and Auger-mediated Electron Trapping in CdTe Quantum-Dot Solids. *Nano Lett.* 2015, 15 (5), 3056-66.
46. van der Stam, W.; Gudjonsdottir, S.; Evers, W. H.; Houtepen, A. J., Switching between Plasmonic and Fluorescent Copper Sulfide Nanocrystals. *J. Am. Chem. Soc.* 2017, 139 (37), 13208-13217.
47. Yu, D.; Wehrenberg, B. L.; Jha, P.; Ma, J.; Guyot-Sionnest, P., Electronic transport of n-type CdSe quantum dot films: Effect of film treatment. *J. Appl. Phys.* 2006, 99 (10), 104315.
48. Grimaldi, G.; van den Brom, M. J.; du Fosse, I.; Crisp, R. W.; Kirkwood, N.; Gudjonsdottir, S.; Geuchies, J. J.; Kinge, S.; Siebbeles, L. D. A.; Houtepen, A. J., Engineering the Band Alignment in QD Heterojunction Films via Ligand Exchange. *J Phys Chem C Nanomater Interfaces* 2019, 123 (49), 29599-29608.
49. Amelia, M.; Lincheneau, C.; Silvi, S.; Credi, A., Electrochemical properties of CdSe and CdTe quantum dots. *Chem. Soc. Rev.* 2012, 41 (17), 5728-43.
50. Yu, D.; Wang, C.; Wehrenberg, B. L.; Guyot-Sionnest, P., Variable range hopping conduction in semiconductor nanocrystal solids. *Phys. Rev. Lett.* 2004, 92 (21), 216802.
51. Houtepen, A. J.; Kockmann, D.; Vanmaekelbergh, D., Reappraisal of Variable-Range Hopping in Quantum-Dot Solids. 2008, Vol. 8 (10), 3516-3520.
52. Elgrishi, N.; Rountree, K. J.; McCarthy, B. D.; Rountree, E. S.; Eisenhart, T. T.;

- Dempsey, J. L., A Practical Beginner's Guide to Cyclic Voltammetry. J. Chem. Educ. 2017, 95 (2), 197-206.
53. van der Stam, W.; du Fosse, I.; Grimaldi, G.; Monchen, J. O. V.; Kirkwood, N.; Houtepen, A. J., Spectroelectrochemical Signatures of Surface Trap Passivation on CdTe Nanocrystals. Chem. Mater. 2018, 30 (21), 8052-8061.
54. van der Stam, W.; de Graaf, M.; Gudjonsdottir, S.; Geuchies, J. J.; Dijkema, J. J.; Kirkwood, N.; Evers, W. H.; Longo, A.; Houtepen, A. J., Tuning and Probing the Distribution of Cu(+) and Cu(2+) Trap States Responsible for Broad-Band Photoluminescence in CuInS<sub>2</sub> Nanocrystals. ACS Nano 2018, 12 (11), 11244-11253.
55. Houtepen, A. J. Charge injection and transport in quantum confined and disordered systems. Utrecht University, 2007.
56. Gao, J.; Li, Y.; Yu, G.; Heeger, A. J., Polymer light-emitting electrochemical cells with frozen junctions. J. Appl. Phys. 1999, 86 (8), 4594-4599.



# 2



## The role of dopant ions on charge injection and transport in electrochemically doped quantum dot films

---

In Chapter 1, electrochemical doping is introduced as a promising way of controllably doping porous semiconductor films, where electrolyte ions can be regarded as external dopant ions. In order to make stable electrochemically doped films at room temperature, the role of the electrolyte ions in the doping process needs to be known. To gain insight into the doping mechanism and the role of the external dopant ions, we investigate charge injection in ZnO nanocrystal assemblies for a large series of charge compensating electrolyte ions with spectro-electrochemical and electrochemical transistor measurements. We show that charge injection is limited by the diffusion of cations in the nanocrystal films as their diffusion coefficient are found to be  $\sim 7$  orders of magnitude lower than those of electrons. We further show that the rate of charge injection depends strongly on the cation size and cation concentration. Strikingly, the onset of electron injection varies up to 0.4 V, depending on the size of the electrolyte cation. For the small ions  $\text{Li}^+$  and  $\text{Na}^+$  the onset is at significantly less negative potentials. For larger ions ( $\text{K}^+$ , quaternary ammonium ions) the onset is always at the same, more negative potential, suggesting that intercalation may take place for  $\text{Li}^+$  and  $\text{Na}^+$ . Finally, we show that the nature of the charge compensating cation does not affect the source-drain electronic conductivity and mobility, indicating that shallow donor levels from intercalating ions fully hybridize with the quantum confined energy levels and that the reorganization energy due to intercalating ions does not strongly affect electron transport in these nanocrystal assemblies.

This chapter is based on: S. Gudjonsdottir, W. van der Stam, N. Kirkwood, W. H. Evers, A. J. Houtepen. J. Am. Chem. Soc. 2018, 140 (21), 6582-6590

## 2.1 Introduction

Quantum dots (QDs) are known for their tunable optoelectronics properties, processability and cheap and facile solution-based synthesis.<sup>1-3</sup> For these reasons they are promising for optoelectronic applications such as displays,<sup>4-6</sup> solar cells<sup>3, 7-8</sup> and LEDs.<sup>3,9-10</sup> To optimize the potential of QDs for such applications, control over electronic doping is essential.<sup>11</sup> Traditionally, doping of semiconductors is achieved by introducing impurity atoms into the crystal that act as electron donors and acceptors. For QDs there have been many attempts to dope them in a similar manner.<sup>12-14</sup> However, due to charge compensation by localized counter charges on the surface of the nanocrystals, introduced impurities rarely contribute excess carriers in conduction or valence states.<sup>13</sup> Additionally, significant distortion of the QD crystal structure even at one dopant per QD<sup>12</sup> can make this approach difficult. In practice, it still remains a challenge to fully and reversibly control the charge carrier density.<sup>13</sup> A less invasive and potentially more controllable approach is to use external dopants that reside outside the QD but still dope it electronically. Chemical redox doping has been used for this purpose.<sup>15-16</sup> More recently, photochemical doping<sup>17-18</sup> has also been shown to be efficient in tuning the charge carrier density.

However, arguably the most controllable method to dope QD films is by electrochemical doping. In this approach, electrons or holes are injected via an electrode and their charge is compensated by electrolyte ions that diffuse into the QD film.<sup>19-21</sup> Ideally, the charge compensation by electrolyte ions is uniform due to the porous nature of QD films, resulting in a uniform charge density and absence of band bending. This method enables reversible carrier density tuning in a wide range and allows to set the Fermi-level on demand by controlling the potential with a potentiostat. Furthermore, electrochemical and spectro-electrochemical methods have been used to examine many different properties of QDs such as the band gap energies, QDs trap states, QDs valence and conduction band energy levels and the effect of charge injection on blinking of the QDs.<sup>20, 22-23</sup> The versatility of electrochemical methods to dope QDs is demonstrated by the wide range of QD compositions studied, such as CdSe, CdTe, core shell quantum dots (CdSe-ZnS, CdSe-CdS-ZnS)<sup>23-24</sup>, PbSe quantum dot superstructures<sup>25</sup>, Cu<sub>2</sub>S<sup>26</sup>, HgTe<sup>13</sup> and ZnO<sup>27</sup>. For electrochemical charge injection, the charge compensating electrolyte ions can be regarded as external dopants. It is to be expected that the nature of these dopant ions affects the rate and energetics of charge injection and may also influence electron transport in these films. However, the role of the electrolyte ions has not been studied in detail before.

In this Chapter, we investigate the role of the electrolyte cation in electron injection into QD films. ZnO QD films were selected as they exhibit very stable and reversible charge injection, allowing in-depth electrochemical investigations, including performing many different experiments on the same ZnO QD film.<sup>15</sup> By using differential capacitance and source-drain electronic conductance measurements combined with spectro-electrochemical measurements, both the mobility of electrons moving perpendicular through the film (out-of-plane) during charge injection and the mobility of electrons moving parallel to the substrate (in-plane) in a source-drain configuration can be determined. The out-of-plane electron mobility is shown to be 7 orders of magnitude lower than the in-plane mobility. By performing cyclic voltammetry (CV) at different scan rates, it is shown that the concentration and the size of the electrolyte cation affects the electron injection rate.

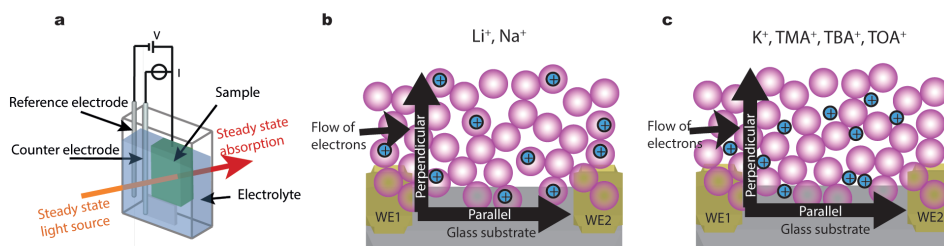


**Figure 2.1.** Schematic representation of the (a) Three electrode (spectro)-electrochemical setup. The cell contains a Ag wire pseudoreference electrode, Pt sheet counter electrode and the sample on a working electrode. The solution is typically a 0.1 M LiClO<sub>4</sub> acetonitrile electrolyte solution. The steady state absorption can be measured during the electrochemical measurements. (b) The ZnO film on the IDE with Li<sup>+</sup> or Na<sup>+</sup> as an electrolyte cation. The ions have intercalated into the ZnO QDs upon electron injection. The schematic includes the parallel (in-plane) and perpendicular (out-of-plane) flow of electrons. (c) The ZnO film on the IDE with K<sup>+</sup>, TMA<sup>+</sup>, TBA<sup>+</sup> or TOA<sup>+</sup> as an electrolyte ion. The ions occupy the voids of the film. The schematic includes parallel and perpendicular flow of electrons.

We conclude that ion diffusion limits charge injection and we determine the diffusion coefficients for different cations. Interestingly, cyclic voltammograms show a lower onset of electron injection into the ZnO QDs by up to 0.4 V for smaller ions (Li<sup>+</sup>, Na<sup>+</sup>), suggesting that they may intercalate into the ZnO lattice. Finally, it is shown that the size of the cation does not affect the in-plane conductivity or mobility of the electrons. This shows that the electrons tunnel between QDs independent of the positive counterions. The implications of this are discussed.

## 2.2 Results and Discussions

### 2.2.1 Flow of electrons in the ZnO film

Figure 2.1a shows the experimental approach as previously described by Boehme et al.<sup>21,28</sup> (Spectro)electrochemical and conductivity measurements are done in an electrochemical cell with three electrodes (for CV and for differential capacitance measurements) or four electrodes (source-drain conductivity measurements) with a home-built interdigitated electrode (IDE, see Methods). Two types of electron currents are monitored (Fig. 2.1b and c): perpendicular (out-of-plane) to the electrode during charge injection, or parallel (in-plane) to the electrode during source-drain conductivity measurements. We find that there is a great difference between the parallel and perpendicular conductivities.

In the electrochemical experiment charge is injected into the QDs. To compensate for the charge, cations flow into the voids of the film. Here, we inject electrons into ZnO QDs film in six different electrolyte solutions of different concentrations. From the results it is possible to separate the different electrolyte cations into two groups (Fig. 2.1b and c). The former one includes the smaller electrolyte cations, Li<sup>+</sup> and Na<sup>+</sup>. For these ions, electron injection occurs at more positive potential than for the larger ions, which might be due to intercalation. The second group includes the larger electrolyte cations K<sup>+</sup>, TMA<sup>+</sup>, TBA<sup>+</sup> and TOA<sup>+</sup>. They are able to diffuse into the voids of the ZnO QDs but their size hinders intercalation.

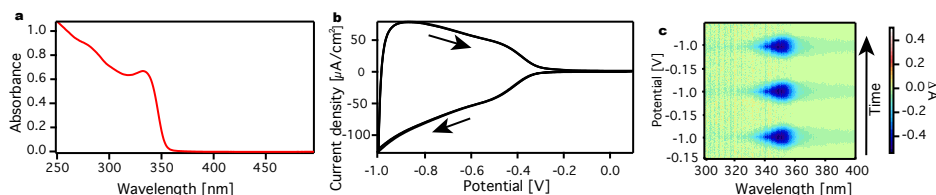


**Figure 2.2 Spectro-electrochemical measurements for a ZnO QD film.** (a) Absorption spectrum of a ZnO QD suspension in ethanol. (b) Cyclic voltammogram for a ZnO QD film on ITO in 0.1 M LiClO<sub>4</sub> acetonitrile electrolyte solution. The scan was started at 0.1 V, which is in the band gap of the ZnO QDs, arrows indicate the scan direction. The scan speed was 25 mV/s and the scan is repeated three times. (c) The differential absorption during CV scans. As electrons are injected in the conduction band of the ZnO QDs (around -0.4 V), a negative differential absorbance of the 1Se conduction level is measured (blue area).

## 2.2.2 General properties of electron injection

The ZnO QDs were synthesized as outlined in the Experimental Section. Figure 2.2a shows the absorption spectrum of the ZnO QDs in ethanol, with the first absorbance peak around 350 nm. By using an empirical correlation from Meulenkamp et al.<sup>29</sup> the diameter of the ZnO QDs was calculated to be 3.8 nm. Figure 2.2b shows the cyclic voltammogram for a ZnO QD film on an ITO electrode in a 0.1 M LiClO<sub>4</sub> in acetonitrile electrolyte solution, where the potential was scanned from 0.1 V vs. the Ag pseudoreference electrode in negative direction to -1.0 V at 25 mV/s, and back to 0.1 V. The scan was repeated three times and is completely reproducible. From the voltammogram it can be seen that the current density starts to increase around -0.4 V and keeps increasing until the potential is reversed. This current density corresponds to electron injection into the ZnO QDs.<sup>20</sup> The symmetry and the reproducibility of these cyclic voltammetry (CV) measurements show that the electron injection is reversible and stable. Figure 2.2c shows the change in absorption during CV for a ZnO QD film over time for three scans. Time runs from bottom to top and the scan starts at -0.15 V. Around -0.5 V, a change in absorption around 350 nm can be seen which corresponds to a bleach of the band edge absorption due to the injection of electrons in the 1Se conduction level of the ZnO QDs (see Appendix, Figure A2.1).<sup>30</sup> Like the CV measurements, the spectro-electrochemical measurements are highly reversible and stable. We note that this is due to the rigorous water and oxygen free conditions of the experiments.

## 2.2.3 In-plane versus out-of-plane electron current

We now compare the electron current in the parallel (in-plane) and perpendicular (out-of-plane) directions with respect to the WE surface. Figure 2.3a shows the results of differential capacitance measurements (see Methods), which we use to calculate the total charge injected into the ZnO QD film. The measurements were performed with a potential step of 35 mV from 0 V to -1.0 V to 0 V again, on a gold IDE. In the bandgap of the ZnO QD the current is low, however, when electron injection occurs (~-0.4 V, represented by red curves), an initial peak current is seen that decays in ~0.5 s. From Figure 2.3a the differential capacitance can be determined after each potential step as described in the Methods. The outcome is depicted in Figure 2.3b in units of C/V and corrected for

background currents. At potentials more negative than -0.4 V, electrons are injected into the QD film (negative currents in Fig. 2.3a). The amount of injected charge increases until the scan is reversed (at -1.0 V). When the scan is reversed, the number of withdrawn electrons (positive currents in Fig. 2.3a) is very close to the number of injected electrons. This again shows the ability of ZnO to receive and release electrons reversibly. The right axis in Fig. 2.3b shows the density of states, calculated from the differential capacitance,  $\Delta Q/\Delta V$ , and the film volume,  $V_{\text{film}}$  according to equation 2.1:

$$\rho(V) = \Delta Q(V) / (\Delta V \times V_{\text{film}} \times e) \quad 2.1$$

From Figure 2.3a it is also possible to calculate the resistance of the film. If the film acts as a capacitor, the current response of a step potential is given by,<sup>31</sup>

$$I(t) = \frac{E}{R_{\perp}} e^{-\frac{t}{\tau_{\perp}}} = \frac{E}{R_{\perp}} e^{-\frac{t}{R_{\perp} \times C}} \quad 2.2$$

Where E is the potential step,  $R_{\perp}$  is the out-of-plane film resistance,  $\tau_{\perp}$  is the relaxation time, also known as the RC-time, and C is the film capacitance. We note that the charging currents in Figure 2.3a are not perfectly exponential (see Appendix, Figure A2.2). For simplicity we therefore determine  $\tau_{\perp}$  as the time where the current has dropped to 1/e of the maximum.

As the capacitance C is known directly from integrating the current (Fig. 2.3b) we determine  $R_{\perp}$  and relate it to the film conductivity,  $\sigma_{\perp}$ , by equation 2.3:

$$\sigma_{\perp} = \frac{h_{\text{film}}}{A_{\text{film}} \times R_{\perp}} \quad 2.3$$

where  $h_{\text{film}}$  is the height of the film and  $A_{\text{film}}$  is the area of the film. The resulting out-of-plane conductivity,  $\sigma_{\perp}$ , is plotted as a function of applied potential for both the forward and the backward scan (black line in Figure 2.3c).

For the same film, source-drain electronic conductance measurements were performed after each differential capacitance measurement (see Methods). The corresponding source-drain currents can be seen in Appendix, Figure A2.3. The conductivity can be calculated as shown in the Methods. The resulting in-plane conductivity,  $\sigma_{\parallel}$ , is plotted as a function of applied potential as well for both the forward and the backward scan (red line in Figure 2.3c). When the two conductivities are compared, we find that the out-of-plane electronic conductivity is seven orders of magnitude lower than the in-plane electronic conductivity ( $10^{-9}$  S/cm vs  $10^{-2}$  S/cm). As both  $\sigma_{\perp}$  and  $\sigma_{\parallel}$  are determined on the same film during the same potential scan, the charge carrier density, n, is necessarily the same, showing that the mobility (given by  $\mu = \sigma / (n \cdot e)$ ) also differs by 7 orders of magnitude. The charge carrier density (Appendix, Figure A2.4) is derived by dividing the total injected charge obtained from Figure 2.3b (see Methods) by the film volume ( $1.4 \times 10^{-10}$  m<sup>3</sup>). The in-plane mobility,  $\mu_{\parallel}$  is plotted as a red line and the out-of-plane mobility  $\mu_{\perp}$  is plotted as a black line in Figure 2.3d.

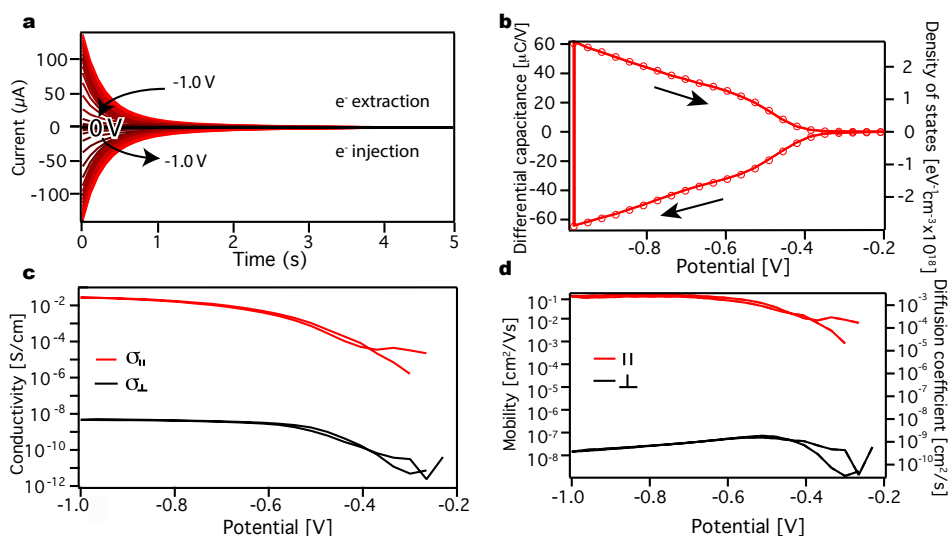


**Figure 2.3 Differential capacitance and electronic source-drain conductance measurements.** (a) Differential capacitance measurements performed on a ZnO QD film on an IDE in 0.1 M  $\text{LiClO}_4$  in acetonitrile electrolyte solution. Potential steps of 35 mV were taken and the current was measured for 5 seconds until equilibrium was reached. The potential was stepped from 0 V to -1.0 V and then reversed to 0 V. (b) The differential capacitance of the QD film with units of C/V is on the left axis while the density of states is shown on the right axis, arrows indicate the scan direction. (c) Calculated parallel source-drain electron conductivity (red line) compared to the perpendicular electron conductivity (black line). (d) Difference in parallel source-drain electron mobility (red) and the perpendicular mobility (black) on the left axis and the parallel (red) and perpendicular (black) diffusion coefficients on the right axis.

The great difference in conductivities and mobilities can be explained by the role of the electrolyte cations in the electronic doping of the QD film. In the out-of-plane conductivity electrons are injected into the film, to compensate for the negative injected charge in the film, the electrolyte cations diffuse into the pores of the film. Therefore, the out-of-plane conductivity of the electrons is limited by the diffusion of the cations. This is not seen in the in-plane source-drain conductivity as the electrons have already been injected into the film, and no additional charging takes place. These experiments are performed under steady state conditions where the electron density (and hence also the ion density) is constant and hence diffusion of ions is not required. The in-plane mobility varies over several orders of magnitude with potential, or equivalently with charge density. This is expected for electron transport in a disordered semiconductor system.<sup>32-33</sup> The maximum value of the in-plane mobility ( $10^{-1} \text{ cm}^2/\text{Vs}$ ) is found to be similar to previous experimental values of the source-drain mobility ( $10^{-2} \text{ cm}^2/\text{Vs}$ ).<sup>30</sup> The out-of-plane mobility is orders of magnitude lower ( $10^{-8} \text{ cm}^2/\text{Vs}$ ).

The diffusion coefficient,  $D$ , of an ordered system can be calculated with the Einstein relation:

$$D = (\mu k_b T) / e \quad 2.4$$

where  $k_b$  is the Boltzmann constant,  $T$  is the temperature and  $e$  is the elemental charge. We note that the Einstein relation may not strictly be valid in the case of strongly interacting or highly disordered systems.<sup>33</sup> However, for reasons of simplicity and given the 7-orders of magnitude difference between in-plane and out-of-plane mobilities we are interested in here, we will disregard this effect. The calculated diffusion coefficients are shown in Figure 2.3d, right axis. We find that  $D_{\perp}$  is  $\sim 10^{-9}$  cm<sup>2</sup>/s. This value is lower than for diffusion of ions in solvents. However, such low values are not uncommon for ion diffusion in porous solids.<sup>34</sup> Hence, we conclude that charge injection, and the corresponding out-of-plane conductivity, is limited by diffusion of charge compensating cations through the porous NC film.

### 2.2.4 Effects of the cation on charge injection

To investigate the diffusion of the counterions in more detail we performed scan-rate dependent cyclic voltammetry measurements. The diffusion coefficient of the electrolyte cations can be determined by the Randles-Sevcik equation which states that for diffusion limited currents, the peak current ( $i_p$ ) can be connected to the scan rate ( $v$ ) according to:

$$i_p = 0.4463 n F A C^* \left( \frac{n F v D}{RT} \right)^{1/2} \quad 2.5$$

where  $n$  is the number of electrons,  $F$  is the Faradaic constant,  $A$  is the area of the working electrode,  $C^*$  is the concentration of the electrolyte and  $D$  is the diffusion coefficient. The Randles-Sevcik equation assumes diffusion of a reactant from a bulk solution to a smooth electrode surface. Although a QD film is nanoporous and not a smooth surface, this formalism is also often used for porous electrodes<sup>35-36</sup> and we do the same. In the Appendix we argue that the Randles-Sevcik equation also holds in the porous QD film investigated here.

To see the effect of the cation concentration on electron injection, a ZnO QD film was immersed in solutions of LiClO<sub>4</sub> in acetonitrile with three different concentrations: 0.01 M, 0.1 M and 1 M. CV measurements were performed with scan rates between 0.0075 V/s and 1.0 V/s and the peak current density ( $J_p$ ) was plotted against the scan rate (Fig. 2.4). For increasing Li<sup>+</sup> concentration the current density ( $J_0$ ) increases and the CVs become more symmetric. Furthermore, the log-log plot of the peak current density versus the scan rate for 0.01 M LiClO<sub>4</sub> shows that the peak current density is linearly dependent on the scan rates at low scan rates (<0.2 V/s) but at higher scan rates (>0.2 V/s) it scales with  $\sqrt{v}$ . This behavior clearly shows that at low scan rates charging is limited by the capacitance of the film, while at higher scan rates the current is limited by counter ion diffusion. This diffusion limitation becomes apparent around 0.18 V/s.

By increasing the concentration of LiClO<sub>4</sub> the diffusion limitations appear at higher scan rates, that is at around 0.4 V/s for 0.1 M LiClO<sub>4</sub> and >1 V/s for 1 M LiClO<sub>4</sub>. This shows that at low concentrations of the cation, the diffusion current of the cations inside the pores of

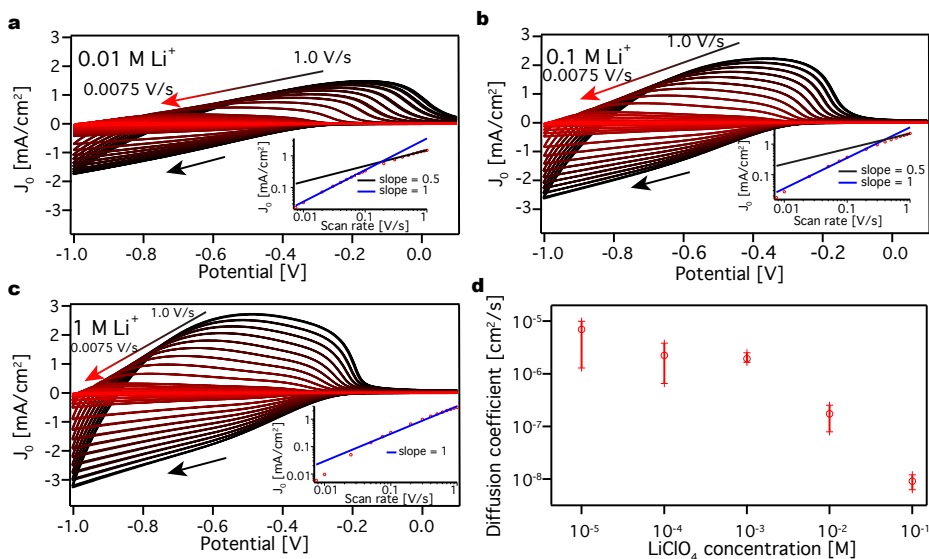


**Figure 2.4 Determination of diffusion coefficients in LiClO<sub>4</sub> acetonitrile electrolyte solution.** Cyclic voltammograms at different scan rates for a ZnO QD film in (a) 0.01 M LiClO<sub>4</sub> in acetonitrile electrolyte solution, (b) 0.1 M LiClO<sub>4</sub> in acetonitrile electrolyte solution and (c) 1 M LiClO<sub>4</sub> in acetonitrile electrolyte solution.  $J_0$  stands for the current density. The panels include a peak current density versus scan rate plot on a log-log scale. The scans have negative direction, indicated by a black arrow. By increasing the electrolyte concentration, the current and the symmetry increases. (d) Average diffusion coefficient and the standard deviation obtained from 3 different measurements for different concentration of LiClO<sub>4</sub> acetonitrile electrolyte solution.

the QD film is lower. By using the Randles-Sevcik equation, the diffusion coefficients were determined to be  $7.9 \times 10^{-8}$  cm<sup>2</sup>/s and  $6.3 \times 10^{-9}$  cm<sup>2</sup>/s at 0.01 M and 0.1 M, respectively. For the 1 M electrolyte solution, the peak current density does not depend on the square root of the scan rates within the investigated range, therefore it is not possible to calculate a diffusion coefficient. By increasing the concentration of the cation, the diffusion coefficient decreases, which shows that something is slowing the process down such as “jamming” of cations in the pores of the film. If this is the case, one would expect the diffusion coefficient to become constant at lower Li<sup>+</sup> concentrations. Figure 2.4d shows such measurements for a concentration range from 10  $\mu$ M to 0.1M. Fig 2.4d shows the average obtained diffusion coefficient and the standard deviation obtained from 3 measurements. Below 1 mM concentration, a concentration independent diffusion coefficient of  $\sim 10^{-5}$  cm<sup>2</sup>/s is obtained.

In addition to the ion concentration, we investigate the type and size of the cation and its effect on electron injection. In previous studies on Cu<sub>2</sub>S<sup>26</sup> and CdSe<sup>21</sup> our group has showed a strong effect of the size of the charge compensating ions on the reduction of nanocrystals. Furthermore, it has been shown by Brozek et al.<sup>37</sup> that the charge compensating cation can affect both the injected electron stability and the chemical reduction of ZnO nanocrystals greatly. Therefore, a ZnO QD film was subsequently immersed in four different electrolyte

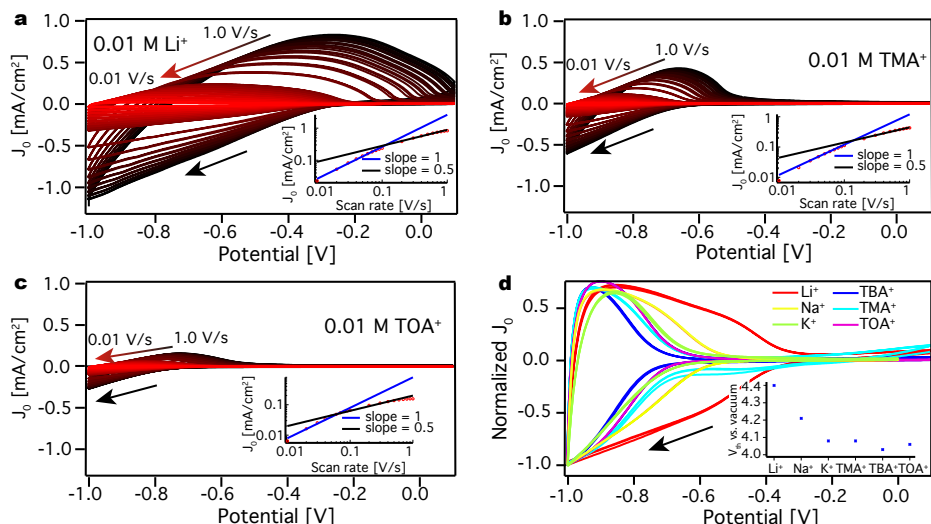


**Figure 2.5 Cyclic voltammograms for a ZnO QD film.** (a) CVs at different scan rates in 0.01 M LiClO<sub>4</sub> in acetonitrile electrolyte solution. The panel includes a peak current density versus scan rate plot on a log-log scale. (b) CVs at different scan rates in 0.01 M TMAPF<sub>6</sub> in acetonitrile electrolyte solution. The panel includes a peak current density versus scan rate plot on a log-log scale. (c) CVs at different scan rates in 0.01 M TOABF<sub>4</sub> in acetonitrile electrolyte solution. The panel includes a peak current density versus scan rate plot on a log-log scale. (d) CVs measured at 0.1 V/s for different electrolyte cations in a 0.1 M in acetonitrile electrolyte solution. The panel includes a plot of the threshold potential versus vacuum for the different ions. By increasing the size of the electrolyte cation, charge injection occurs at lower potentials. The scans have negative direction, indicated by a black arrow, and are repeated three times for every scan rate.  $J_0$  stands for current density.

solutions, containing different cations: lithium (Li<sup>+</sup>), tetramethylammonium (TMA<sup>+</sup>), tetrabutylammonium (TBA<sup>+</sup>) and tetraoctylammonium (TOA<sup>+</sup>). Furthermore, three different concentrations were investigated: 0.01 M, 0.1 M and 0.5 M. (The solubility of tetraalkylammonium salts in acetonitrile does not permit experiments at 1M). All experiments were done on the same ZnO QD film starting from the largest cation (TOA<sup>+</sup>) to the smallest one (Li<sup>+</sup>). Figure 2.5a-c shows the cyclic voltammograms for the ZnO QD film in 0.01 M Li<sup>+</sup>, TMA<sup>+</sup> and TOA<sup>+</sup> acetonitrile electrolyte solution. For simplicity, the CVs are plotted on the same scale, which allows for direct comparison of the current density between the different counterions (magnifications of the CVs including the one for TBA<sup>+</sup> are shown in the Appendix, Figure A2.6). As can be seen in Figure 2.5a-c, increasing the size of the cation dramatically decreases the peak current density by an order of magnitude. By using the Randles-Sevcik equation, the diffusion coefficient was determined for the different cations in a 0.01 M and 0.1 M in acetonitrile electrolyte solution (Table 2.1). As before, at the highest concentration charge injection is not diffusion limited in the range of scan rates investigated and hence it is not possible to calculate a diffusion coefficient. Table 2.1 shows that by increasing the size of the ion, the diffusion coefficient decreases. This trend can be seen for both concentrations. As for Li<sup>+</sup> the diffusion coefficient for the different ions decreases with higher concentration.

**Table 2.1.** Calculated diffusion coefficients in  $\text{cm}^2/\text{s}$  for the four different cations in 0.01 M and 0.1 M concentrations

	$\text{Li}^+$	$\text{TMA}^+$	$\text{TBA}^+$	$\text{TOA}^+$
0.01 M	$7.90 \cdot 10^{-8}$	$1.89 \cdot 10^{-8}$	$9.18 \cdot 10^{-9}$	$2.14 \cdot 10^{-9}$
0.1 M	$6.30 \cdot 10^{-9}$	$1.24 \cdot 10^{-9}$	$7.70 \cdot 10^{-10}$	$4.61 \cdot 10^{-10}$

Furthermore, Figure 2.5a-c shows that the onset for charge injection is around -0.4 V for  $\text{Li}^+$  while it is around -0.8 V for the other ions. The same difference in current and onset potential for  $\text{Li}^+$  compared to the other cations ( $\text{TMA}^+$ ,  $\text{TBA}^+$  and  $\text{TOA}^+$ ) can be seen at concentrations of 0.1 M and 0.5 M in acetonitrile electrolyte solution (Appendix, Figures A2.7 and A2.8). To examine the difference in the onset of charge injection for the different electrolyte cations in more detail, two additional measurements were performed with  $\text{Na}^+$  ( $r^+ = 116$  pm) and  $\text{K}^+$  ( $r^+ = 150$  pm), which have ionic radii in between  $\text{Li}^+$  ( $r^+ = 90$  pm) and  $\text{TMA}^+$  ( $r^+ = 320$  pm). Figure 2.5d shows CV scans at 0.1 V/s for the six different ions ( $\text{Li}^+$ ,  $\text{Na}^+$ ,  $\text{K}^+$ ,  $\text{TMA}^+$ ,  $\text{TBA}^+$  and  $\text{TOA}^+$ ). To make the onset of the electron injection clearer, the current density was normalized. An injection threshold potential  $V_{\text{th}}$  (vs. vacuum) is determined for every ion by identifying the first minimum in the second derivative of the first forward scan and is shown in Figure 2.5d. For  $\text{K}^+$ ,  $\text{TMA}^+$ ,  $\text{TBA}^+$  and  $\text{TOA}^+$  the threshold potentials are very similar ( $\sim 4.06$  V vs. vacuum) while for  $\text{Na}^+$  (4.21 V vs. vacuum) and for  $\text{Li}^+$  (4.4 V vs. vacuum) it is more positive.

We can rule out that mass transfer effects cause a different onset of charge injection, since the CVs are fully reversible at the low scan rates used in Figure 2.5d. Further, source-drain conductance measurements, which are performed at steady state for the different ions, show the same offset in potential (Appendix, Fig A2.9). Therefore, the difference in potential cannot be explained by faster diffusion of the smaller  $\text{Li}^+$  and  $\text{Na}^+$  ions. Since the differential capacitance and total injected charge (see also below where this is discussed in more detail) are indistinguishable for the different ions we can rule out that there exist differences in the portion of the film that gets charged, due to smaller ions penetrating deeper into the QD film. We conclude that the differences in the onset of charge injection must reflect a true thermodynamic free energy difference.

We believe that the observed differences with  $\text{Li}^+$  and  $\text{Na}^+$  are due to intercalation of these ions into the ZnO QDs, while the other ions are too large to intercalate into the ZnO QDs.  $\text{Li}^+$  is a known interstitial donor in bulk ZnO.<sup>38-39</sup> Moreover, both  $\text{Li}^+$  and  $\text{Na}^+$  have been reported to occupy interstitial sites and form shallow donors in ZnO QDs<sup>39</sup> and the syntheses of intentionally  $\text{Li}^+$  and  $\text{Na}^+$  doped ZnO nanocrystals have previously been reported.<sup>40-41</sup> In fact, ZnO and ZnO nanostructures are considered as anode material in Li ion batteries that rely on Li intercalation, albeit at more negative electrochemical potentials.<sup>42</sup> Kushima et al. have proven  $\text{Li}^+$  intercalation in ZnO nanowires under large electrochemical bias by the use of in situ transmission electron microscopy.<sup>43</sup> Additionally, J. Hupp et al.<sup>44</sup> saw a similar trend in electrochemical charging of  $\text{TiO}_2$  where the electron injection onset was  $\sim 0.8$  V more negative when using  $\text{TBA}^+$  compared to either  $\text{Li}^+$  or  $\text{Na}^+$ .

By using a combination of reflectance and electrochemical quartz crystal microbalance they observed that both  $\text{Na}^+$  and  $\text{Li}^+$  intercalated into the  $\text{TiO}_2$  while  $\text{TBA}^+$  did not due to steric hindrance. A similar shift of the onset potential for charging with cation size was reported by Boehme et al.<sup>21</sup> for CdSe QD films and was explained by the increased proximity of the charge on the cation and the electrons. Recently Puntambekar et al.<sup>45</sup> have claimed  $\text{Li}^+$  intercalation in CdSe QDs upon electrochemical charge injection.

Taken together, our experimental results and the discussed literature reports strongly suggest that  $\text{Li}^+$  and  $\text{Na}^+$  intercalate into the ZnO lattice resulting in a less negative onset potential for electron injection. In any case it is clear from the above experiments that the type, size and the concentration of the electrolyte cation affect the electron injection rate and energy greatly.

### 2.2.5 Effect of the cation on the source-drain conductivity

The presence of dopant ions is known to strongly affect charge transport. To investigate if this is the case, we compare the in-plane conductivity and mobility for the different cations. Figure 2.6a shows the source-drain conductivity for a ZnO QD film immersed in a 0.1 M acetonitrile electrolyte solution for four different ions:  $\text{Li}^+$ ,  $\text{TMA}^+$ ,  $\text{TBA}^+$  and  $\text{TOA}^+$ . All the measurements were performed with the same film starting with the largest dopant ion  $\text{TOA}^+$ . As the onset for charge injection is different for each ion (Appendix, Figure A2.9) a threshold potential  $V_{\text{th}}$  for charge injection was determined for every ion by finding the minimum residual between the in-plane conductivity of  $\text{Li}^+$  and the other ions (see Appendix). Fig. 2.6a shows the conductivity and mobility vs.  $V - V_{\text{th}}$ . The source-drain conductivities for all cations are very similar. Figure 2.6b shows the charge carrier density of the film for the four different ions. Similar to the in-plane conductivity, the charge carrier density is very similar for the different ions. Consequently, the electron mobility for the different ions, shown as the inset in Fig. 2.6b, is also very similar. Alternatively, the conductivity can be plotted against the charge carrier density for the different ions, eliminating the need to determine a threshold potential, see Appendix Figure 2.10. Also in this case the conductivities are almost identical. We argue that any differences observed are within the experimental error and that the type, size and location of the dopant ion (intercalating or occupying voids between QDs) do not significantly affect the electron mobility.

This observation is remarkable if one considers that there are various ways the cationic dopants could influence electron transport. In bulk semiconductors, the dominant effect is ionized impurity scattering.<sup>46</sup> However, charge transport in nanocrystal films typically takes place via tunneling between NCs and not via band-like transport, with concomitant lower mobilities and much shorter mean free paths. It is unlikely that ionized impurity scattering will be the limiting factor for charge transport in such systems.

Alternatively, intercalating ions could add energy levels close to the conduction band (shallow donor levels) that may take part in electron transport. Interstitial hydrogen shallow donor levels have for instance recently been shown to strongly affect electron transport in nanoporous  $\text{TiO}_2$ .<sup>47</sup> Hydrogen is also known to form an interstitial donor in bulk ZnO with a shallow donor level 58 meV below the conduction band.<sup>48-49</sup> Similarly,

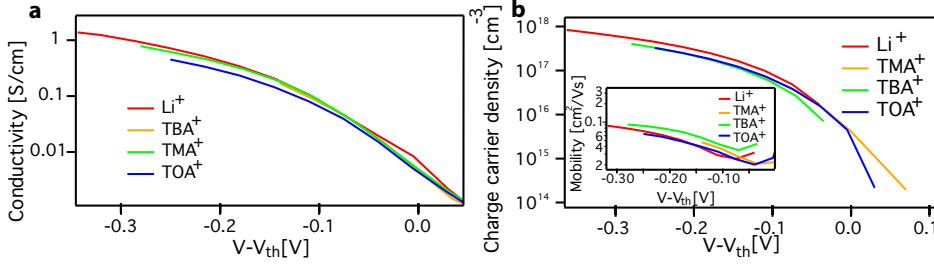


**Figure 2.6 Source-drain measurements for a ZnO QD film for four different cations.** (a) The source-drain conductivity for a ZnO QD film on an IDE immersed in acetonitrile electrolyte solution for four different ions:  $Li^+$ ,  $TMA^+$ ,  $TBA^+$  and  $TOA^+$  concentration of 0.1 M. A threshold potential was subtracted from the original potential. (b) Charge carrier density of the ZnO QD film as a function of potential for  $Li^+$ ,  $TMA^+$ ,  $TBA^+$  and  $TOA^+$  electrolyte solutions (concentration 0.1 M). The panel includes the parallel mobility for the film for the four different ions.

$Li^+$  and  $Na^+$  have been shown to form shallow donors in ZnO.<sup>39</sup> However, the similarity of the electron mobilities shown in Fig. 2.6b shows that intercalated  $Li^+$  and  $Na^+$  donor ions do not significantly affect electron transport in this ZnO QD film.

This can be understood by realizing that in quantum-confined crystals the shallow donor level merges with the 1Se electron level. One can see this quickly by looking at the equation for the exciton Bohr radius  $a_B$

$$a_B = \frac{4\pi\epsilon_r\epsilon_0\hbar^2}{\mu m_e e^2} = \epsilon_r \left( \frac{1}{m_e^*} + \frac{1}{m_h^*} \right) a_0 \quad 2.6$$

where  $\mu$  is the reduced effective mass of the exciton,  $m_e^*$  and  $m_h^*$  are the relative electron and hole effective masses respectively,  $\epsilon_r$  is the relative dielectric constant of the material and  $a_0 = 0.53\text{\AA}$  is the Bohr radius of atomic hydrogen. For an interstitial shallow donor, the Bohr radius is determined by the same equation, except that the hole effective mass is the ion mass and hence falls out of the equation. However, since the hole effective mass in ZnO is much larger than the electron mass ( $m_e^* \sim 0.24$  and  $m_h^* \sim 0.8$ )<sup>50</sup> the shallow donor and exciton Bohr radii are very similar. This implies that if ZnO is quantum confined, the shallow donor state will also be quantum confined. As the 1Se electron level and the shallow donor are delocalized over the nanocrystal it is in fact a single state, as also concluded previously based on DFT calculations,<sup>51</sup> which is simply the solution to the Schrodinger equation of a particle in a box with a positive point charge. The energy of this state is lower than without the presence of the positive point charge, as reflected in the lower onset of electrochemical charging for intercalating  $Li^+$  or  $Na^+$  compared to non-intercalating ions.

Charge transport will in both the case of intercalating and non-intercalating ions take place via electron tunneling between NCs. The moderate variation in energy levels between intercalating and non-intercalating ions apparently does not affect the tunneling rate significantly. For the case of larger crystals that are not quantum confined intercalating

ions add additional energy levels below the conduction band (the shallow donor level) that may strongly affect transport, as reported for electron transport in bulk-like  $\text{TiO}_2$  nanocrystal films.<sup>47</sup>

Finally, it is conceivable that polarization of cations after an electron transfer event leads to a significant reorganization energy that may depend on the nature of the cation. In a Marcus-type electron transport picture this can strongly affect the electron transfer rate and hence also the electron mobility. The fact that this is not observed suggests that there are no significant differences in reorganization energy for the different electrolyte ions, or that the reorganization energy due to these ions is small in all cases.

## 2.3 Conclusions

In summary, we have shown that the electrolyte cations play an important role in electrochemical charging of QD films. Charge injection is limited by cation diffusion, inducing a 7-fold difference between the in plane (steady state) and out of plane (charging) conductivity. The size of the electrolyte cations is shown to dramatically affect the rate of electron injection, by changing the diffusion coefficients of the cations. When the electrolyte concentration is increased, the diffusion coefficient of the electrolyte ions decreases, as a result of jamming of the cations inside the pores of the film. Interestingly, for the smaller cations,  $\text{Li}^+$  and  $\text{Na}^+$ , the electron injection onset occurs at higher potentials in the CV scans. This points to intercalation of the  $\text{Li}^+$  and  $\text{Na}^+$  ions into the ZnO QDs while the steric hindrance of the larger ions hinders the intercalation. Finally, it was shown that electronic conductivity in source-drain measurements is not affected by the type, size or location of the dopant ion. This observation indicates that shallow donor levels from intercalating ions fully hybridize with the quantum confined energy levels and that the reorganization energy due to ions does not strongly affect electron transport in these nanocrystal assemblies. These findings shed light on the role of the electrolyte ions as external dopants, and the effect it has on electron injection into a porous semiconductor film. Additionally, it is clear that the energy of charge injection, and thereby the conduction band edge, can be adjusted by the choice of the electrolyte cation, without affecting charge transport properties of the doped films. This information gives an important insight into the electrochemical doping process, and bring us one step closer in gaining stable electrochemically doped semiconductor films at room temperature.

## 2.4 Methods

**Materials.** Zinc acetate dihydrate ( $\text{Zn}(\text{CH}_3\text{COO})_2 \cdot 2\text{H}_2\text{O}$  reagent grade), potassium hydroxide (KOH pellets), lithium perchlorate ( $\text{LiClO}_4$ , 99.99%), tetramethylammonium hexafluorophosphate ( $(\text{CH}_3)_4\text{N}(\text{PF}_6)$ ,  $\geq 98\%$ ), tetrabutylammonium perchlorate ( $(\text{CH}_3(\text{CH}_2)_3)_4\text{N}(\text{ClO}_4)$ ,  $\geq 99\%$ ) and tetraoctylammonium tetrafluoroborate ( $(\text{CH}_3(\text{CH}_2)_7)_4\text{N}(\text{BF}_4)$ ,  $\geq 97\%$ ), anhydrous methanol, ethanol and toluene were purchased from Sigma Aldrich. Anhydrous acetonitrile was purchased from Alfa Aesar. Acetonitrile was dried before use in an Innovative Technology PureSolv Micro column. All other chemicals were used as received.

**ZnO QD synthesis.** ZnO QDs were synthesized in air by a modification of two known procedures.<sup>52-53</sup> Typically, 3.425 mmol of zinc acetate dihydrate and 50 mL ethanol were added to a flask and heated to 60 °C. In a separate flask, 6.25 mmol KOH and 5 mL methanol were combined and stirred at room

temperature. When both reagents had dissolved, the potassium hydroxide mixture was dropwise added to the stirred zinc acetate dihydrate mixture. The solution was stirred for one additional minute before the heat source was removed. The QDs were purified by adding toluene until the solution became turbid. The flocculates were isolated by centrifugation at 2000 rpm for 1 minute and redissolved in ethanol. The QD dispersion was stored at -20 °C to avoid further growth by Ostwald ripening.

**ZnO QD film preparation.** QD films were drop-cast on two different types of working electrodes and annealed at 60 °C for one hour in air. The typical film thickness was approximately 700 nm. One type of working electrode was indium-doped tin oxide (ITO) on glass while the second one was a home-built interdigitated electrode (IDE). The IDE is a glass substrate coated with four separate gold working electrodes prepared in house via optical lithography. These four working electrodes provide five source-drain gaps of different sensitivities, that is, it is possible to choose between four different gap lengths: 8.825 mm, 6.8 cm, 0.3403 m and 0.8548 m.

**Electrochemical measurements.** All electrochemical measurements were performed according to a procedure performed previously with an Autolab PGSTAT128N potentiostat including an additional dual-mode bipotentiostat BA module in a nitrogen glovebox to ensure oxygen- and water-free conditions.<sup>26, 54</sup> The QD film deposited on the WE is immersed in a container containing 0.1 M LiClO<sub>4</sub> acetonitrile electrolyte solution unless stated otherwise. The container furthermore contained an Ag wire pseudoreference electrode and Pt sheet counter electrode. The Ag wire pseudoreference electrode was calibrated multiple times throughout the course of the experiments with a ferrocene/ferrocenium couple<sup>55</sup> and its potential was found to be constant at -4.79 eV vs. vacuum.

**Spectro-electrochemical measurements.** All spectro-electrochemical measurements were performed with an ITO working electrode. In the measurements, the absorption changes were measured with a fiber based UV-vis spectrometer, Ocean Optics USB2000 using an Ocean Optics DH 2000 lamp as a light source.

**Differential capacitance measurements.** The differential capacitance was measured as described elsewhere.<sup>19</sup> The ZnO QD film deposited on IDE serves as the WE. The same electrochemical cell as described above was used. Potential steps of 35 mV were applied and after each potential step the electrochemical charging current was measured for 5 seconds. The initial peak current decays quickly in about a second to a constant current which is attributed to a background current of the electrolyte. This background current was subtracted to obtain the charging current of the film. To obtain the differential capacitance (in C/V) the charging current was integrated and divided by the potential step. By multiplying the differential capacitance (units of C/V) with the potential (in V) the total injected charge is obtained (units of C).

**Source-drain electronic conductance measurements.** The electronic conductance measurements were performed on ZnO QD films on the IDE with a gold source-drain geometry. The width of the source-drain gap was 25 μm while the gap length was 6.8 cm. These measurements were performed in each potential step in the differential capacitance measurements after equilibrium was reached. When equilibrium was reached, the potential of WE1 was scanned in a CV manner around the fixed potential of WE2. The change in potential for WE1 was ± 10 mV compared to the potential of WE2. The slope of the current versus the potential gives the in-plane (or parallel) conductance,  $G_{||}$ , of the film. From the conductance, it is possible to calculate the in-plane source-drain electron conductivity,

$\sigma_{||}$ :

$$\sigma_{||} = (G_{||} \times w) / (l \times h) \quad 2.7$$

where  $w$  is the source-drain gap width,  $l$  is the gap length and  $h$  is the height of the film. The in-plane mobility,  $\mu_{||}$ , can then be calculated with equation 2.8:

$$\mu_{||} = \sigma_{||} / (n \times e) \quad 2.8$$

where  $n$  is the charge carrier density and  $e$  is the elemental charge.

## References

1. Bailey, R. E.; Nie, S., Alloyed semiconductor quantum dots: Tuning the optical properties without changing the particle size. *J. Am. Chem. Soc.* 2003, 125 (23), 7100-7106.
2. Wang, X.; Zhuang, J.; Peng, Q.; Li, Y., A general strategy for nanocrystal synthesis. *Nature* 2005, 437 (7055), 121-4.
3. Talapin, D. V.; Lee, J.-S.; Kovalenko, M. V.; Shevchenko, E. V., Prospects of colloidal nanocrystals for electronic and optoelectronic applications. *Chem. Rev.* 2009, 110 (1), 389-458.
4. Zhang, F.; Zhong, H.; Chen, C.; Wu, X.-g.; Hu, X.; Huang, H.; Han, J.; Zou, B.; Dong†, Y., Brightly Luminescent and Color-Tunable Colloidal CH<sub>3</sub>NH<sub>3</sub>PbX<sub>3</sub> (X = Br, I, Cl) Quantum Dots: Potential Alternatives for Display Technology. *ACS Nano* 2015, 9 (4), 4533-4542.
5. Maksym V. Kovalenko; Manna, L.; Cabot, A.; Hens, Z.; Talapin, D. V.; Kagan, C. R.; Klimov, V. I.; Rogach, A. L.; Reiss, P.; Milliron, D. J.; Guyot-Sionnest, P.; Konstantatos, G.; Parak, W. J.; Hyeon, T.; Korgel, B. A.; Murray, C. B.; Heiss, W., Prospects of nanoscience with nanocrystals. *ACS Nano* 2015, 9 (2), 1012-1057.
6. Bourzac, K., Quantum dots go on display: adoption by TV makers could expand the market for light-emitting nanocrystals. *Nature News* 2013, 493 (7432).
7. Carey, G. H.; Abdelhady, A. L.; Ning, Z.; Thon, S. M.; Bakr, O. M.; Sargent, E. H., Colloidal Quantum Dot Solar Cells. *Chem. Rev.* 2015, 115 (23), 12732-63.
8. Lan, X.; Voznyy, O.; Garcia de Arquer, F. P.; Liu, M.; Xu, J.; Proppe, A. H.; Walters, G.; Fan, F.; Tan, H.; Liu, M.; Yang, Z.; Hoogland, S.; Sargent, E. H., 10.6% Certified Colloidal Quantum Dot Solar Cells via Solvent-Polarity-Engineered Halide Passivation. *Nano Lett.* 2016, 16 (7), 4630-4.
9. Sun, Q.; Wang, Y. A.; Li, L. S.; Wang, D.; Zhu, T.; Xu, J.; Yang, C.; Li, Y., Bright, multicoloured light-emitting diodes based on quantum dots. *Nat. Photonics* 2007, 1 (12), 717-722.
10. Shirasaki, Y.; Supran, G. J.; Bawendi, M. G.; Bulović, V., Emergence of colloidal quantum-dot light-emitting technologies. *Nat. Photonics* 2012, 7 (1), 13-23.
11. Shim, M.; Wang, C.; Norris, D. J.; Guyot-Sionnest, P., Doping and Charging in Colloidal Semiconductor Nanocrystals. *MRS Bull.* 2001, 26 (12), 1005-1008.
12. Mocatta, D.; Cohen, G.; Schattner, J.; Millo, O.; Rabani, E.; Banin, U., Heavily Doped Semiconductor Nanocrystal Quantum Dots. *Science* 2011, 332, 77-81.

13. Schimpf, A. M.; Knowles, K. E.; Carroll, G. M.; Gamelin, D. R., Electronic doping and redox-potential tuning in colloidal semiconductor nanocrystals. *Acc. Chem. Res.* 2015, 48 (7), 1929-37.
14. Sahu, A.; Kang, M. S.; Kompch, A.; Notthoff, C.; Wills, A. W.; Deng, D.; Winterer, M.; Frisbie, C. D.; Norris, D. J., Electronic impurity doping in CdSe nanocrystals. *Nano Lett.* 2012, 12 (5), 2587-94.
15. Shim, M.; Guyot-Sionnest, P., n-type colloidal semiconductor nanocrystals. *Letters to nature* 2000, 407, 981-983.
16. Koh, W. K.; Koposov, A. Y.; Stewart, J. T.; Pal, B. N.; Robel, I.; Pietryga, J. M.; Klimov, V. I., Heavily doped n-type PbSe and PbS nanocrystals using ground-state charge transfer from cobaltocene. *Sci. Rep.* 2013, 3, 2004.
17. Schimpf, A. M.; Gunthardt, C. E.; Rinehart, J. D.; Mayer, J. M.; Gamelin, D. R., Controlling carrier densities in photochemically reduced colloidal ZnO nanocrystals: size dependence and role of the hole quencher. *J. Am. Chem. Soc.* 2013, 135 (44), 16569-77.
18. Rinehart, J. D.; Schimpf, A. M.; Weaver, A. L.; Cohn, A. W.; Gamelin, D. R., Photochemical electronic doping of colloidal CdSe nanocrystals. *J. Am. Chem. Soc.* 2013, 135 (50), 18782-5.
19. Vanmaekelbergh, D.; Houtepen, A. J.; Kelly, J. J., Electrochemical gating: A method to tune and monitor the (opto)electronic properties of functional materials. *Electrochim. Acta* 2007, 53 (3), 1140-1149.
20. Guyot-Sionnest, P., Charging colloidal quantum dots by electrochemistry. *Microchim. Acta* 2008, 160 (3), 309-314.
21. Boehme, S. C.; Wang, H.; Siebbeles, L. D. A.; Vanmaekelbergh, D.; Houtepen, A. J., Electrochemical charging of CdSe quantum dot films: Dependence on voids size and counterion proximity. *ACS Nano* 2013, 7 (3), 2500-2508.
22. Boehme, S. C.; Azpiroz, J. M.; Aulin, Y. V.; Grozema, F. C.; Vanmaekelbergh, D.; Siebbeles, L. D.; Infante, I.; Houtepen, A. J., Density of Trap States and Auger-mediated Electron Trapping in CdTe Quantum-Dot Solids. *Nano Lett.* 2015, 15 (5), 3056-66.
23. Amelia, M.; Lincheneau, C.; Silvi, S.; Credi, A., Electrochemical properties of CdSe and CdTe quantum dots. *Chem. Soc. Rev.* 2012, 41 (17), 5728-43.
24. Gooding, A. K.; Gómez, D. E.; Mulvaney, P., The Effects of Electron and Hole Injection on the Photoluminescence of CdSe:CdS:ZnS Nanocrystal Monolayers. *ACS Nano* 2008, 2 (4), 669-676.
25. Alimoradi Jazi, M.; Janssen, V.; Evers, W. H.; Tadjine, A.; Delerue, C.; Siebbeles, L. D. A.; van der Zant, H. S. J.; Houtepen, A. J.; Vanmaekelbergh, D., Transport Properties of a Two-Dimensional PbSe Square Superstructure in an Electrolyte-Gated Transistor. *Nano Lett.* 2017, 17 (9), 5238-5243.
26. van der Stam, W.; Gudjonsdottir, S.; Evers, W. H.; Houtepen, A. J., Switching between Plasmonic and Fluorescent Copper Sulfide Nanocrystals. *J. Am. Chem. Soc.* 2017, 139 (37), 13208-13217.
27. Hoyer, P.; Eichberger, R.; Weller, H., Spectroelectrochemical Investigations of Nanocrystalline ZnO Films. *Ber. Bunsenges. Phys. Chem* 1993, 97, 630-635.
28. Boehme, S. C.; Vanmaekelbergh, D.; Evers, W. H.; Siebbeles, L. D. A.; Houtepen, A. J., In Situ Spectroelectrochemical Determination of Energy Levels and Energy

- Level Offsets in Quantum -Dot Heterojunctions. *J. Phys. Chem. C* 2016, 120 (9), 5164-5173.
29. Meulenkamp, E. A., Synthesis and Growth of ZnO Nanoparticles. *J. Phys. Chem. B* 1998, 102 (29), 5566–5572.
  30. Roest, A. L.; Kelly, J. J.; Vanmaekelbergh, D.; Meulenkamp, E. A., Staircase in the electron mobility of a ZnO quantum dot assembly due to shell filling. *Phys. Rev. Lett.* 2002, 89 (3), 036801.
  31. Bard, A. J.; Faulkner, L. R., *Electrochemical methods. Fundamentals and applications*. 2nd ed.; John Wiley & sons, INC.: New York, United states of America, 2001.
  32. Chandler, R. E.; Houtepen, A. J.; Nelson, J.; Vanmaekelbergh, D., Electron transport in quantum dot solids: Monte Carlo simulations of the effects of shell filling, Coulomb repulsions, and site disorder. *Phys. Rev. B* 2007, 75 (8).
  33. van de Lagemaat, J., Einstein relation for electron diffusion on arrays of weakly coupled quantum dots. *Phys. Rev. B* 2005, 72 (23).
  34. Page, C. L.; Short, N. R.; Tarras, A. E., Diffusion of chloride ions in hardened cement pastes. *Cem. Concr. Res.* 1981, 11 (3), 395-406.
  35. Laoire, C. O.; Mukerjee, S.; Abraham, K. M., Elucidating the Mechanism of Oxygen Reduction for Lithium-Air Battery Applications. *J. Phys. Chem. B* 2009, 113 (46), 20127–20134.
  36. Shen, J.; Wang, H.; Zhou, Y.; Ye, N.; Li, G.; Wang, L., Anatase/rutile TiO<sub>2</sub> nanocomposite microspheres with hierarchically porous structures for high-performance lithium-ion batteries. *The Royal Society of Chemistry* 2012, 2, 9173-9178.
  37. Brozek, C. K.; Hartstein, K. H.; Gamelin, D. R., Potentiometric Titrations for Measuring the Capacitance of Colloidal Photodoped ZnO Nanocrystals. *J. Am. Chem. Soc.* 2016, 138 (33), 10605-10.
  38. Özgür, Ü.; Alivov, Y. I.; Liu, C.; Teke, A.; Reshchikov, M. A.; Doğan, S.; Avrutin, V.; Cho, S. J.; Morkoç, H., A comprehensive review of ZnO materials and devices. *J. Appl. Phys.* 2005, 98 (4), 041301.
  39. Orlinskii, S. B.; Schmidt, J.; Baranov, P. G.; Hofmann, D. M.; de Mello Donega, C.; Meijerink, A., Probing the wave function of shallow Li and Na donors in ZnO nanoparticles. *Phys. Rev. Lett.* 2004, 92 (4), 047603.
  40. Joshi, A. G.; Sahai, S.; Gandhi, N.; Krishna, Y. G. R.; Haranath, D., Valence band and core-level analysis of highly luminescent ZnO nanocrystals for designing ultrafast optical sensors. *Appl. Phys. Lett.* 2010, 96 (12), 123102.
  41. Saáedi, A.; Yousefi, R.; Jamali-Sheini, F.; Zak, A. K.; Cheraghizade, M.; Mahmoudian, M. R.; Baghchesara, M. A.; Dezaki, A. S., XPS studies and photocurrent applications of alkali-metals-doped ZnO nanoparticles under visible illumination conditions. *Physica E: Low-dimensional Systems and Nanostructures* 2016, 79, 113-118.
  42. Zhang, J.; Gu, P.; Xu, J.; Xue, H.; Pang, H., High performance of electrochemical lithium storage batteries: ZnO-based nanomaterials for lithium-ion and lithium-sulfur batteries. *Nanoscale* 2016, 8 (44), 18578-18595.
  43. Kushima, A.; Liu, X. H.; Zhu, G.; Wang, Z. L.; Huang, J. Y.; Li, J., Leapfrog Cracking and Nanoamorphization of ZnO Nanowires during In Situ Electrochemical

- Lithiation. *Nano Lett.* 2011, 11 (11), 4535-4541.
44. Lyon, L. A.; Hupp, J. T., Energetics of Semiconductor Electrode/Solution Interfaces-EQCM Evidence for Charge-Compensating Cation Adsorption and Intercalation during Accumulation Layer Formation in the Titanium Dioxide/Acetonitrile System. *J. Phys. Chem.* 1995, (99), 15718-15720.
  45. Puntambekar, A.; Wang, Q.; Miller, L.; Smieszek, N.; Chakrapani, V., Electrochemical Charging of CdSe Quantum Dots: Effects of Adsorption versus Intercalation. *ACS Nano* 2016, 10 (12), 10988-10999.
  46. Neamen, D. A., *Semiconductor physics and devices: Basic principles*. 4th ed.; McGraw-Hill Education: New York, United States, 2012.
  47. Halverson, A. F.; Zhu, K.; Erslev, P. T.; Kim, J. Y.; Neale, N. R.; Frank, A. J., Perturbation of the electron transport mechanism by proton intercalation in nanoporous TiO<sub>2</sub> films. *Nano Lett.* 2012, 12 (4), 2112-6.
  48. Cox, S. F.; Davis, E. A.; Cottrell, S. P.; King, P. J.; Lord, J. S.; Gil, J. M.; Alberto, H. V.; Vilao, R. C.; Piroto Duarte, J.; Ayres de Campos, N.; Weidinger, A.; Lichti, R. L.; Irvine, S. J., Experimental confirmation of the predicted shallow donor hydrogen state in zinc oxide. *Phys. Rev. Lett.* 2001, 86 (12), 2601-4.
  49. Gil, J. M.; Alberto, H. V.; Vilão, R. C.; Piroto Duarte, J.; Ayres de Campos, N.; Weidinger, A.; Krauser, J.; Davis, E. A.; Cottrell, S. P.; Cox, S. F. J., Shallow donor muonium states in II-VI semiconductor compounds. *Phys. Rev. B* 2001, 64 (7).
  50. Enright, B.; Fitzmaurice, D., Spectroscopic Determination of Electron and Hole Effective Masses in a Nanocrystalline Semiconductor Film. *J. Phys. Chem.* 1995, 100, 1027-1035.
  51. Goings, J. J.; Schimpf, A. M.; May, J. W.; Johns, R. W.; Gamelin, D. R.; Li, X., Theoretical Characterization of Conduction-Band Electrons in Photodoped and Aluminum-Doped Zinc Oxide (AZO) Quantum Dots. *J. Phys. Chem. C* 2014, 118 (46), 26584-26590.
  52. Wood, A.; Giersig, M.; Hilgendorff, M.; Vilas-Campos, A.; Liz-Marzan, L. M.; Mulvaney, P., Size effect in ZnO. The cluster to quantum dot transition. *Aust. J. Chem.* 2003, 56, 1051-1057.
  53. Mashford, B. S.; Stevenson, M.; Popovic, Z.; Hamilton, C.; Zhou, Z.; Breen, C.; Steckel, J.; Bulovic, V.; Bawendi, M.; Coe-Sullivan, S.; Kazlas, P. T., High-efficiency quantum-dot light-emitting devices with enhanced charge injection. *Nat. Photonics* 2013, 7 (5), 407-412.
  54. Boehme, S. C.; Vanmaekelbergh, D.; Evers, W. H.; Siebbeles, L. D. A.; Houtepen, A. J., In Situ Spectroelectrochemical Determination of Energy Levels and Energy Level Offsets in Quantum-Dot Heterojunctions. *J. Phys. Chem. C* 2016, 120 (9), 5164-5173.
  55. Ruch, P. W.; Cericola, D.; Hahn, M.; Kötz, R.; Wokaun, A., On the use of activated carbon as a quasi-reference electrode in non-aqueous electrolyte solutions. *J. Electroanal. Chem.* 2009, 636 (1-2), 128-131.

## Appendix

2

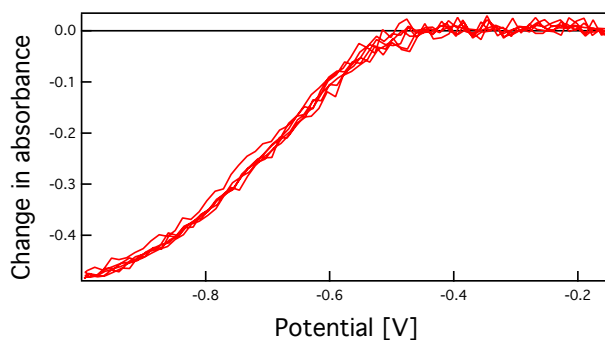


**Figure A2.1** Change in absorbance during a CV scan for a ZnO QD film immersed in 0.1 M LiClO<sub>4</sub> acetonitrile electrolyte solution. This is at the 1s peak of the ZnO QD film. The scan is in negative direction and repeated three times.

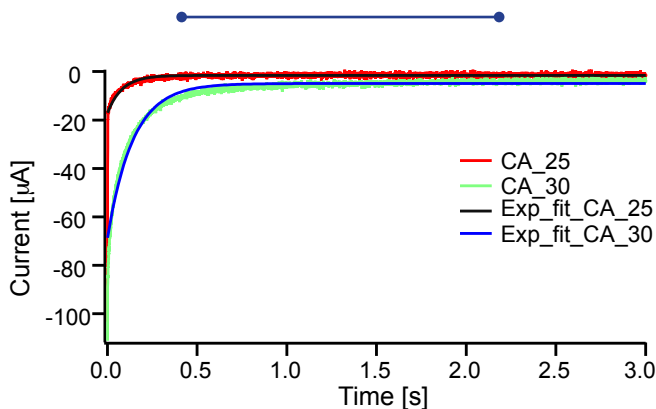


**Figure A2.2** Exponential fit for charging currents. An exponential fit suits the curves well after initial drop of the current.

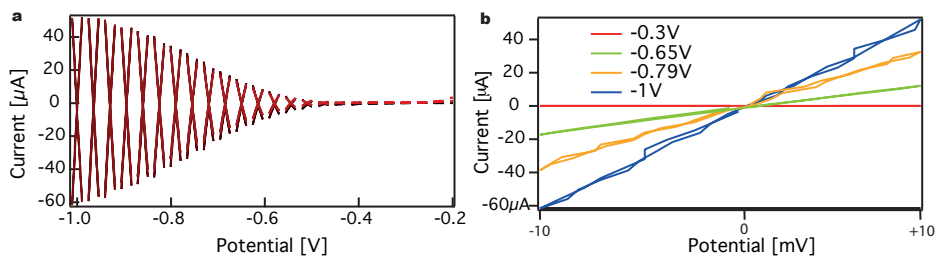


**Figure A2.3** Source-drain electron conductivity measurements. (a) The CVs from both WE1 and WE2. WE1 is scanned  $\pm 10$  mV around the potential of WE2 and a potential step of 35 mV is taken between each measurement. (b) The source-drain output for WE2 for picked potentials. The slope gives the conductance.

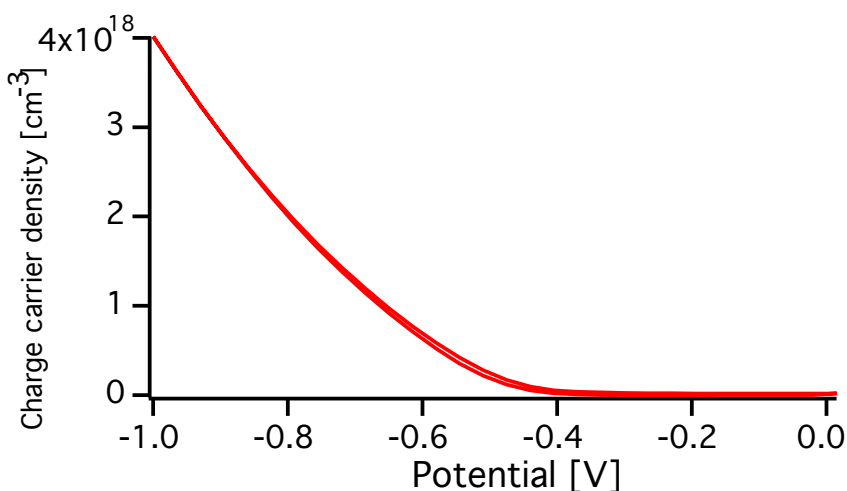


**Figure A2.4** Charge carrier density calculated from the differential capacitance measurements.

#### Randles-Sevcik equation for porous QD films

We use the Randles-Sevcik equation to calculate the diffusion coefficient for different electrolyte cations. This can be rationalized by considering that the concentration profile for diffusion of excess  $\text{Li}^+$  is similar to a concentration profile of diffusion of reactant from a bulk solution (Fig. A2.5). When the QD film is immersed in the electrolyte solution, some ions diffuse into the voids of the film. However, the concentration of ions in the film is not necessarily the same as in the bulk,  $C^*$ , as it may be more difficult for the ions to diffuse into the voids than out of them. Therefore, the concentrations are related via the partition coefficient,  $\gamma$  (Fig. A2.5).<sup>31</sup> The potential of the working electrode can be changed compared to a reference electrode, and if a negative enough potential is applied, electrons can flow into the QD film. To compensate for the charge, cations flow into the voids of the film. As more electrons are injected, more cations are required to compensate the injected charge and the concentration of excess cations (cations that do not participate to neutralize the film) decreases in the film. This process will start at the electrode surface resulting in a concentration profile such as is shown in Figure A2.5. The diffusion current,  $i$ , can be related to the diffusion coefficient,  $D$ , and the ion concentration,  $c$ , by equation A2.1:

$$i = eD \left( \frac{dc}{dx} \right) \quad \text{A2.1}$$

where  $x$  is the distance from the working electrode. The concentration gradient, and hence the diffusion current, will decrease with time. The solution to this problem for ions in solution in contact with a flat electrode is the Randles-Sevcik equation. The solution ion diffusion in a porous film can be expected to be similar.

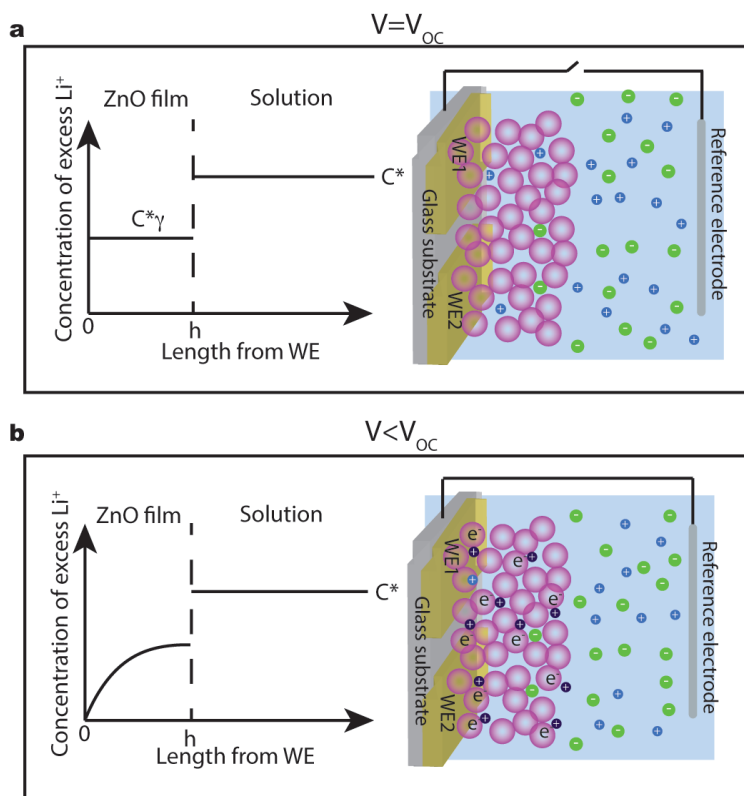


**Figure A2.5** Schematic of the QD film after immersion in the electrolyte. (a) The concentration of  $\text{Li}^+$  is the same throughout the QD film.  $h$  stands for the film height,  $C^*$  for the bulk concentration and  $\gamma$  is the partition coefficient. (b) The concentration of excess  $\text{Li}^+$  decreases in the film as  $\text{Li}^+$  neutralizes injected charge and new  $\text{Li}^+$  need to diffuse from the bulk solution.

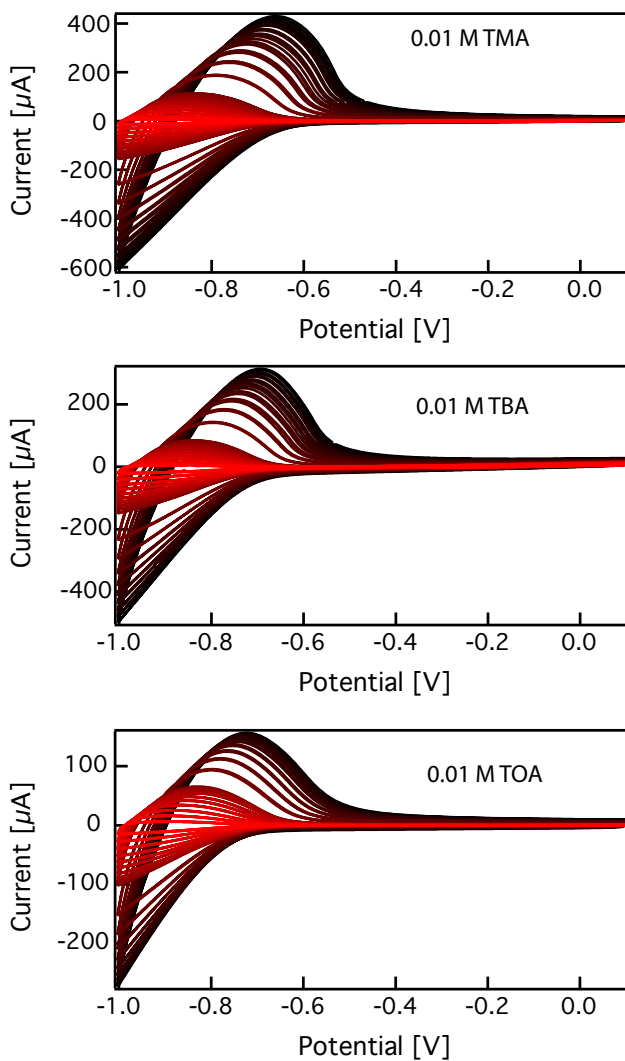


**Figure A2.6** A magnification of the CVs in Figure 5 in the manuscript. CVs taken at different scan rates for 0.01 M TMA<sup>+</sup>, TBA<sup>+</sup> or TOA<sup>+</sup> in acetonitrile electrolyte solution. The scans have negative direction and are repeated three times for every scan rate.

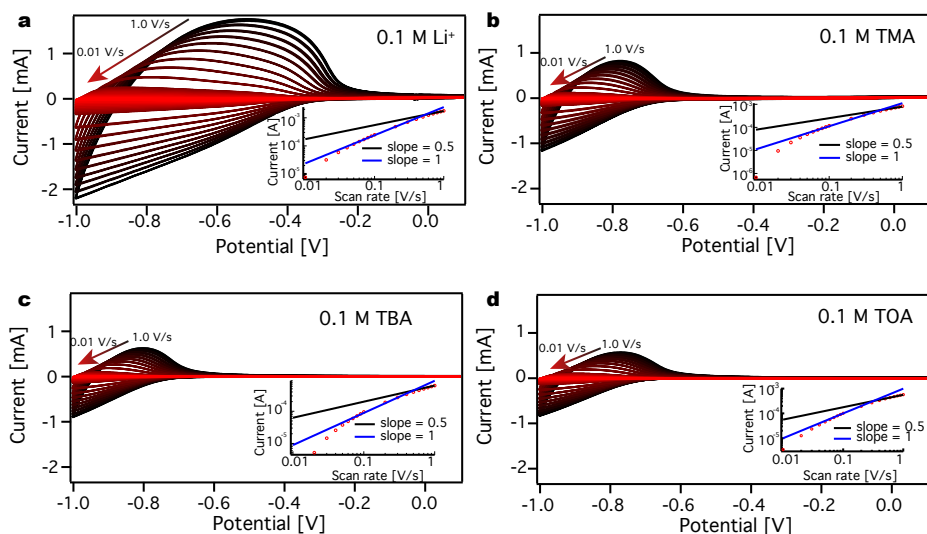


**Figure A2.7** CVs for ZnO QD films immersed in (a) 0.1 M  $\text{LiClO}_4$  in acetonitrile electrolyte solution, (b) 0.1 M tetramethylammonium hexafluorophosphate ( $\text{CH}_3)_4\text{N}(\text{PF}_6)$  in acetonitrile electrolyte solution, (c) 0.1 M tetrabutylammonium perchlorate ( $\text{CH}_3(\text{CH}_2)_3\text{N}(\text{ClO}_4)$ ) in acetonitrile electrolyte solution and (d) 0.1 M tetraoctylammonium tetrafluoroborate ( $\text{CH}_3(\text{CH}_2)_7\text{N}(\text{BF}_4)$ ) in acetonitrile electrolyte solution. The scan rates are between 0.01 V/s to 1.0 V/s, the scan starts in negative direction and is repeated three times for each scan rate. Each panel includes a log-log plot of the peak current versus scan rate.

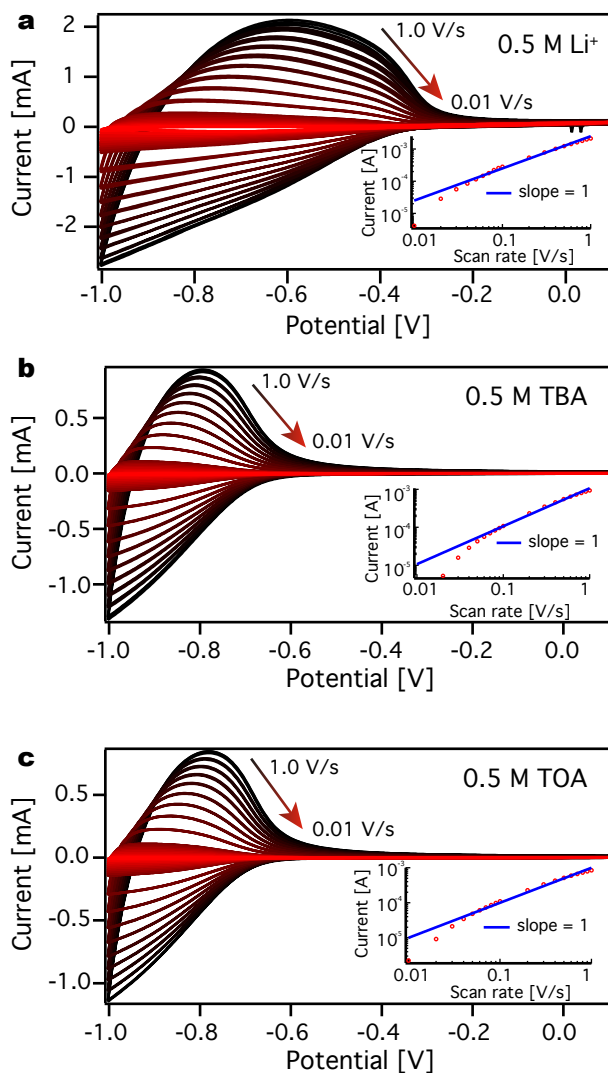


**Figure A2.8** CVs for ZnO QD films immersed in (a) 0.5 M  $\text{LiClO}_4$  in acetonitrile electrolyte solution, (b) 0.5 M tetrabutylammonium perchlorate ( $\text{CH}_3(\text{CH}_2)_3\text{N}(\text{PF}_6)_4$ ) in acetonitrile electrolyte solution and (c) 0.5 M tetraoctylammonium tetrafluoroborate ( $\text{CH}_3(\text{CH}_2)_7\text{N}(\text{BF}_4)_4$ ) in acetonitrile electrolyte solution. The scan rates are between 0.01 V/s to 1.0 V/s, the scan starts in negative direction and is repeated three times for each scan rate. Each panel includes a log-log plot of the peak current versus scan rate.

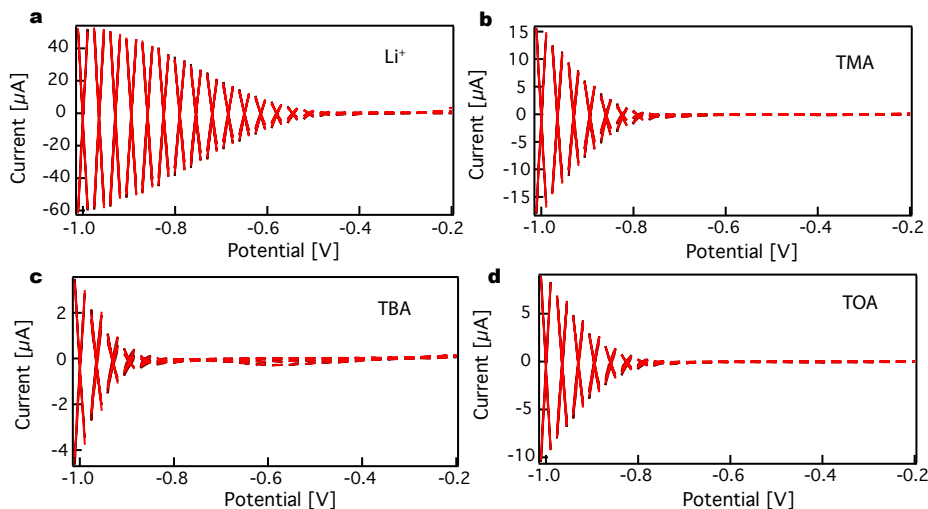


**Figure A2.9** Source-drain electron conduction measurements in (a) 0.1 M LiClO<sub>4</sub> in acetonitrile electrolyte solution, (b) 0.1 M tetramethylammonium hexafluorophosphate (CH<sub>3</sub>)<sub>4</sub>N(PF<sub>6</sub>) in acetonitrile electrolyte solution, (c) 0.1 M tetrabutylammonium perchlorate (CH<sub>3</sub>(CH<sub>2</sub>)<sub>3</sub>)<sub>4</sub>N(ClO<sub>4</sub>) in acetonitrile electrolyte solution and (d) 0.1 M tetraoctylammonium tetrafluoroborate (CH<sub>3</sub>(CH<sub>2</sub>)<sub>7</sub>)<sub>4</sub>N(BF<sub>4</sub>) in acetonitrile electrolyte solution. The CVs are both from WE1 and WE2. WE1 is scanned  $\pm 10$  mV around the potential of WE2 and a potential step of 35 mV is taken between each measurement.

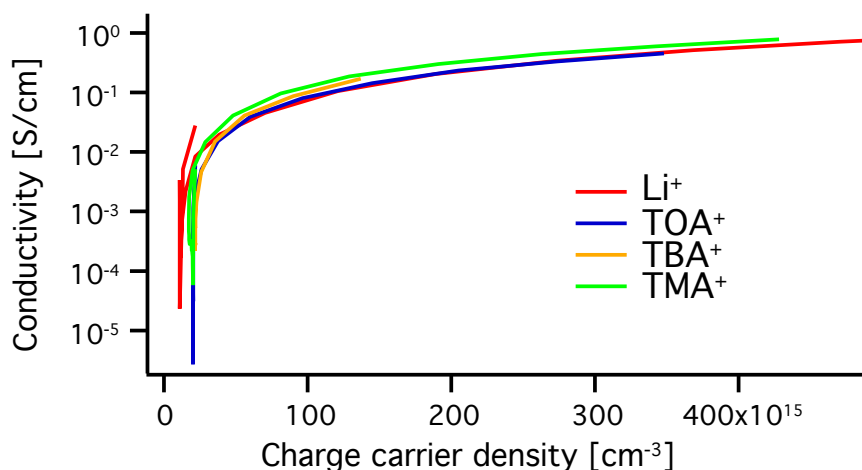


**Figure A2.10** Calculated conductivity vs. the charge carrier density for 0.1 M acetonitrile electrolyte solution. The used electrolytes are lithium perchlorate, tetramethylammonium hexafluorophosphate, tetrabutylammonium perchlorate and tetraoctylammonium tetrafluoroborate.

### Determination of the threshold potential

In order to determine the threshold potential, the potential of the conductivity for each cation was shifted compared to the potential of the conductivity of  $\text{Li}^+$ . That is, the threshold potential was determined by finding the minimum of the following equation:

$$\sigma_{\text{Li}^+} - \sigma_{\text{Cat}^+} (V - V_{\text{th}}) \quad \text{A2.2}$$

Where  $\sigma_{\text{Li}^+}$  is the conductivity when  $\text{Li}^+$  is the electrolyte cation,  $\sigma_{\text{Cat}^+}$  is the conductivity when other ions than  $\text{Li}^+$  are used,  $V$  is the potential and  $V_{\text{th}}$  is the threshold potential.





# 3



## On the stability of permanent electrochemical doping of quantum dot, fullerene and conductive polymer films in frozen electrolytes

---

Chapter 2 gave us information about the effect the electrolyte ions have on charge injection into semiconductor films. In this Chapter, various electrolyte solvents are investigated to see if stable electrochemically doped film can be gained at room temperature. In our measurements we use a wide variety of semiconductor materials, namely inorganic semiconductors (ZnO NCs, CdSe NCs, CdSe/CdS core/shell NCs) and organic semiconductors (P3DT, PCBM and  $C_{60}$ ). We show that by charging the semiconductors at elevated temperatures in solvents with melting points above room temperature, the charge stability at room temperature increases greatly, from seconds to days. At reduced temperature ( $-75\text{ }^{\circ}\text{C}$  when using succinonitrile as electrolyte solvent) the injected charge becomes entirely stable on the time scale of our experiments (up to several days). Other high melting point solvents such as dimethyl sulfone, ethylene carbonate and polyethylene glycol (PEG) also offer increased charge stability at room temperature. Especially the use of PEG increases the room temperature charge stability by several orders of magnitude compared when using acetonitrile. We discuss how this improvement of the charge stability is related to the immobilization of electrolyte ions and impurities. While the electrolyte ions are immobilized, conductivity measurements show that electrons in the semiconductor films remain mobile. These results highlight the potential of using solidified electrolytes to stabilize injected charges, which is a promising step toward making semiconductor devices based on electrochemically doped semiconductor thin films.

This chapter is based on: S. Gudjonsdottir, W. van der Stam, C. Koopman, B. Kwakkenbos, W. H. Evers, A. J. Houtepen. ACS Applied Nano Materials 2019.

### 3.1 Introduction

Over the last decades, several new promising semiconductor materials have emerged, including quantum dots (QDs), conductive polymers, fullerenes and other small organic semiconductors. These materials are known for their cheap synthesis and tunable optical properties.<sup>1-7</sup> A general feature of the greatest importance for semiconductor devices is to control the charge carrier density. The abovementioned materials have in common that the charge carrier density is not easily tuned via methods of impurity doping that have been developed for bulk inorganic semiconductors such as silicon.<sup>8-10</sup> However, as we show below, these semiconductor materials can all be doped efficiently using electrochemistry.

For electrochemical doping, a semiconductor film is deposited on a conductive electrode that forms the working electrode in an electrochemical cell, and charge is injected into the material from a counter electrode. To neutralize the injected charge, electrolyte cations of the opposite charge diffuse into the film and act as external dopants (Figure 3.1).<sup>11</sup> Because of the efficient nanoscale charge compensation it is possible to reach extremely high doping densities of up to  $10^{21} \text{ cm}^{-3}$ .<sup>12</sup> Further, since the electrolyte ions are external dopants that are typically not incorporated into the semiconductor materials itself, they do not lead to a disruption of the crystal lattice or molecular structure. Additionally, as the ions are stable in the ionized form (e.g.  $\text{Li}^+$  would only reduce to Li at very negative electrochemical potentials) there is no problem with the activation of dopants, as is the case e.g. for common p-type impurity doping in II-VI semiconductors.<sup>13</sup> The same point implies that electrochemical doping does not introduce states in the bandgap that could act as recombination centers for electrons and holes, as is the case for substitutional impurity doping. Finally, the amount of the injected charge and thus the placement of the Fermi level is easily controlled with the touch of a button on the potentiostat.<sup>12, 14-15</sup>

Electrochemical measurements have been used to investigate many different QDs and organic semiconductors.<sup>12, 16-20</sup> Such electrochemically doped films could also be ideal for use in devices. A particularly interesting example of such a device that employs electrochemical doping is the light-emitting electrochemical cell (LEC). LECs are made by an electroluminescent semiconductor, most often a conjugated polymer, sandwiched between a cathode and an anode. The semiconductor layer also includes an ionic transport medium and electrolyte ions, and by applying voltages higher than the band gap energy of the semiconductor a p-n junction diode can be created.<sup>21-22 23-24</sup> However, when the voltage source is disconnected, it is invariably observed that the injected charge disappears, both in the case of charged QD films<sup>14, 25</sup> and in polymer LECs.<sup>25</sup> As will be discussed in detail below, the loss of charge density can be due to electrochemical reactions with impurities or intrinsic electrochemical reactions with the material itself. Moreover, when used in junctions, potential differences can lead to diffusion of the dopant ions, resulting in a change of the charge density.

Several approaches have been used to increase the room temperature doping stability in LECs. One way is to reduce ion transport in the electrolyte solvent. Tang et al. polymerized the electrolyte with the counter ions<sup>26</sup> and Wantz et al. used polymer electrolytes with high glass transition temperatures.<sup>27</sup> Another way is to chemically fix the electrolyte counterions. To do so, Hoven et al. used a cationic conjugated polyelectrolyte containing

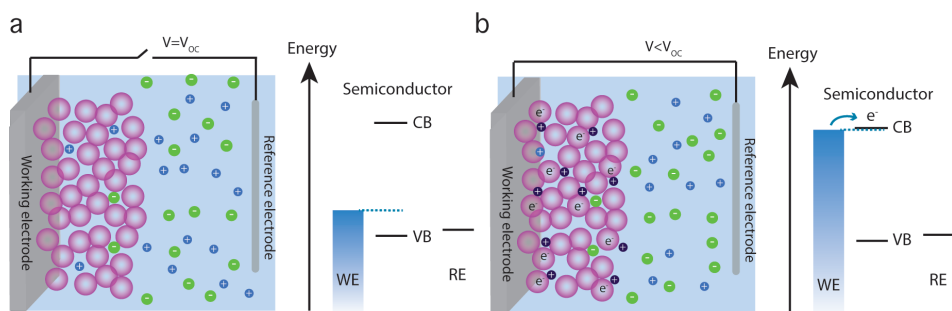


**Figure 3.1 Schematic of electrochemical charge injection into a semiconductor film.** (a) When no potential is applied to the WE, the Fermi level is inside the band gap of the semiconductor. (b) When a negative potential is applied to the WE compared to the RE, the Fermi level moves to the conduction band of the semiconductor which leads to electron injection. To neutralize the charge, electrolyte cations diffuse into the pores of the film.

fluoride counter anions, with an underlayer of a neutral conjugated polymer that had anion trapping functional groups.<sup>28</sup>

Despite intense studies, complete doping stability has not been achieved at room temperature. Gao et al. made a stable LEC at 100 K, which freezes the electrolyte solvent.<sup>22</sup> At this temperature, the electrolyte solvent is frozen and both external dopants and impurities are immobilized. In addition, electrochemical side reactions of the semiconductor material itself are slowed down. Similarly, Guyot-Sionnest et al. and Houtepen et al. showed that the charge density in different quantum dots (CdSe, PbSe and ZnO nanocrystals) and organic polymers (poly(p-phenylene vinylene, PPV) is stable for days at cryogenic temperatures in various electrolyte solvents.<sup>29–32</sup>

In this chapter we investigate the possibility of stabilizing electrochemically doped semiconductor films at room temperature using a large variety of electrolyte solvents with melting points above room temperature (RT). The charge is injected into the system when the solvent is liquid. The system is then cooled down to room temperature causing the solvent to freeze. This could enable the use of electrochemically doped semiconductor devices at room temperature.

In this work we show electrochemical doping for three different QD materials (ZnO, CdSe and CdSe/CdS QDs), two fullerenes ( $C_{60}$  and PCBM) and two conductive polymers (P3DT and P3HT). We investigate how stable the doping is by measuring the electrochemical potential over time for different electrolyte solvents at different temperatures. When using acetonitrile as the electrolyte solvent, for CdSe, CdSe/CdS QDs and PCBM it takes less than 30 s for the electrochemically injected electrons to spontaneously leave the conduction band, even under stringent anaerobic conditions. By using a ZnO QD film in a succinonitrile supporting electrolyte, which has a melting point of 57 °C, charge stability at RT is improved by two orders of magnitude. By decreasing the temperature to -75 °C, the injected electrons become entirely stable on the time scale of our experiments (hours

to days), and cannot be removed even by applying positive potentials, showing that the cations that compensate the electrons have become immobilized.

In a search for a similar improved charge stability at RT, we have investigated a range of different electrolyte solvents with melting points above room temperature. All solvents showed improved RT charge stability compared to acetonitrile; the best results were obtained for polyethylene glycol (PEG) with molecular weight  $\geq 4000$ . In that electrolyte solvent injected charges remained in the conduction or valence band for over an hour at RT for all materials. Optimized measurements on ZnO NCs show that even after several days the Fermi-level remained in the conduction band.

## 3

## 3.2 Results and Discussion

### 3.2.1 Electrochemical charging of various semiconductor films

Figure 3.2 shows spectro-electrochemical measurements on ZnO QDs, CdSe QDs, P3DT and PCBM performed inside a glovebox, where electrochemical charge injection takes place. Spectro-electrochemical measurements for CdSe/CdS core/shell QDs, P3HT and  $C_{60}$  are shown in Appendix, Figures A3.1 and A3.2. For comparison a CV of a blank ITO is shown in Appendix, Figure A3.3. For all films it is observed that, as the potential is changed into the conduction band (QDs and fullerenes) or valence band (conducting polymers), the current increases, the band edge absorbance decreases and the conductivity increases drastically (measured in the case of ZnO and P3DT).<sup>29, 33</sup> In the SI we also show for ZnO QD films that this is accompanied with an increase of absorption in the IR due to intraband absorption of the injected charges (Appendix, Fig A3.4). All these effects are a clear demonstration of charge injection into the conduction or valence band of the semiconductors.

From Figure 3.2 it is clear that the CVs of P3DT and ZnO are almost symmetric.<sup>34</sup> Charge injection for CdSe and PCBM is not as reversible; when the scan is reversed only a small positive current can be seen in the CVs. This means that the injected electrons are not extracted.<sup>14</sup> This is a first sign of the instability of injected charges.

Similar electrochemical measurements have been used in literature as a means to study the optical and electrical properties of semiconductor thin films.<sup>14, 35-39</sup> However, here we want to investigate whether electrochemical doping can also be used to prepare doped films that can be used in semiconductor devices. Hence, we investigate next how long the injected charge remains if the potentiostat is disconnected.

### 3.2.2 Electrochemical doping stability

To determine the stability of electrochemically injected charge the counter electrode is disconnected and the potential of the working electrode (with respect to the reference electrode) is recorded over time (see Methods section). Similar measurements have been performed before by Pei et al. for LECs.<sup>25</sup> We call this experiment a Fermi-level stability measurement. If the injected electrons or holes leave the system, the potential will change from the initially applied potential value (just before disconnecting the CE) back to the original  $V_{oc}$ . By simultaneously recording the absorption bleach we verified that we are indeed measuring the potential of the working electrode correctly with such a Fermi-level

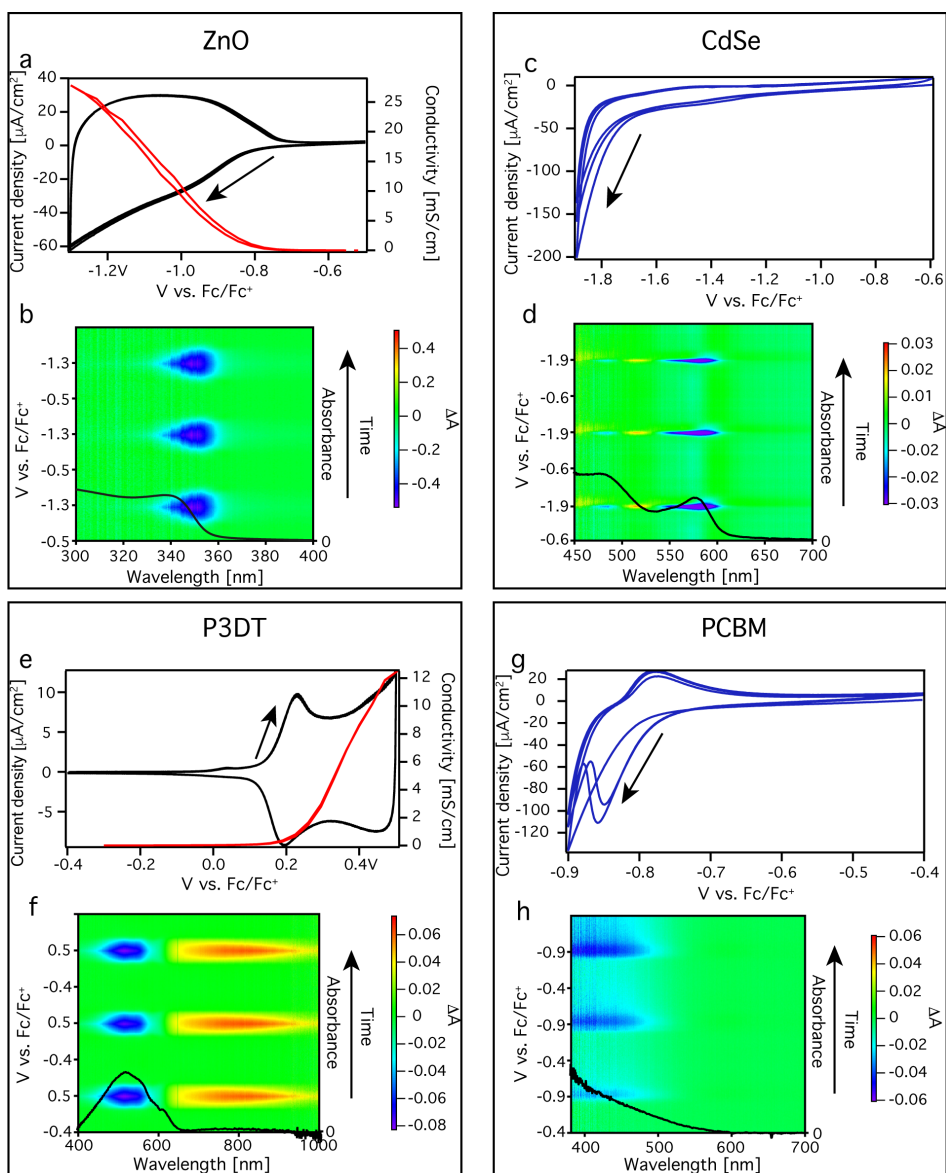


**Figure 3.2 Spectro-electrochemical measurements for different semiconductor films.** (a), (c), (e) and (g) show the CVs (black or blue trace) for a (a) ZnO QD film (c), CdSe QD film, (e) P3DT film and a (g) PCBM film. The measurements are performed on an ITO substrate in 0.1 M LiClO<sub>4</sub> acetonitrile solution with a scan speed of 50 mV/sec. The scans start at the  $V_{oc}$  of the system and are repeated three times; the arrows indicate the scan directions. (a) and (e) furthermore show the source-drain electronic conductivity in red. (b), (d), (f) and (h) show the change in absorbance during the three scans. The color plot includes the absorbance of the film. A negative change in absorbance is shown in blue and a positive change is shown in red.

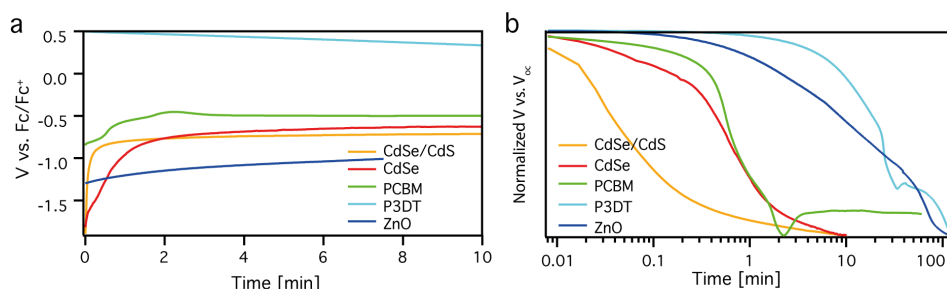


**Figure 3.3 Fermi-level stability measurements for different semiconductor films.** (a) Fermi-level stability measurements for the semiconductors in 0.1 M  $LiClO_4$  acetonitrile electrolyte solution for the duration of 10 minutes. The injected charge gradually leaves all semiconductor films. (b) The same measurements as in (a) with the normalized initial potential after the  $V_{oc}$  is set as 0.

stability measurements (Appendix, Figure A3.5)

Figure 3.3a shows Fermi-level stability measurements for all investigated semiconductor films in 0.1 M  $LiClO_4$  acetonitrile solutions. For comparison Fermi-level stability measurements normalized to 1 at the potential set before disconnecting the counter electrode and to 0 at the initial  $V_{oc}$  are shown in Figure 3.3b. For CdSe, CdSe/CdS QDs and PCBM it takes  $<35$ s for the potential to be half of the maximum. In contrast, for ZnO QDs and P3DT it takes  $\sim 14$  minutes and  $\sim 23$  minutes, respectively. Both ZnO and P3DT are clearly much more stable than the other systems, in line with the more symmetric CVs for these materials in Figure 3.2.

The loss of charge density and potential shown in Figure 3.3 is similar to self-discharge in batteries.<sup>40</sup> We consider three possible causes for the observed loss. First of all, impurities can extract the charges from the conduction/valence band of the material. The most common impurity is molecular oxygen, which can be reduced to its radical anion superoxide by electrons in the conduction band of the semiconductor materials. Indeed, performing the same experiments for ZnO QDs outside the glovebox results in much less symmetric CVs and a rapid loss of electrons (Appendix, Figure A3.6). While the glovebox atmosphere contains  $\leq 0.1$  ppm oxygen, on timescales of minutes to hours this may still lead to significant reactions with electrons.

Second, intrinsic electrochemical reactions can occur with the material itself.<sup>14</sup> The strong differences between e.g. ZnO QDs and CdSe QDs in Figs 3.2 and 3.3 hint towards a strong contribution of intrinsic reduction reactions in the latter material. Such reactions have been observed and discussed before and have sometimes been assigned to the reduction of surface  $Cd^{2+}$  to  $Cd^0$ .<sup>41–44</sup> However, the occurrence and nature of such surface electrochemical reactions, and their potential reversibility, is largely unknown.

Finally, movement of counterions can lead to the loss of injected charges. This process should not occur spontaneously as the counterions are Coulombically bound to the injected charge carriers and should not diffuse out of the film unless there is another mechanism (i.e. the first two mechanisms above) that removes the injected charge carriers.

**Table 3.1.** Melting point of electrolyte solvents.

Solvent	Acetonitrile	Ethylene Carbonate	Succinonitrile	PEG 6000	Dimethyl sulfone
Melting point	-45 °C	37 °C	57 °C	56-63 °C	109 °C

However, if electric fields are present, as is the case in any semiconductor junction or any device under operation, they will cause counterions to migrate with an associated loss of injected charge carrier density.

In order to make a permanently doped semiconductor system by the means of electrochemistry, that can also be used in a device, these processes need to be controlled. As was discussed above, several methods have been explored to make stable LECs at room temperature.<sup>26-28</sup> While an increase in doping stability was achieved, none of these methods proved successful in fully stabilizing the charge density at room temperature. Until now the only successful way of obtaining truly stable electrochemical charge injection has been at cryogenic temperatures.<sup>22, 29-31, 45</sup> This is clearly not suitable for real world applications. However, freezing does not necessarily require low temperatures.

Want et al. used polymer electrolyte solvents with higher glass transition temperatures and gained a higher stability at room temperature for conductive polymer LECs, however the devices decayed and were undoped after 100 hours.<sup>27</sup> However, many other types of solvents have proven to be good electrolyte solvents for either fuel cells or batteries.<sup>46-49</sup> We sought solvents that are chemically similar to common electrolyte solvents, but with higher melting points (see Table 3.1).

### 3.2.3 Enhanced doping stability by using room temperature freezing

We use ZnO as a model system due to its stable and reversible electrochemistry, as highlighted in Figure 3.2 and 3.3, but the results are general and many of the measurements are shown for the other semiconductor materials either in this Chapter or in the Appendix. Figure 3.4a shows CVs for a ZnO QD film on an ITO electrode in 0.1 M LiClO<sub>4</sub> in succinonitrile electrolyte solution at temperatures between -77 °C and 60 °C. It is clear that by lowering the temperature, the current density decreases, and the positive peak current density occurs at more positive potentials. Both of these observations can be explained by the reduced diffusion of the electrolyte ions as the temperature decreases. At -77 °C, no features are seen in the CV and no charging occurs (see Appendix, Figure A3.7).

Figure 3.4b shows the peak current density obtained from the CVs at -1.36 V at different temperatures (left axis). As we showed in detail recently,<sup>17</sup> charge injection is limited by counterion diffusion. Under these conditions it is possible to estimate the diffusion coefficient of the Li<sup>+</sup> cation at each temperature with the Randles-Sevcik equation:

$$j_p = 0.4463nFC^* \left( \frac{nFvD}{RT} \right)^{1/2} \quad 3.1$$

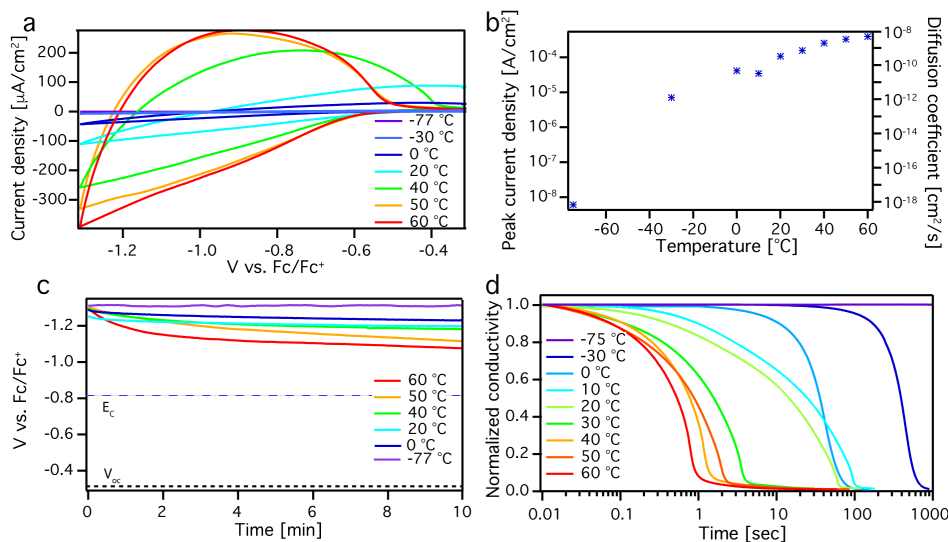


**Figure 3.4** Electrochemical measurements for a ZnO QD film in succinonitrile performed at temperatures between  $-77^\circ\text{C}$  and  $60^\circ\text{C}$ . (a) CVs at different temperatures. The potential is scanned between  $-0.36$  V and  $-1.36$  V at  $50$  mV/s scan rate. (b) The peak current obtained from the CVs for different temperatures (left axis) and the corresponding diffusion coefficient (right axis). Both of them are plotted with the same symbol (blue stars). By lowering the temperature, the  $\text{Li}^+$  diffusion coefficient decreases due to the solidifying of the solvent. (c) Fermi-level stability measurements performed at different temperatures. The graph includes the conduction band edge ( $E_c$ , blue dashed line) and the open circuit potential of the ZnO QD film ( $V_{oc}$ , black dashed line). When the temperature is lowered the potential becomes much more stable. (d) Conductivity measurements after a potential step from  $-1.36$  V to  $-0.36$  V. The initial conductivity at each temperature is normalized. The conductivity drops as a result of electrons that leave the ZnO QDs film upon discharging. At lower temperatures discharging becomes much slower and stops altogether at  $-75^\circ\text{C}$ .

where  $j_p$  is the peak current density,  $n$  is the number of electrons,  $F$  is the Faradaic constant,  $C^*$  is the concentration of the electrolyte,  $v$  is the scan rate,  $D$  is the diffusion coefficient,  $R$  is the gas constant and  $T$  is the temperature. The resulting estimated diffusion coefficient values are plotted vs. the right axis in Figure 3.4b. By cooling down from  $60^\circ\text{C}$  to  $20^\circ\text{C}$ , the cation diffusion coefficient reduces by an order of magnitude. At  $-77^\circ\text{C}$ , the cation diffusion coefficient is estimated to be  $\sim 10^{-18} \text{ cm}^2/\text{s}$ , ten orders of magnitude lower than at  $60^\circ\text{C}$ . With such a diffusion coefficient it would take a  $\text{Li}^+$  ion  $\sim 1010 \text{ s}$  ( $=450 \text{ yr}$ ) to diffuse out of a  $1 \mu\text{m}$  thick ZnO NC film. This shows that by freezing the electrolyte solvent, the diffusion coefficient of the  $\text{Li}^+$  cation decreases greatly, which should lead to increased electron stability after charge injection. At the same time, freezing the electrolyte should also prevent impurity diffusion, which will also increase the stability of doped semiconductor films.

For the same sample, Fermi-level stability measurements were performed for the duration of 10 minutes. The results are shown in Fig. 3.4c. Measurements on a longer time-scales are shown in Appendix, Figure A3.8. A potential of  $-1.36$  V vs. ferrocene is

applied to the sample at temperatures where charge injection can occur (around 60 °C). While continuously applying this potential, the temperature is lowered to the desired temperature, where the Fermi-level stability measurements are initiated. For measurements performed at temperatures above the melting point of succinonitrile, a significant increase in potential is observed on the timescale of minutes. By lowering the temperature, the potential increases more gradually. At RT it takes around 145 minutes for the potential to reach the value of -1.17 V vs. ferrocene (the whole measurement is shown in Figure 3.5a), while in acetonitrile the same potential is reached after only 92 seconds. However, while the RT charge stability is much higher when using succinonitrile as a solvent, it is not until -77 °C that the injected electrons are entirely stable for at least 10 minutes. This indicates that complete crystallization of the solvent in the crowded pores between the QDs where the cation concentration is high is much more difficult, resulting in a very strong melting point depression.

In the Fermi-level stability measurements no electric field is applied and the electrons leave the semiconductor spontaneously, through reacting with either impurities or via intrinsic surface electrochemical reactions. However, in devices electric fields are present which could cause ions to migrate and the doping density to change. To investigate this we actively apply a potential close to the original  $V_{oc}$  after charging the sample. This change in potential will force ions out of the film via migration, if they are mobile, and will cause discharging of the film. However, if ions are immobile such discharge should be prevented. This process hence depends on ion mobility and not on reactions with impurities or intrinsic surface electrochemical reactions.

Figure 3.4d shows normalized source-drain conductivity measurements of a ZnO QD sample on an IDE. In the measurement, a potential of -1.36 V is applied to the ZnO QDs when the solvent is liquid (around 60 °C), then the temperature is lowered, and at the desired temperature the potential is changed to the original  $V_{oc}$  (-0.36 V) while the source-drain current is recorded. Since the conductance depends linearly on the electron concentration this measurement detects the drop in charge density in a sensitive way. At 60 °C, when succinonitrile is liquid, it takes <1 s to discharge the film, while at -30 °C it takes ~1000 s. At -75 °C the conductivity does not drop at all showing that at this temperature the electrolyte cations are immobilized in the frozen solvent.

The temperature dependent source-drain conductance is shown in Figure A3.9 and A3.10 in the Appendix. From those figures, and from Fig. 3.4d it is clear that even at -75 °C, when the ions are immobilized and the film cannot be discharged, electrons can still move between the ZnO QDs. This is a crucial requirement for using such electrochemically doped films in devices.

By looking at the temperature dependent potential and discharging results (Figures 3.4c and 3.4d), it is clear that even when succinonitrile is well below its reported melting temperature (57 °C), diffusion of ions and impurities is still possible. Apparently, the solvent does not properly freeze until at -75 °C, a surprising 132 °C lower than the reported melting point of succinonitrile. Differential scanning calorimetry shows only around 30 °C melting point depression for 0.1 M LiClO<sub>4</sub> succinonitrile (Appendix, Figure A3.11)

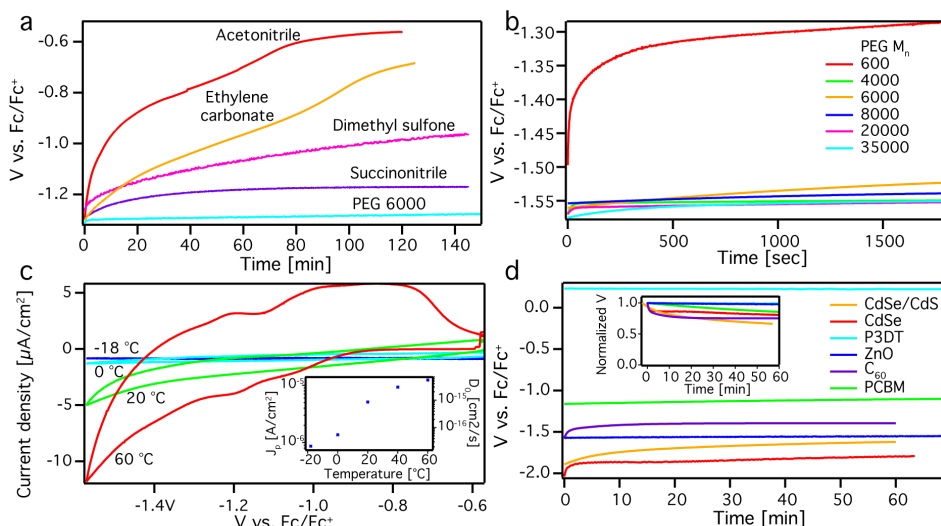


**Figure 3.5 Electrochemical measurements performed with different electrolyte solvents.** (a) Fermi-level stability measurements for a ZnO QD film in different electrolyte solvents with different melting points measured at room temperature. (b) Fermi-level stability measurements for a ZnO QD film measured in PEG with different number average molecular weights,  $M_n$ , (from 600 to 35,000) at room temperature. (c) CVs for a ZnO QD film in 11 wt%  $LiClO_4$  PEG 6000 performed at temperatures between -18 °C and 60 °C. The figure includes an inset containing the peak current density,  $J_p$  (left axis), and the calculated  $Li^+$  diffusion coefficient,  $D_0$  (right axis), versus the temperature. (d) Fermi-level stability measurements for different semiconductor systems in an 11 wt%  $LiClO_4$  in either PEG 4000 or PEG 6000 electrolyte solvent. The panel includes an inset where the initial  $V_{oc}$  is set as a 0 and the measured potential has been normalized. It takes longer than an hour for the injected charge to leave the conduction/valence band of the materials.

and furthermore both solvents are solid at room temperature. Further melting point depression is most likely caused by the inability of the solvent to crystallize in crowded environment of the nanopores in the QD film. Due to these factors, electrolyte solvents with higher melting points than succinonitrile are most likely better suited.

To investigate whether an even larger improvement of the RT charge stability is possible, measurements with other electrolyte solvents were performed. Figure 3.5a shows Fermi-level stability measurement for ZnO QD films with  $LiClO_4$  in acetonitrile, ethylene carbonate, dimethyl sulfone, succinonitrile and PEG 6000 at room temperature. It is clear that polyethylene glycol (PEG) offers the greatest RT charge stability. After 170 minutes, the potential of the ZnO QD film in PEG has increased from -1.30 V to -1.273 V while it only takes 11 seconds for a ZnO QD film to reach this potential in acetonitrile. We observe that PEG has a lower melting point than dimethyl sulfone (56-63 °C vs. 109 °C) but shows a much better charge stability. We hypothesize that the better stability in PEG can be caused by the combination of high viscosity, resulting in slower diffusion of impurities, and by a lower impurity solubility.

As both the viscosity and the melting point increase with increasing PEG chain length,

Fermi-level stability measurements were performed with PEG with number average molecular weights,  $M_n$ , between 600 and 35000 (Fig 3.5b). Of these only PEG 600 is liquid at room temperature and it shows the most rapid change in the measured potential. This confirms our conclusion above that solidifying the electrolyte is a promising strategy to create permanently doped nanocrystal films with electrochemical doping. PEG 4000 was chosen for Fermi-level stability measurements with a ZnO QD sample over a weekend (Appendix, Figure A3.12). After 65 hours, the potential had only increased by 0.2 V (to -1.35 V), which is still 0.55 V more negative than the conduction band edge of the ZnO QDs. The sample thus remained degenerately doped after several days. Wantz et al. used polymer electrolytes with different glass transition temperatures for conductive polymer LECs, and tested their stability at room temperature. Their best operation half-lifetime at room temperature was between 10 to 20 hours.<sup>27</sup> A direct comparison to this half-lifetime of LEC operation is difficult, but it appears the doping stability with the present approach is better.

To investigate the diffusion of counterions in PEG in more detail, CVs were performed on a ZnO QD film in 11 w%  $\text{LiClO}_4$  PEG 6000 solution at temperatures between -18 °C and 60 °C (Fig 3.5c). These CVs show a much larger separation between forward and backward peaks than for succinonitrile (Fig. 3.4a), in line with the higher viscosity of PEG and the associated smaller diffusion coefficient of  $\text{Li}^+$  in that solvent. By lowering the temperature, the peak current density decreases and the peak separation increases further. Using eq. 2 we find that the diffusion coefficient of  $\text{Li}^+$  in PEG 6000 (inset of Figure 3.5c) is a few orders of magnitude lower than in succinonitrile ( $10^{-14}$  cm<sup>2</sup>/s vs.  $10^{-8}$  cm<sup>2</sup>/s, both at 60 °C). Similar measurements were performed for a P3DT film in 11 w% PEG 6000 and show the same trend (Appendix, Figure A3.13).

Fermi-level stability measurements with solvents from Table 3.1 were also performed for CdSe QDs, CdSe/CdS QDs, P3DT, PCBM and  $\text{C}_{60}$  (Appendix, Figure A3.14). In all cases, the stability of injected charges is better when solvents with melting points above room temperature are used and is best when using PEG with  $M_n \geq 4000$ . An overview of the charge stability for all systems in PEG is shown in Figure 3.5d. The Figure includes an inset where the potential is normalized (the  $V_{oc}$  before charging is set to 0 and the initial applied potential is normalized to 1). When the results are compared to the measurements performed with acetonitrile (Figure 3.3), it is clear that for all materials the electrochemically injected charge is much more stable in PEG. As before, the potential is not completely stable as it gradually relaxes to the original  $V_{oc}$ , but a great enhancement is achieved. For all materials, charge is still present in the conduction/valence band after at least an hour.

While PEG proved to give the best charge stability at room temperature, likely due to a combination of the lowest impurity concentration and impurity diffusion coefficient, the overall best result was obtained for succinonitrile at -75 °C. We were not able to measure the charge stability in PEG at such low temperatures as going through the glass transition of PEG<sup>50</sup> resulted in a loss of contact to the electrodes. However, even if we could solve these experimental problems we consider it is unlikely that PEG can crystallize into a very dense crystal structure required for the immobilization of counterions and impurities.

This is evidenced by the fact that upon solidification the diffusion coefficient of  $\text{Li}^+$  in PEG 6000 is reduced by about two orders of magnitude (Fig. 3.5c), while for succinonitrile a reduction of 10 orders of magnitude is observed (Fig. 3.4b). The diffusion coefficient of  $\text{Li}^+$  in succinonitrile at  $-70\text{ }^\circ\text{C}$  is  $\sim 10^{-18}\text{ cm}^2/\text{s}$ , which is two orders of magnitude below the lowest diffusion coefficient found for PEG6000 ( $\sim 10^{-16}\text{ cm}^2/\text{s}$  at  $-10\text{ }^\circ\text{C}$ ).

We are currently looking for other solvents, such as nitriles with even higher melting points than succinonitrile, to see if we can extend the full stability of injected charges to room temperature. Additionally, the use of different ions than  $\text{Li}^+$  might show a further reduction of the diffusion coefficient, and a gain in stability.

### 3.3 Conclusions

In summary, we have shown electrochemical doping for a broad range of semiconductor films. In all cases when acetonitrile is used, the injected charge disappears quickly when the films are disconnected from the external applied potential, due to reactions with impurities and intrinsic electrochemical reactions at the surface of the semiconductors. For ZnO QDs, the injected charge is stable for 37 minutes or less under stringent air-free conditions, and for some materials the stability lasts only a few seconds (CdSe and CdSe/CdS QDs). We have shown that this charge stability at room temperature is greatly improved for all investigated semiconductor films by charging the films at elevated temperature in different solvents with melting points above room temperature. In terms of room temperature charge stability, the best solvent was PEG with molecular weight of  $\geq 4000$ , which increases the lifetime of injected charges to several days. Further improvements in charge stability should be possible as experiments at  $-75\text{ }^\circ\text{C}$  in succinonitrile showed that the electrochemically injected charge becomes entirely stable on experimental time scales. By investigating the role of impurities in the disappearance of injected charges, and nitriles with melting points higher than succinonitrile, there is a great chance to gain stable electrochemically doped films at room temperature.

### 3.4 Methods

**Materials.** Zinc acetate dihydrate ( $\text{Zn}(\text{CH}_3\text{COO})_2 \cdot 2\text{H}_2\text{O}$  reagent grade), potassium hydroxide (KOH pellets), cadmium acetate ( $\text{CdAc}_2$ , 99.999%, ChemPur), oleic acid (OA, 90%), 1-octadecene (ODE, 90%), selenium powder (Se, ChemPur) trioctylphosphine (TOP, 90%), trioctylphosphine oxide (TOPO, 99%), octadecylamine (ODA, 90%), oleylamine (OLAM, 70%), 1-octanethiol ( $\geq 98.5\%$ ), 1,4-butanedithiol (BDT, 97%), Poly(3-decylthiophene-2,5-diyl) (P3DT, regioregular), Poly(3-hexylthiophene-2,5-diyl) (P3HT, regiorandom), Phenyl-C61-butyric acid methyl ester (PCBM, 99%), fullerene ( $\text{C}_{60}$ , 99.9%), 1,2-dichlorobenzene (99%), chlorobenzene (99.8%), Indium-doped Tin Oxide substrates (ITO, PGO Germany), lithium perchlorate ( $\text{LiClO}_4$ , 99.99%), ferrocene (Fc, 98%), decamethylferrocene (97%), anhydrous ethylene carbonate ( $(\text{CH}_2\text{O})_2\text{CO}$ , 99.8%), succinonitrile (99%), dimethyl sulfone (98%), poly(ethylene glycol) (PEG Mn of 600, 4000, 6000, 8000, 20000 and 35000) and anhydrous solvents (acetonitrile, 99.99%, methanol, 99.8%, ethanol (max 0.01%  $\text{H}_2\text{O}$ ), toluene, 99.8%, hexane, 95%, butanol, 99.8%). All chemicals were purchased from Sigma Aldrich unless stated otherwise. Acetonitrile was dried before use in an Innovative Technology PureSolv Micro column. All other chemicals were used as received.

**ZnO QD synthesis.** The ZnO QDs were synthesized as previously described.<sup>17</sup> 3.425 mmol of zinc

acetate dihydrate and 50 mL ethanol were combined at 60 °C in an Erlenmeyer flask. A potassium hydroxide mixture (6.25 mmol KOH in 5 mL methanol) was added dropwise to the stirred zinc acetate dihydrate mixture. After 1 additional minute in reaction time, the heat source was removed. The QDs were purified by the addition of hexane and the flocculates were isolated by centrifugation at 2000 rpm for 1 minute. The QDs were redissolved in ethanol and the dispersion was stored at -20 °C to avoid further growth by Ostwald ripening.

**CdSe QD synthesis.** The CdSe QD cores were synthesized according to the procedure of Qu et. al.<sup>51</sup> The Cd-precursor containing 0.66 g of CdAc<sub>2</sub>, 3.68 g OA and 25.9 g ODE was degassed for three hours. For the Se-precursor, 1.42 g Se powder was dissolved at 200 °C in 7.5 g TOP and 11.9 g ODE. 1.11 g TOPO, 3.2 g ODA 90% and 5.2 g of the Se-precursor were added to a 3 neck round bottom flask and heated to 300 °C. At 300 °C, 4.9 g of the Cd-precursor was injected into the bottle. The reaction was kept at around 280 °C for 9 minutes and cooled down by an air gun. When the solution reached 100 °C, it was quenched with 5 mL of anhydrous toluene. The CdSe particles were precipitated by addition of methanol and butanol in a 1:1:1 crude solution:anhydrous methanol:anhydrous butanol ratio. The flocculates were isolated by centrifugation at 2800 rpm for 8 minutes and redissolved in toluene.

**CdSe/CdS shell growth.** The CdS shell growth was synthesized by a known procedure.<sup>52</sup> 400 nmol of CdSe QDs in toluene were combined with 3 mL of OLAM and 4 mL of ODE and degassed for 1 hour at room temperature and for 20 minutes at 120 °C under vacuum. The reaction solution was heated up to 310 °C under N<sub>2</sub>, and when the temperature reached 240 °C, the Cd precursor (as in the core synthesis, desired amount diluted in 1 mL of ODE) and 1-octanethiol (1.2 equivalent amounts to Cd-oleate diluted in 3.4 mL of ODE) are injected dropwise into the reaction solution at the rate of 1 monolayer per hour, by syringe pumps. When the injection is finished, 1 mL oleic acid was injected and the NCs were annealed at 310 °C for an hour. Afterwards, the solution is cooled down to 50 °C. The CdSe/CdS QDs were precipitated by the addition of butanol and methanol and centrifuged at 3800 rpm for 5 minutes. The QDs were redissolved in hexane.

**Film preparation.** All films were prepared on two different working electrodes (WE), on indium-doped tin oxide (ITO) substrates or on home-built interdigitated gold electrodes (IDEs). The IDE is a glass substrate containing four different gold working electrodes prepared by optical lithography. The four working electrodes provide four different sensitivities in the measurements.

ZnO QD films were drop-casted in air and annealed for 1 hour at 60 °C.

CdSe and CdSe/CdS films were made by layer-by-layer dip-coating procedure in a nitrogen filled glovebox. The substrate was immersed in a QD dispersion for 30 seconds, thereafter in a solution containing 0.2 M 1,4-butanedithiol cross-linking ligands in methanol for 30 seconds and ultimately it was dipped in methanol to rinse excess ligands.

For P3DT film preparation, 10 mg of P3DT was dissolved in 1 mL of 1,2-Dichlorobenzene. The substrate was coated by spin-coating for 60 seconds at 3000 RPM with a ramp of 1000 RPM/s.

For PCBM films, 50 µL of 3 wt% PCBM chlorobenzene solution was spin-coated for 45 seconds at 3000 RPM with a ramp of 1000 RPM/s. The substrate was placed on a hot plate at 100 °C for 10 minutes to ensure the evaporation of chlorobenzene.<sup>53</sup>

C<sub>60</sub> films were prepared by a physical vapor deposition technique using an AJA ATC Orion evaporator at high vacuum ( $\leq 1 \times 10^{-6}$  mbar). The C<sub>60</sub> powder was placed in a crucible and heated to sublimation temperature. The temperature was kept fixed during the evaporation.<sup>54</sup>

**Electrochemical measurements.** All electrochemical measurements were performed in a nitrogen filled glovebox with moisture  $\leq 0.5$  ppm and O<sub>2</sub> levels  $\leq 0.1$  ppm. The measurements were performed with an Autolab PGSTAT128N potentiostat with a bipotentiostat BA module. Two different three electrode electrochemical cells were used (Appendix, Figure A3.15). The former one was a cuvette cell where the sample was deposited on a WE and immersed in a LiClO<sub>4</sub> electrolyte solution. The solution further contained a Ag pseudo reference electrode (RE) and a Pt sheet as a counter electrode (CE). The latter electrochemical cell was a flat cell containing a well where the sample on the WE was placed inside the well and the solvent was placed on top of the sample. On top of the solvent a glass substrate was placed containing a Ag pseudo RE and a Pt mesh CE (see Appendix, Figure A3.16). It was made sure both the RE and the CE touched the solvent but not the WE in order to avoid short circuiting. The flat cell is used when smaller volumes of solvents are needed or when the solvents are very viscous.

Both cell designs were used for cyclic voltammetry measurements (CVs) for different semiconductor materials. The CVs were performed in a LiClO<sub>4</sub> electrolyte solution starting from the open circuit potential ( $V_{oc}$ ) of the material. The potential was scanned at 50 mV/s in either the positive/negative direction until charge was injected into the valence/conduction band of the material. The CVs were repeated three times.

Before the measurements, the Ag pseudoreference electrode was calibrated with a ferrocene/ferrocenium couple<sup>55</sup> (cuvette cell) or a decamethylferrocene/decamethylferrocenium couple (flat cell).<sup>56</sup> The difference between the decamethylferrocene/decamethylferrocenium and the ferrocene/ferrocenium couple was measured as 0.57 V. All potentials are given versus the ferrocene/ferrocenium couple.

**Spectro-electrochemical measurements.** The absorbance changes in the spectro-electrochemical measurements were measured as a function of the applied electrochemical potential with a fiber-based UV-VIS spectrometer, Ocean Optics USB2000, using an Ocean Optics DH 2000 lamp as a light source.

**Source-drain electronic conductance measurements.** Source-drain electronic conductance measurements were performed as previously described by the use of the home-built IDE.<sup>17</sup> During the measurements, two WEs were used in a source-drain configuration, the source-drain gap width was 25  $\mu\text{m}$  while the gap length was 6.8 cm. The potential is stepped and after the system reached equilibrium, the potential of WE1 was scanned in a CV manner around the fixed potential of WE2 with a difference of  $\pm 10$  mV. The slope of the current versus the potential gives the conductance, G. From the conductance, the conductivity,  $\sigma$ , can be calculated with Equation 3.2.

$$\sigma = (G \times w) / (l \times h) \quad 3.2$$

where w is the source-drain width, l is the gap length and h is the height of the sample.

**Fermi-level stability measurements.** Fermi-level stability measurements were performed following a procedure similar to Pei et al.<sup>25</sup> The measurements were performed after charge injection into the

conduction band or the valence band of the different semiconductors. When equilibrium was reached, the CE was disconnected from the WE and the RE electrode. By doing so, no additional charge can be injected into the film while the potential between the WE and the RE is measured. This potential is equal to the Fermi level of the working electrode vs. the Fermi level of the reference electrode. If injected charges leave the semiconductor, this will result in a drop of the Fermi-level and a change in potential. When solvents that are solid at room temperature are used, the sample is charged at elevated temperature when the solution is liquid, after which the temperature is lowered while the same potential is applied. When the desired temperature is reached, the CE is disconnected from the WE and the RE.

## References

1. Bailey, R. E.; Nie, S., Alloyed semiconductor quantum dots: Tuning the optical properties without changing the particle size. *J. Am. Chem. Soc.* 2003, 125 (23), 7100-7106.
2. Talapin, D. V.; Lee, J.-S.; Kovalenko, M. V.; Shevchenko, E. V., Prospects of colloidal nanocrystals for electronic and optoelectronic applications. *Chem. Rev.* 2009, 110 (1), 389-458.
3. Geffroy, B.; le Roy, P.; Prat, C., Organic light-emitting diode (OLED) technology: materials, devices and display technologies. *Polym. Int.* 2006, 55 (6), 572-582.
4. Facchetti, A., Semiconductors for organic transistors. *Materials Today* 2007, 10 (3), 28-37.
5. Schöll, A.; Schreiber, F., Molecular Beam Epitaxy. In *From research to mass production* [Online] Henini, M., Ed. Elsevier: USA, 2013; pp. 591-609.
6. Coropceanu, V.; Cornil, J. r.; Filho, D. A. d. S.; Olivier, Y.; Silbey, R.; Bredas, J.-L., Charge Transport in Organic Semiconductors. *Chem. Rev.* 2007, 107, 926-952.
7. Würthner, F., Bay-substituted perylene bisimides: Twisted fluorophores for supramolecular chemistry. *Pure Appl. Chem.* 2006, 78 (12), 2341-2349.
8. Shim, M.; Wang, C.; Norris, D. J.; Guyot-Sionnest, P., Doping and Charging in Colloidal Semiconductor Nanocrystals. *MRS Bull.* 2001, 26 (12), 1005-1008.
9. Schimpf, A. M.; Knowles, K. E.; Carroll, G. M.; Gamelin, D. R., Electronic doping and redox-potential tuning in colloidal semiconductor nanocrystals. *Acc. Chem. Res.* 2015, 48 (7), 1929-37.
10. Salzmann, I.; Heimel, G.; Oehzelt, M.; Winkler, S.; Koch, N., Molecular Electrical Doping of Organic Semiconductors: Fundamental Mechanisms and Emerging Dopant Design Rules. *Acc. Chem. Res.* 2016, 49 (3), 370-8.
11. Boehme, S. C.; Wang, H.; Siebbeles, L. D. A.; Vanmaekelbergh, D.; Houtepen, A. J., Electrochemical charging of CdSe quantum dot films: Dependence on voids size and counterion proximity. *ACS Nano* 2013, 7 (3), 2500-2508.
12. Boehme, S. C.; Vanmaekelbergh, D.; Evers, W. H.; Siebbeles, L. D. A.; Houtepen, A. J., In Situ Spectroelectrochemical Determination of Energy Levels and Energy Level Offsets in Quantum-Dot Heterojunctions. *J. Phys. Chem. C* 2016, 120 (9), 5164-5173.
13. Bard, A. J.; Faulkner, L. R., *Electrochemical methods. Fundamentals and*

- applications. 2nd ed.; John Wiley & sons, INC.: New York, United states of America, 2001.
14. Guyot-Sionnest, P., Charging colloidal quantum dots by electrochemistry. *Microchim. Acta* 2008, 160 (3), 309-314.
  15. Vanmaekelbergh, D.; Houtepen, A. J.; Kelly, J. J., Electrochemical gating: A method to tune and monitor the (opto)electronic properties of functional materials. *Electrochim. Acta* 2007, 53 (3), 1140-1149.
  16. Hulea, I. N.; Brom, H. B.; Houtepen, A. J.; Vanmaekelbergh, D.; Kelly, J. J.; Meulenkaamp, E. A., Wide energy-window view on the density of states and hole mobility in poly(p-phenylene vinylene). *Phys. Rev. Lett.* 2004, 93 (16), 166601.
  17. Gudjonsdottir, S.; van der Stam, W.; Kirkwood, N.; Evers, W. H.; Houtepen, A. J., The Role of Dopant Ions on Charge Injection and Transport in Electrochemically Doped Quantum Dot Films. *J. Am. Chem. Soc.* 2018, 140 (21), 6582-6590.
  18. van der Stam, W.; Gudjonsdottir, S.; Evers, W. H.; Houtepen, A. J., Switching between Plasmonic and Fluorescent Copper Sulfide Nanocrystals. *J. Am. Chem. Soc.* 2017, 139 (37), 13208-13217.
  19. Shimotani, H.; Diguët, G.; Iwasa, Y., Direct comparison of field-effect and electrochemical doping in regioregular poly(3-hexylthiophene). *Appl. Phys. Lett.* 2005, 86 (2), 022104.
  20. ECHEGOYEN, L.; ECHEGOYEN, L. E., Electrochemistry of Fullerenes and Their Derivatives. *Acc. Chem. Res.* 1998, 31, 593-601.
  21. Pei, Q.; Yu, G.; Zhang, C.; Yang, Y.; Heeger, A. J., Polymer Light-Emitting Electrochemical Cells. *Science* 1995, 269, 1086-1088.
  22. Gao, J.; Yu, G.; Heeger, A. J., Polymer light-emitting electrochemical cells with frozen p-i-n junction. *Appl. Phys. Lett.* 1997, 71 (10), 1293-1295.
  23. Matyba, P.; Maturova, K.; Kemerink, M.; Robinson, N. D.; Edman, L., The dynamic organic p-n junction. *Nat. Mater.* 2009, 8 (8), 672-6.
  24. S., T.; L., E., Light-Emitting Electrochemical Cells: A Review on Recent Progress. In: Armaroli N., Bolink H. (eds) *Photoluminescent Materials and Electroluminescent Devices*. Springer, Cham: 2017.
  25. Pei, Q.; Yang, Y.; Yu, G.; Zhang, C.; Heeger, A. J., Polymer Light-Emitting Electrochemical Cells: In Situ Formation of a Light-Emitting p-n Junction. *J. Am. Chem. Soc.* 1996, 118 (16), 3922-9.
  26. Tang, S.; Irgum, K.; Edman, L., Chemical stabilization of doping in conjugated polymers. *Organic Electronics* 2010, 11 (6), 1079-1087.
  27. Wantz, G.; Gautier, B.; Dumur, F.; Phan, T. N. T.; Gigmes, D.; Hirsch, L.; Gao, J., Towards frozen organic PN junctions at room temperature using high-Tg polymeric electrolytes. *Organic Electronics* 2012, 13 (10), 1859-1864.
  28. Hoven, C. V.; Wang, H.; Elbing, M.; Garner, L.; Winkelhaus, D.; Bazan, G. C., Chemically fixed p-n heterojunctions for polymer electronics by means of covalent B-F bond formation. *Nat. Mater.* 2010, 9, 249-252.
  29. Yu, D.; Wang, C.; Wehrenberg, B. L.; Guyot-Sionnest, P., Variable range hopping conduction in semiconductor nanocrystal solids. *Phys. Rev. Lett.* 2004, 92 (21), 216802.
  30. Houtepen, A. J.; Kockmann, D.; Vanmaekelbergh, D., Reappraisal of Variable-Range Hopping in Quantum-Dot Solids. 2008, Vol. 8 (10), 3516-3520.

31. Houtepen, A. J. Charge injection and transport in quantum confined and disordered systems. Utrecht University, 2007.
32. Wehrenberg, B. L.; Yu, D.; Ma, J.; Guyot-Sionnest, P., Conduction in Charged PbSe Nanocrystal Films. *J. Phys. Chem. B* 2005, 109, 20192-20199.
33. Shim, M.; Guyot-Sionnest, P., n-type colloidal semiconductor nanocrystals. *Letters to nature* 2000, 407, 981-983.
34. Hoyer, P.; Weller, H., Potential-Dependent Electron Injection in Nanoporous Colloidal ZnO Films. *J. Phys. Chem.* 1995, 99 (38), 14096-14100.
35. Boehme, S. C.; Azpiroz, J. M.; Aulin, Y. V.; Grozema, F. C.; Vanmaekelbergh, D.; Siebbeles, L. D.; Infante, I.; Houtepen, A. J., Density of Trap States and Auger-mediated Electron Trapping in CdTe Quantum-Dot Solids. *Nano Lett.* 2015, 15 (5), 3056-66.
36. Murphy, A. R.; Frechet, J. M. J., Organic Semiconducting Oligomers for Use in Thin Film Transistors. *Chem. Rev.* 2007, 107, 1066-1096.
37. Tsumura, A.; Koezuka, H.; Ando, T., Macromolecular electronic device: Field-effect transistor with a polythiophene thin film. *Appl. Phys. Lett.* 1986, 49 (18), 1210-1212.
38. Jehoulet, C.; Bard, A. J., Electrochemical Reduction and Oxidation of C60 Films. *J. Am. Chem. Soc* 1991, 113, 5457-5459.
39. Flagg, L. Q.; Giridharagopal, R.; Guo, J.; Ginger, D. S., Anion-Dependent Doping and Charge Transport in Organic Electrochemical Transistors. *Chem. Mater.* 2018, 30 (15), 5380-5389.
40. Niu, J.; Conway, B. E.; Pell, W. G., Comparative studies of self-discharge by potential decay and float-current measurements at C double-layer capacitor and battery electrodes. *J. Power Sources* 2004, 135 (1-2), 332-343.
41. Zhao, J.; A, M.; Holmes; Osterloh, F. E., Quantum Confinement Controls Photocatalysis- A Free Energy Analysis for Photocatalytic Proton Reduction at CdSe Nanocrystals. *ACS Nano* 2013, 7 (5), 4316-4325.
42. Tsui, E. Y.; Hartstein, K. H.; Gamelin, D. R., Selenium Redox Reactivity on Colloidal CdSe Quantum Dot Surfaces. *J. Am. Chem. Soc.* 2016, 138 (35), 11105-8.
43. Tsui, E. Y.; Carroll, G. M.; Miller, B.; Marchioro, A.; Gamelin, D. R., Extremely Slow Spontaneous Electron Trapping in Photodoped n-Type CdSe Nanocrystals. *Chem. Mater.* 2017, 29 (8), 3754-3762.
44. du Fossé, I.; ten Brinck, S.; Infante, I.; Houtepen, A. J., Role of Surface Reduction in the Formation of Traps in n-Doped II-VI Semiconductor Nanocrystals: How to Charge without Reducing the Surface. *Chem. Mater.* 2019.
45. Wehrenberg, B. L.; Yu, D.; Ma, J.; Guyot-Sionnest, P., Conduction in Charged PbSe nanocrystal films. *J. Phys. Chem. B* 2005.
46. Verma, P.; Maire, P.; Novák, P., A review of the features and analyses of the solid electrolyte interphase in Li-ion batteries. *Electrochim. Acta* 2010, 55 (22), 6332-6341.
47. Xu, K., Nonaqueous Liquid Electrolytes for Lithium-Based Rechargeable Batteries. *Chem. Rev.* 2004, 104, 4303-4417.
48. Chen, R.; Liu, F.; Chen, Y.; Ye, Y.; Huang, Y.; Wu, F.; Li, L., An investigation of functionalized electrolyte using succinonitrile additive for high voltage lithium-

- ion batteries. *J. Power Sources* 2016, 306, 70-77.
49. Kim, J. G.; Son, B.; Mukherjee, S.; Schuppert, N.; Bates, A.; Kwon, O.; Choi, M. J.; Chung, H. Y.; Park, S., A review of lithium and non-lithium based solid state batteries. *J. Power Sources* 2015, 282, 299-322.
  50. P.Törmälä, Determination of glass transition temperature of poly(ethylene glycol) by spin probe technique. *Eur. Polym. J.* 1974, 10 (6), 519-521.
  51. Qu, L.; Peng, Z. A.; Peng, X., Alternative Routes toward High Quality CdSe Nanocrystals. *Nano Lett.* 2001, 1 (6), 333-337.
  52. Chen, O.; Zhao, J.; Chauhan, V. P.; Cui, J.; Wong, C.; Harris, D. K.; Wei, H.; Han, H. S.; Fukumura, D.; Jain, R. K.; Bawendi, M. G., Compact high-quality CdSe-CdS core-shell nanocrystals with narrow emission linewidths and suppressed blinking. *Nat. Mater.* 2013, 12 (5), 445-51.
  53. Hutter, E. M.; Hofman, J.-J.; Petrus, M. L.; Moes, M.; Abellón, R. D.; Docampo, P.; Savenije, T. J., Charge Transfer from Methylammonium Lead Iodide Perovskite to Organic Transport Materials: Efficiencies, Transfer Rates, and Interfacial Recombination. *Advanced Energy Materials* 2017, 7 (13), 1602349.
  54. Aulin, Y. V.; Felter, K. M.; Genbas, D. D.; Dubey, R. K.; Jager, W. F.; Grozema, F. C., Morphology-Independent Efficient Singlet Exciton Fission in Perylene Diimide Thin Films. *ChemPlusChem* 2018, 83 (4), 230-238.
  55. Ruch, P. W.; Cericola, D.; Hahn, M.; Kötz, R.; Wokaun, A., On the use of activated carbon as a quasi-reference electrode in non-aqueous electrolyte solutions. *J. Electroanal. Chem.* 2009, 636 (1-2), 128-131.
  56. Noviandri, I.; Brown, K. N.; Fleming, D. S.; Gulyas, P. T.; Lay, P. A.; Masters, A. F.; Phillips, L., The Decamethylferrocenium:Decamethylferrocene Redox Couple- A Superior Redox Standard to the Ferrocenium:Ferrocene Redox Couple for Studying Solvent Effects on the Thermodynamics of Electron Transfer. *J. Phys. Chem. B* 1999, 103, 6713-6722.

## Appendix

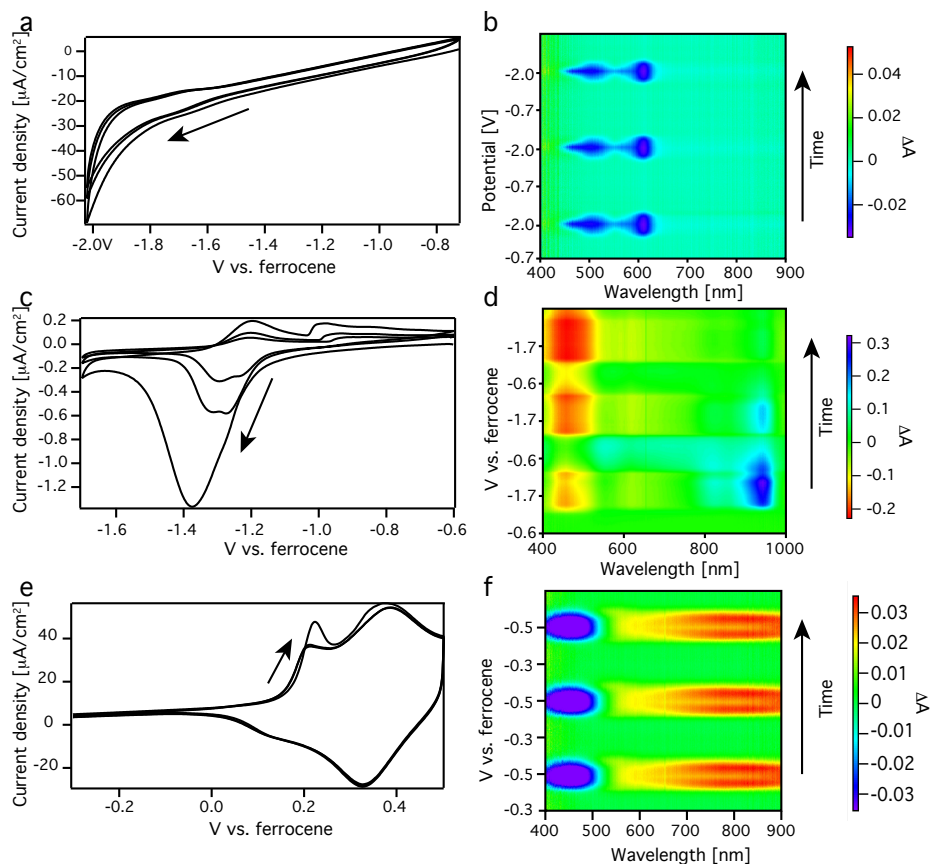


**Figure A3.1** Spectro-electrochemical measurements for different porous semiconductor films. (a), (c) and (e) show the CVs for (a) CdSe/CdS QD film (b),  $\text{C}_{60}$  film and (e) P3HT film. The measurements are performed in 0.1 M  $\text{LiClO}_4$  acetonitrile solution with a scan speed of 50 mV/sec. The scans are started at the  $V_{oc}$  of the system and the scans are repeated three times, the arrow indicates the scan direction. (b), (d) and (f) show the change in absorbance during the three scans.

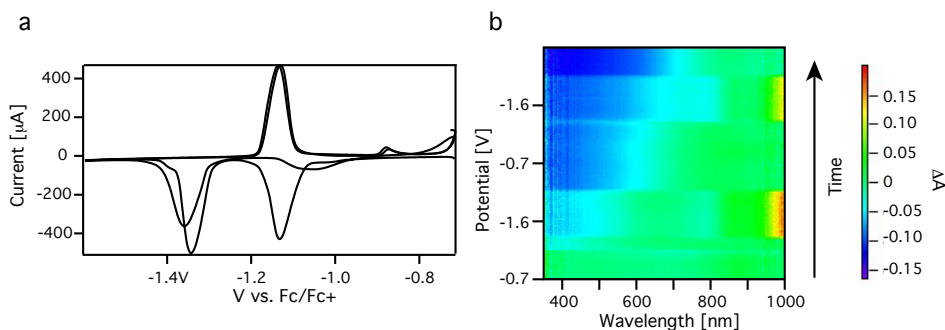


**Figure A3.2** Spectro-electrochemical measurement for a  $\text{C}_{60}$  film. (a) CV measurement that is performed in 0.1 M  $\text{TBAClO}_4$  acetonitrile solution with a scan speed of 20 mV/sec. The scans are started at the  $V_{\text{oc}}$  of the system and the scans are repeated two times. (b) shows the change in absorbance during the three scans. The sample is not stable throughout the measurements.

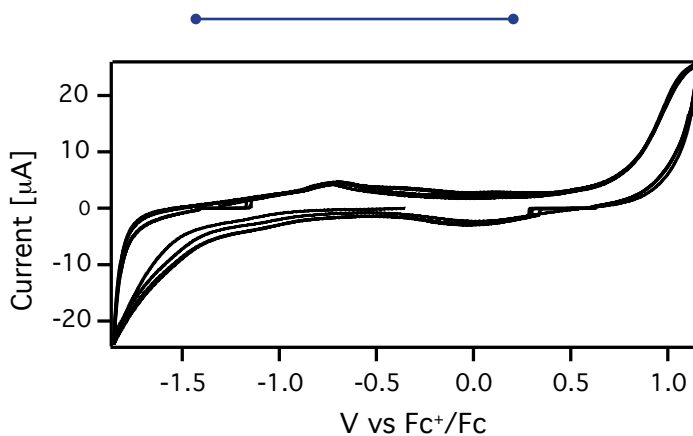


**Figure A3.3** A CV measurement performed on a blank ITO in 0.1 M  $\text{LiClO}_4$  acetonitrile solution.

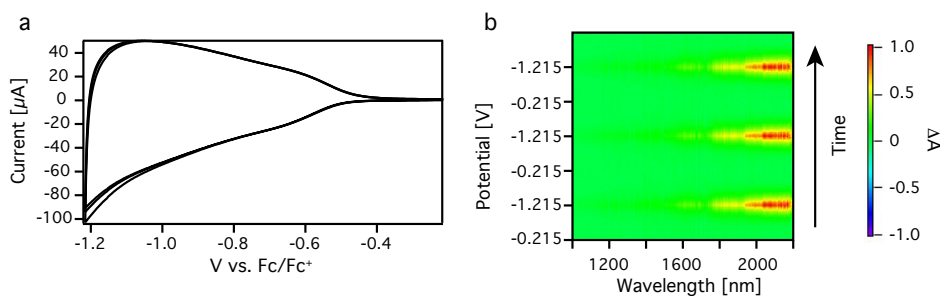


**Figure A3.4** Spectro-electrochemical measurement for a ZnO QD film. (a) CV measurement in 0.1 m  $\text{LiClO}_4$  acetonitrile solution with a scan speed of 50 mV/sec. The scans are repeated three times. (b) Differential absorbance spectra measured in the infrared during the CV. As electrons are injected into the conduction band of ZnO QDs, absorbance increases in the NIR due to intraband transitions.

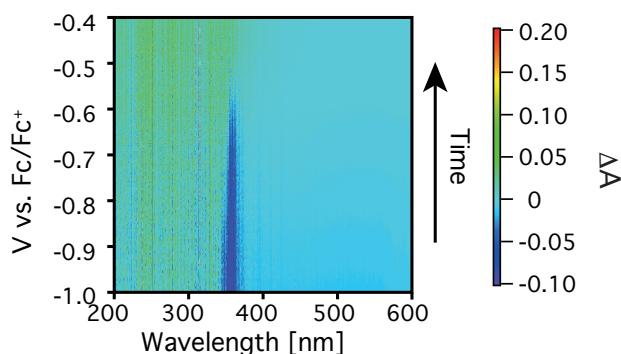


**Figure A3.5** Differential absorbance measurements during a Fermi-level stability measurements on a ZnO QD film. The graph shows the differential absorbance (color plot) vs. potential (y axis). As the potential increases the bleach decreases which means that electrons are leaving the conduction band of the ZnO QDs.

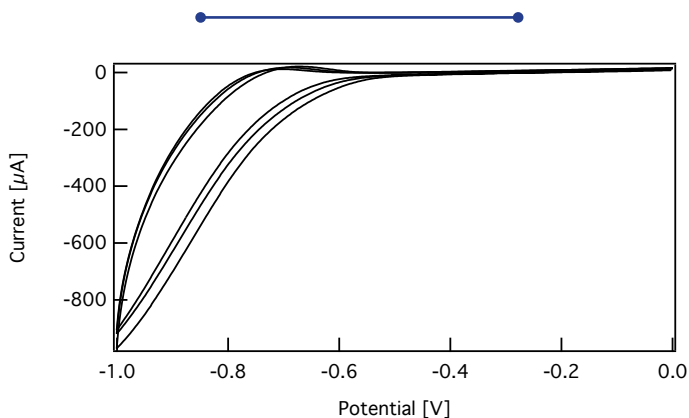


**Figure A3.6** CVs performed on a ZnO QD sample measured in 0.1 M LiClO<sub>4</sub> in air. The CV was measured at a scan rate of 50 mV/s and includes three scans.

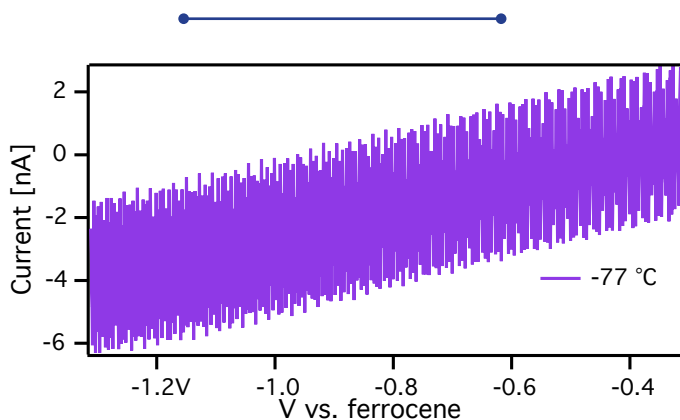


**Figure A3.7** CV for a ZnO QD film in 0.1 M LiClO<sub>4</sub> succinonitrile at -77 °C. The scan rate is 0.05 V/s. No charge injection into the system is seen.

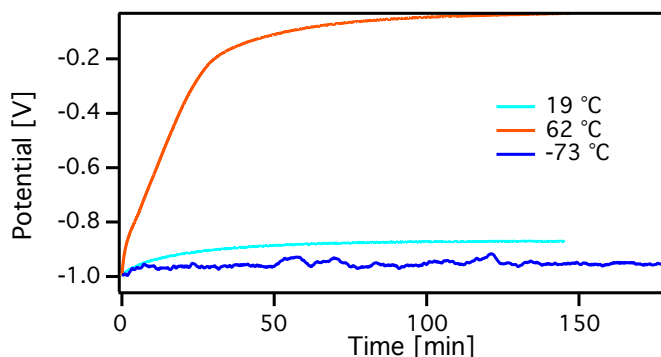


**Figure A3.8** Fermi-level stability measurements performed on ZnO QD films in 0.1 M LiClO<sub>4</sub> succinonitrile solution at different temperatures.

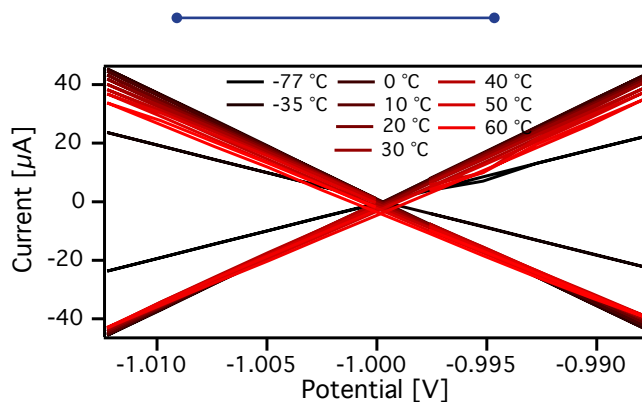


**Figure A3.9** Source-drain electronic conductance measurements at different temperatures. The measurements were performed on a ZnO QD film in 0.1 M LiClO<sub>4</sub> succinonitrile solution. The graph shows CVs for WE1 and WE2. The potential of WE1 is scanned  $\pm 10$  mV around a fixed potential of WE2.

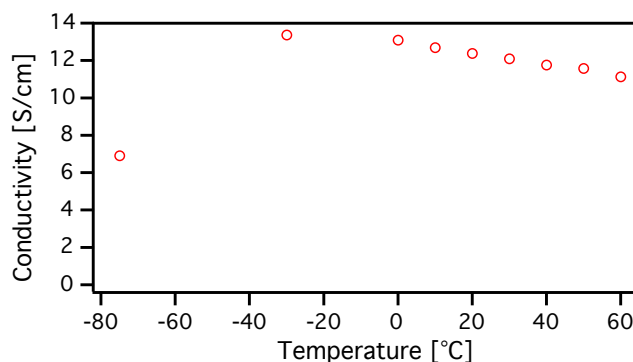


**Figure A3.10** Source-drain conductivity measurements for a ZnO QD film on an IDE at different temperatures derived from the CVs in Figure A3.9. The potential of WE1 was scanned  $\pm 10$  mV around the fixed potential of WE2.

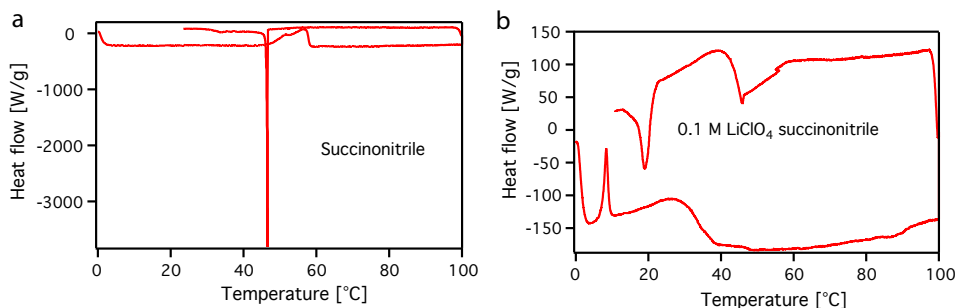


**Figure A3.11** Differential scanning calorimetry measurements performed on a) succinonitrile solution b) 0.1 M  $\text{LiClO}_4$  succinonitrile solution. In both measurements the scan is started at 0 °C and scanned to 100 °C. At 100 °C the scan is reversed.

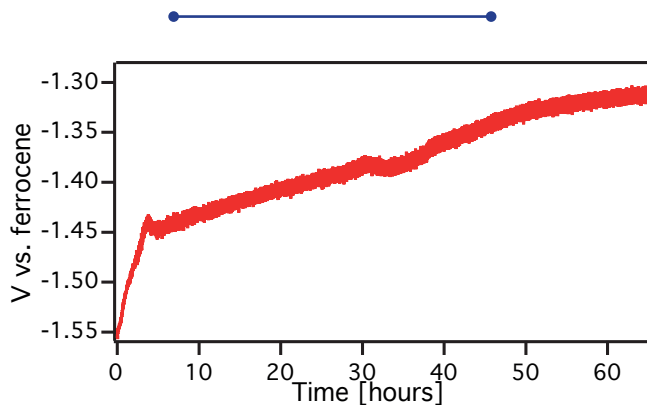


**Figure A3.12** Fermi-level stability measurement for a ZnO QD film in  $\text{LiClO}_4$  PEG 4000 solution.

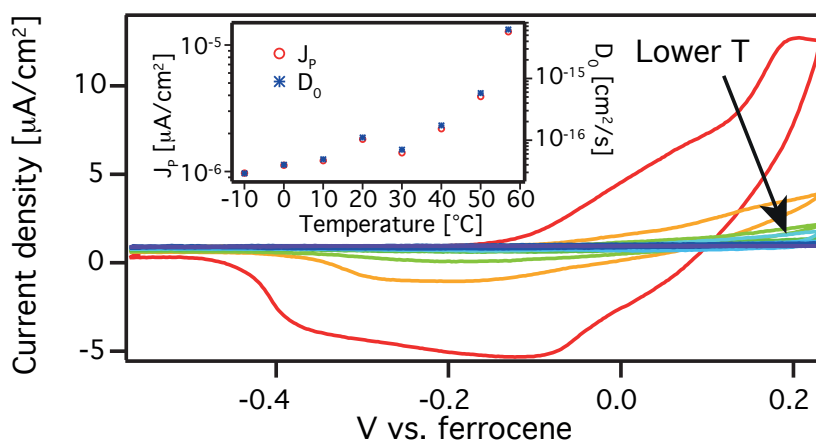


**Figure A3.13** CVs for a P3DT film in 11 wt%  $\text{LiClO}_4$  PEG 6000 performed at temperatures between -10 and 57 °C. The figure includes an inset containing the peak current density,  $J_p$ , and the calculated  $\text{Li}^+$  diffusion coefficient,  $D_0$ , versus the temperature.

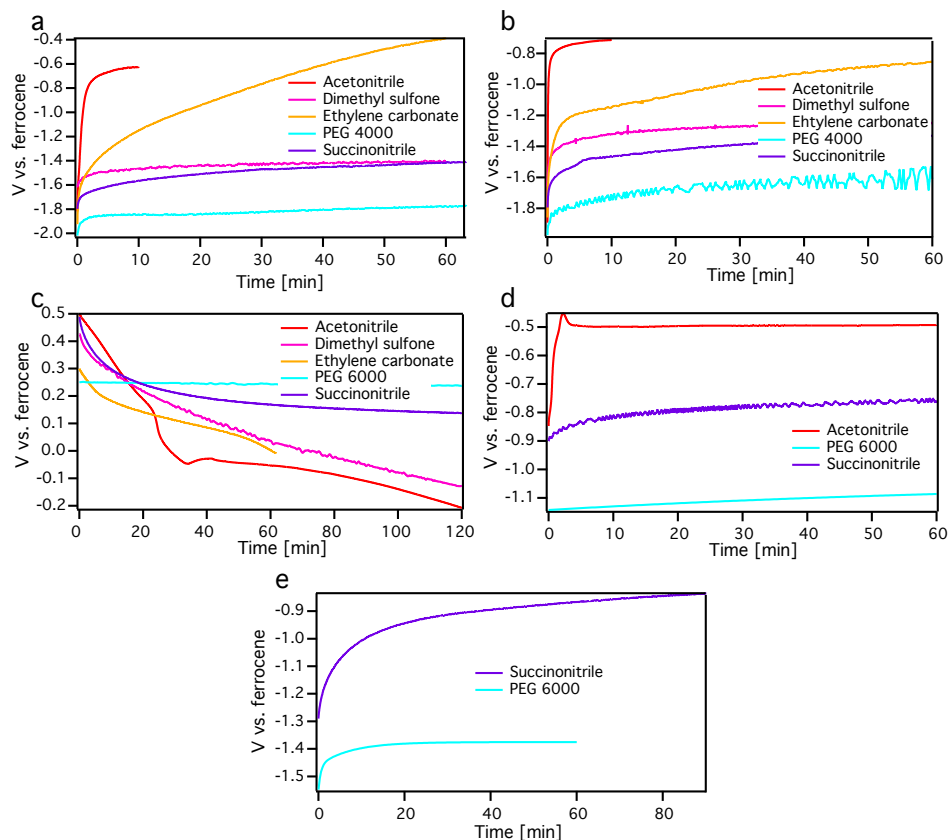


**Figure A3.14** Fermi-level stability measurements for different semiconductor films. (a) CdSe QD film, (b) CdSe/CdS QD film, (c) P3DT film, (d) PCBM film and (e)  $C_{60}$  film in  $LiClO_4$  electrolyte solution at room temperature.

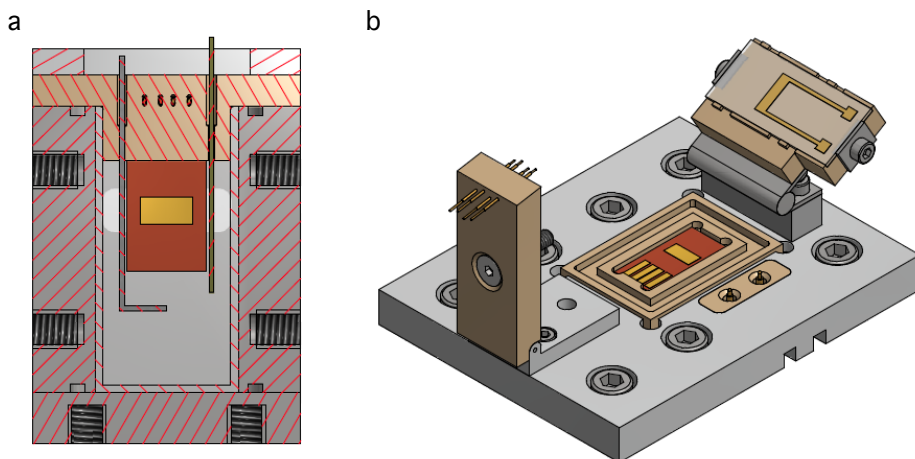


**Figure A3.15** The two used electrochemical cells. (a) The cuvette cell includes a commercial cuvette containing the electrolyte solution that is placed into a metal holder. A cap containing the sample on a WE, the RE and the CE fits in the cuvette. (b) The flat cell includes a well, made out of PEEK which is inert to most chemicals. The WE is placed in the well with the sample on top. Electrical contacts are made to the WE with four gold pogo pins. The solvent is placed on top of the sample and a substrate with the RE and the CE is placed on top of the solvent. The CE and the RE make contact with two gold pogo pins at the base of the cell. The figure is a courtesy of Youp van Goozen.

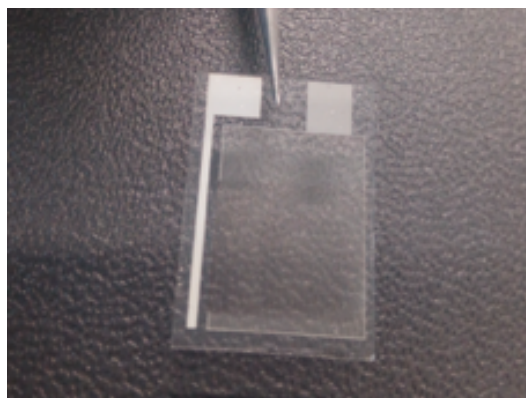


**Figure A3.16** The home-built RE and CE substrate for the flat cell setup. The Ag pseudo-reference electrode is made by a shadow mask while the Pt mesh CE is made by optical lithography. The mesh allows absorbance measurements during electrochemical measurements.



# 4



## Enhancing the stability of the electron density in electrochemically doped ZnO quantum dots

---

In Chapter 3, various electrolyte solvents with melting points above room temperature were investigated in order to gain a stable electrochemically doped semiconductor film at room temperature. Unfortunately, in all cases injected charge gradually left the films. While there are multiple possible causes for this, we demonstrate in this chapter, using n-doped ZnO quantum-dot films of variable thickness that the dominant mechanism is reduction of solvent impurities by the injected electrons. We subsequently investigate two different ways to enhance the doping stability of ZnO QD films. The first method uses pre-emptive reduction of the solvent impurities; the second method involves a solid covering the QD film, which hinders impurity diffusion to the film. Both methods enhance the doping stability of the QD films greatly.

## 4.1 Introduction

Electrochemical doping provides a controlled way of changing the charge carrier density of semiconductor materials. So far, (spectro)-electrochemical measurements have been mainly used as an analytical tool<sup>1-3</sup> for a wide range of semiconductor materials,<sup>4-8</sup> but electrochemistry can also be a powerful method to permanently dope porous semiconductor films. In electrochemical doping, the semiconductor material is deposited on a working electrode (WE) and placed in an electrochemical cell. By changing the potential between the WE and a reference electrode (RE), electrons can be injected into or extracted from the semiconductor film. That is, the Fermi-level and the charge carrier density of the semiconductor film can be tuned by changing the potential.<sup>2,9</sup> The requirement for efficient electrochemical doping is that counterions, that compensate the charge of injected electrons/holes, can diffuse into the material and result in 3D charge compensation.

Electrochemical doping has predominantly been used for conducting polymers.<sup>10</sup> A notable example is that of the Light Emitting Electrochemical cell, wherein a potential difference on a planar two-electrode electrochemical cell results in the in situ formation of a p-i-n junction which exhibits light emission in the i region.<sup>11-12</sup> Electrochemical doping has also been applied to films of semiconductor nanocrystals,<sup>2,4,13-15</sup> fullerenes<sup>16</sup> and carbon nanotubes.<sup>17</sup>

However, stable electrochemical doping has not been achieved, as when the electrochemical cell is disconnected from the potentiostat, the injected charges spontaneously leave the semiconductor film.<sup>2,9,12,18</sup> The loss of injected charges can be caused by either electrochemical reactions of the material itself<sup>2,19-21</sup> or by solvent impurities.<sup>22</sup> It is known that impurities can affect doping stability greatly.<sup>23-24</sup> Gamelin et. al showed that by exposing n-doped nanocrystals to air or other appropriate oxidants, the injected charge was removed and the nanocrystals returned to their original oxidation state.<sup>25-26</sup> Additionally, solvent impurities do not only affect electrochemical doping of the material, they can also induce a large variation in electrochemical measurements.<sup>27-29</sup> It is highly desirable to increase the stability of electrochemically injected charge carriers, so that this technique could be used to prepare active and stable junctions in devices such as light emitting diodes.

In this chapter we investigate the electrochemical doping stability of ZnO QDs in anhydrous acetonitrile solution dried over an activated alumina column (Innovative Technology PureSolv Micro, water content around 5 ppm without 0.1 M LiClO<sub>4</sub> and 11.8 ppm with 0.1 M LiClO<sub>4</sub> measured by Karl-Fischer titration), performed in a nitrogen filled glovebox (oxygen  $\leq 0.1$  ppm and moisture  $\leq 0.5$  ppm). Even under these conditions, it is observed that injected electrons gradually leave the conduction band of the QDs after disconnecting the electrochemical cell. We find that the apparent charge stability is a strong function of ZnO QD film thickness. This implies that solvent impurities, rather than electrochemical reactions in the ZnO QD films, are the dominant cause of the decay of the charge density. Next, we sought methods to eliminate the effect of solvent impurities on the charge stability, by reducing any eventual impurity oxidant before electrochemical doping or by covering the film with a solid film of succinonitrile that prevents impurity diffusion. We

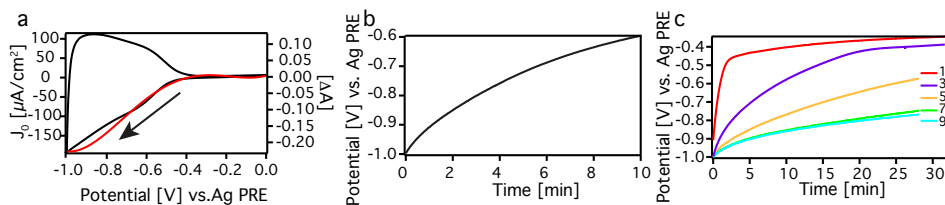


**Figure 4.1 Spectro-electrochemical measurements performed on ZnO QD films in 0.1 M LiClO<sub>4</sub> acetonitrile solution.** a) CV (shown in black) measured at 0.05 V/s, the arrow indicates the scan direction. The graph includes the differential band edge absorbance,  $\Delta A$  (shown in red).  $J_0$  stands for the current density. The sample is made of 3 drop casting steps. b) Fermi-level stability measurement of a ZnO QD film. Before the CE was disconnected the potential was kept at -1.0 V until equilibrium was reached. When the injected electrons leave the QDs, the Fermi-level drops which corresponds to an increase in potential. The sample is made of 3 drop casting steps c) Fermi-level stability measurement for ZnO QD films of different thicknesses. The films were made of 1, 3, 5, 7 and 9 drop casting steps of QD solution. Measured profilometry thicknesses are shown in Appendix, Table A4.1. By increasing the film thickness, the doping stability increases.

show that by using either electrochemical or chemical reduction of the solvent impurities, the doping stability of the doped ZnO QD film increases immensely. When the electrolyte solvent is exposed to a reducing potential (-1.0 V vs. Ag pseudo reference electrode) this results in an 18-fold increase in doping stability, as determined with Fermi-level stability measurements. Chemical reduction of the solvent impurities is achieved by addition of super hydride, Li[Et<sub>3</sub>BH]. This greatly improves the doping stability of the ZnO QDs, by about a factor 100.

Both approaches are effective, but only for a limited time, as more oxidants will inevitably diffuse into the doped film. To prevent this we have used succinonitrile as an alternative solvent with a melting point of 57 °C. After charging at 60 °C the film is quickly removed from the solvent and treated in various ways. This leads to the quick solidification of the succinonitrile and the formation of a protective thin solid film around the doped ZnO QDs. In the best cases the loss of injected charge density is around 4% after 2 hours. These results demonstrate possible avenues for enhancing the stability of electrochemically injected charges in semiconductor films.

## 4.2 Results and Discussions

### 4.2.1 Electrochemical doping of ZnO QD films

Figure 4.1a shows a cyclic voltammogram (CV) and the differential absorbance at the band edge (360 nm) for a ZnO QD film in 0.1 M LiClO<sub>4</sub> acetonitrile solution. The 2D plot of the differential absorbance is shown as Figure A4.1 in the Appendix. The scan starts at 0 V vs. a Ag pseudoreference electrode (PRE), which corresponds to a Fermi level in the bandgap of the ZnO QD film. At around -0.5 V the current becomes more negative and the band edge absorbance decreases due to state filling, which shows that electrons are injected into the conduction band of the QDs.<sup>30</sup> From the measured current,  $I$ , it is possible to calculate of total amount of injected (or extracted on the reverse scan) electrons with Equation 4.1:

$$n_e = \sum \frac{(I * dE)}{v * e * V} \quad 4.1$$

Where  $dE$  is the potential step (here 0.00244 V),  $v$  is the scan rate (here 50 mV/s),  $e$  is the elementary charge and  $V$  is the film volume. By the use of Equation 4.1, we find that the charge density is increased to  $2.24 \times 10^{18} \text{ cm}^{-3}$  at -1.0 V. The ratio between extracted and injected electrons is 0.856 for the measurement in Figure 4.1a. This means that almost 15% of injected electrons are not extracted in the return scan. To investigate this loss of electrons in more detail, so-called Fermi-level stability measurements are performed (Figure 4.1b). In this experiment, the potential is changed to -1.0 V, at which point the counter electrode (CE) is disconnected and the potential of the working electrode (WE) vs. the pseudo reference electrode (PRE) is recorded. If electrons leave the system the potential returns to the original open circuit potential ( $V_{oc}$ , around 0 V). The same trend is also seen from the change in differential absorbance during the Fermi-level stability measurements (Appendix, Figure A4.2). Fig. 4.1b shows that in only 10 minutes the potential increases by about 0.4 V. From the not fully reversible CV and the Fermi-level stability measurement it is clear that many injected electrons are lost.

As previously discussed<sup>31</sup>, we consider three possible reasons for electrons leaving the quantum dot film. First, electrochemical reactions can occur within the material itself.<sup>2, 32-34</sup> For instance, surface  $\text{Zn}^{2+}$  ions on the QDs could potentially reduce to  $\text{Zn}^0$ .<sup>35</sup> Second, counter ions could move out of the film. Such counter ion movement is especially expected in devices where an electric field is present<sup>10</sup>; however in the present experiments such an electric field is not expected to be present. Third, solvent impurities such as water or molecular oxygen can react with injected electrons. Indeed, when similar measurements are performed outside of the glovebox, it leads to much less symmetric CVs (Appendix, Figure A4.3).

To test which mechanism is responsible for the observed spontaneous drop of the Fermi level we performed measurements on films of varying thickness. Increasing the film thickness implies that, for a fixed amount of impurities, the relative change of the electron concentration in the ZnO QD film is smaller. Hence, if solvent impurities are responsible for the electron loss, then increasing the film thickness should improve the doping stability. However, if electrochemical reactions within the ZnO QDs are responsible, increasing the thickness will not help.

Fermi-level stability measurements were performed on ZnO QD films of different thicknesses in a fresh electrolyte solution of the same volume from the same batch of electrolyte solution (Fig 4.1c). The films were made by increasing the number of drop casted steps. To verify the increasing thickness, CVs and profilometer measurements were performed (Appendix, Figure A4.4 and Table A4.1). Figure 4.1c shows that increasing the film thickness indeed leads to a much slower drop of the Fermi level. As the films are highly porous and the solvent permeates throughout the film,<sup>30</sup> this shows that electron extraction is predominantly caused by impurities in the electrochemical environment.

### 4.2.2 Cathodic preconditioning

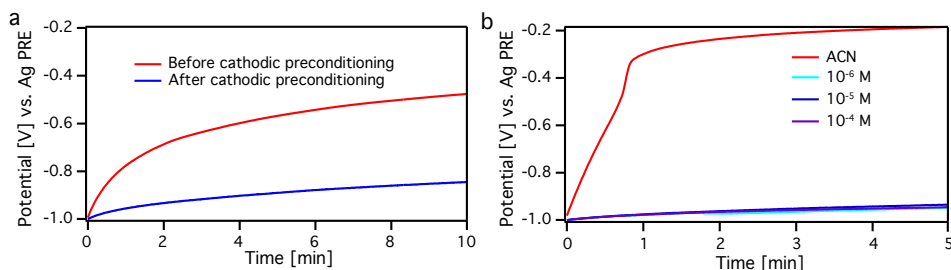


**Figure 4.2 Impurities are reduced in a 0.1 M LiClO<sub>4</sub> acetonitrile (ACN) electrolyte solution.**

a) Fermi-level stability measurements for a ZnO QD film on an ITO before and after a cathodic preconditioning of -1.0 V was applied to the electrolyte solution (with a bare ITO for two hours). b) Fermi-level stability measurements performed with different concentration of Li[Et<sub>3</sub>BH] ranging from 10<sup>-6</sup> to 10<sup>-4</sup> M. By performing a cathodic preconditioning step or by adding super hydride to the solution, the doping stability increases greatly.

To prevent impurities from oxidizing the QDs, it should be possible to reduce them before they react with injected electrons. One way of reducing the solvent impurities is by applying a negative potential to the solution before the measurements with the ZnO QD film, that is by using a cathodic preconditioning. Figure 4.2a shows Fermi-level stability measurements before and after applying the cathodic preconditioning of -1.0 V to the electrolyte solution for two hours. When applying the potential, a bare ITO is used to make sure no changes occur to the ZnO QD film. Without cathodic preconditioning of the electrolyte solution, it takes 32 seconds to get a potential decay of 0.15 V while the same change in potential takes 10 minutes after the solvent preconditioning. This can be seen, somewhat arbitrarily, as an 18-fold increase in doping stability. However, if the electrochemical cell is disconnected from the potentiostat for about four hours between the measurements, the potential decay is again similar to original values (Appendix, Figure A4.5). We tentatively conclude that only a part of the solution is reduced during the treatment. We consider that reduced impurities may again be oxidized at the counter electrode, causing the electrolyte solution to reestablish equilibrium over a couple of hours.

#### 4.2.3 Reducing agent

A supposedly irreversible way<sup>36</sup> of reducing the impurity atoms is by using super hydride, Li[Et<sub>3</sub>BH].<sup>25-26, 36</sup> Upon oxidizing, Li[Et<sub>3</sub>BH] decomposes into hydrogen gas and triethylborane, therefore the reversed reaction does not take place at the same potential.<sup>37-38</sup> Figure 4.2b shows Fermi-level stability measurements for a ZnO QD film in 0.1 M LiClO<sub>4</sub> acetonitrile solution with a concentration of Li[Et<sub>3</sub>BH] ranging from 10<sup>-6</sup> to 10<sup>-4</sup> M. Higher concentrations of super hydride caused sample instability for the ZnO QD film. Both the open circuit potential and the absorbance of the film were measured when the super hydride was added to the acetonitrile solution to make sure that the super hydride did not reduce the ZnO QDs. No bleach and no significant change in the open circuit potential were seen during the addition (see Appendix, Table A4.2). For reference, a Fermi-level stability measurement was performed on the sample before the addition of the Li[Et<sub>3</sub>BH] to the acetonitrile solution.

Adding a small amount of  $\text{Li}[\text{Et}_3\text{BH}]$  greatly increases the doping stability. Before the addition of super hydride, it takes 3 seconds for the potential to reach a decay of 0.05 V, while it takes around 5 minutes after the addition of super hydride. As before, somewhat arbitrarily, this can be seen as a 100-fold increase in doping stability. Increasing the concentration from  $10^{-6}$  to  $10^{-4}$  M improves the stability only marginally.

To quantify the increased doping stability, CVs were performed at every concentration of added  $\text{Li}[\text{Et}_3\text{BH}]$  (Appendix, Figure A4.6). From the CVs the ratio between injected and extracted electrons is calculated and shown in Table 4.1. Without super hydride 89.8% of injected electrons are extracted. This charging/discharging ratio increases to 98.7% for  $10^{-4}$  M super hydride. Thus,  $\text{Li}[\text{Et}_3\text{BH}]$  is able to reduce most solvent impurities which leads to increased charge stability during CVs and Fermi-level stability measurements. However, a small amount of electrons is still lost. This might be due to internal electrochemical reactions of the ZnO QDs themselves or it is possible that residual oxygen or water, or perhaps other impurities, from the glovebox environment diffuse into the electrolyte, making it impossible to remove all impurities.

#### 4.2.4 Solid diffusion barrier

In all experiments so far, the doped ZnO QD film remained submerged in the electrolyte solvent. This is necessary for the Fermi level stability measurements. However, since it appears that impurities in the solvent are dominant in the drop of the charge density it would be interesting to see the charge stability in absence of the electrolyte. To facilitate this we have performed source-drain conductivity experiments vs. time. A ZnO QD film on an interdigitated source-drain electrode is charged, so that the conductance increases strongly. Subsequently the CE is disconnected and the source drain conductance is measured with a Keithly 2400 source meter. This can also be done after the film is removed from the electrochemical cell and is no longer in contact with electrolyte. A decrease in conductance means that the electron density decreases.

Four different conductance measurements were performed on the same ZnO QD film: in an acetonitrile solution, in an acetonitrile solution containing  $10^{-3}$  M super hydride, on a dry film (after the film was taken out of the solution) and on a film dried in vacuum after charging, but before the conductance measurements. As the conductance measurements are not started at exactly the same time after disconnecting the electrochemical cell, the initial conductance varies slightly. Therefore, the normalized results are shown in Figure 4.3a (the original traces are in Appendix, Figure A4.7).

Clearly the quickest decay of the conductance is observed for the film in acetonitrile solution. We note that the conductance in Fig. 4.3a drops more rapidly than the potential in Fig. 4.2 because the potential scales logarithmically with electron density (through the Nernst law), while the conductivity,  $\sigma$ , (and hence also the conductance) scales approximately linearly with the electron density (via  $\sigma = ne\mu$ , where  $n$  is the electron density,  $e$  is the electron charge and  $\mu$  is the electron mobility). As the mobility decreases rapidly with decreasing electrochemical potential in the bandgap,<sup>30</sup> the drop in conductivity is further enhanced.

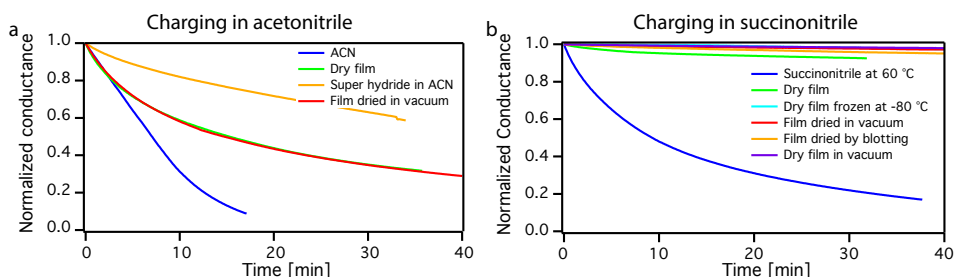


**Figure 4.3 Conductance measurements after charge injection for a ZnO QD film.** a) Measurements performed in 0.1 M  $\text{LiClO}_4$  acetonitrile solution (ACN) (blue), acetonitrile solution with the addition of super hydride (yellow), film taken out of the solution (dry film, green) or for a film dried in vacuum for one minute (red). b) Measurements performed in 0.1 M  $\text{LiClO}_4$  succinonitrile solution at 60 °C (blue), dry film (green), after the sample was blotted with a filter paper (yellow), after the sample was stored under vacuum for one minute (red), after the sample was plunged into THF at -80 °C (cyan) and film measured in vacuum (purple).

Figure 4.3a shows that by taking the film out of the solution the conductance decays more slowly. Additionally, the doping stability of the ZnO QD film does not increase by drying it in vacuum for a minute. Interestingly, the best stability is gained by measuring the conductance in an acetonitrile solution containing super hydride. This suggests that the super hydride treated acetonitrile solution contains less contaminants than the glovebox environment. This also implies that on longer timescales diffusion of impurities from the glovebox environment into the solution may cause the stability to decrease again. Therefore, it is important to avoid diffusion of impurities to the film altogether.

One way to reduce impurity diffusion is to cover the film with a solid protective layer. A convenient way to achieve this is by using an electrolyte solvent that is solid at room temperature. An example is succinonitrile, which is similar in electrochemical stability to acetonitrile, but has a melting point of 57 °C. Therefore, we performed source-drain conductivity measurements on a ZnO QD film measured in 0.1 M  $\text{LiClO}_4$  succinonitrile solution. The film is charged at 60 °C, above the melting point of succinonitrile. After the film is charged at -1.0 V, the CE is disconnected and the film is taken out of the solution. As the sample cools to room temperature, the succinonitrile covering the film solidifies quickly and the source-drain conductance is measured. A CV for a ZnO QD film measured in 0.1 M  $\text{LiClO}_4$  in succinonitrile at 70 °C is shown in Appendix, Figure A4.8.

Figure 4.3b shows the normalized conductance measurements for a ZnO QD film measured in succinonitrile at 60 °C and on a dry film (the original traces are in Appendix, Figure A4.9). A few different measurements were performed on dry films, that is when the film is not in the solution. Firstly, conductance measurements were performed on the film directly after it was taken out of the solvent. Secondly, to minimize the amount of solvent around the film, the film was either blotted by a filter paper or placed under a vacuum for 1 minute. Thirdly, to ensure that the succinonitrile is completely solid, the film was plunged into THF at -80 °C for 10 seconds before the measurement (the conductance was measured at room temperature) and finally the conductance was measured when the film

was under vacuum. The vacuum measurements were performed by placing the sample in a metal tube with electrical feedthroughs, which was connected to a Varian Tri Scroll vacuum pump.

By comparing Figure 4.3a and b it is clear that the charge stability of dry ZnO QD films is a lot better when succinonitrile is used. We attribute this to much reduced impurity diffusion in the solid succinonitrile that covers the film. In Fig. 4.3b dry films show much improved stability compared to the one in liquid succinonitrile at 60 °C. Appendix Figure A4.10 shows a zoom in on the dry films to highlight the differences between them. Of the dry films, the film that was simply taken out of the cell (“dry film”, green line) shows the quickest drop in conductance. By decreasing the amount of succinonitrile (and consequently the total amount of solvent impurities) by either blotting or placing the film under vacuum for one minute, the charge density becomes more stable. The stability increases even further by plunging the film in THF at -80 °C for a short time, allowing the solidification of succinonitrile to occur faster. The best results are obtained when measuring the ZnO QD film with a solid succinonitrile layer around it in vacuum. After a 2 hour measurement the conductance has decreased by about 4 %. Apparently, even if a solid layer is around the ZnO QD film, and the whole sample is in vacuum, the conductance is not completely stable. It might be that succinonitrile is not solid in the nanopores of the QD film<sup>31</sup> or that internal electrochemical reactions of the ZnO QDs are taking place.<sup>35</sup> Despite of the remaining slow decay of the conductance, the doping stability of ZnO QDs is enhanced enormously in solid succinonitrile.

### 4.3 Conclusions

In summary, we have shown by measuring ZnO QD films of different thicknesses that the instability of the charge density in electrochemically doped ZnO QDs films is predominantly due to oxidation by solvent impurities, even under very stringent air and water free conditions. We used two different methods to decrease the influence of solvent impurities on the doping stability. The first one includes reducing the solvent impurities, either electrochemically or chemically, while the second one employs a solid layer covering the ZnO QD film. Using a cathodic preconditioning of the electrolyte solution, we obtained an 18-fold increase of the doping stability. However, after waiting several hours the stability return to its original value. Addition of super hydride Li[Et<sub>3</sub>BH] results in a 100-fold increase in the doping stability. Furthermore, by reducing the solvent impurities the CVs became more reversible. The largest increase in doping stability was obtained by removing the film, after charging it, from a warm succinonitrile solution. The succinonitrile solidifies and forms a solid protective layer around the sample that prevents impurity diffusion. In the best case the charge density decreased by only 4% over the duration of 2 hours. These results increase our understanding in the instability of electrochemically doped semiconductor films. Therefore, by successful protecting of the doped film against impurities such as oxygen, the doping stability will increase immensely.

### 4.4 Methods

**Materials.** Zinc acetate dihydrate ( $\text{Zn}(\text{CH}_3\text{COO})_2 \cdot 2\text{H}_2\text{O}$  reagent grade), potassium hydroxide (KOH pellets), Indium-doped Tin Oxide substrates (ITO), lithium perchlorate ( $\text{LiClO}_4$ , 99.99%), ferrocene (Fc, 98%), anhydrous solvents (acetonitrile, 99.99%, tetrahydrofuran (THF), 99.9%, methanol, 99.8%,

ethanol (max 0.01% H<sub>2</sub>O), hexane, 95%), succinonitrile (99%) and super hydride, (1 M Li[Et<sub>3</sub>BH] in THF). All chemicals were purchased from Sigma Aldrich unless stated otherwise. Acetonitrile and THF were dried before use in an Innovative Technology PureSolv Micro column. All other chemicals were used as received.

**ZnO QD synthesis and film preparation.** The ZnO QDs were synthesized as previously described.<sup>30</sup> 3.425 mmol of zinc acetate dihydrate was combined with 50 mL ethanol in an Erlenmeyer flask at 60 °C. In the meantime, 6.25 mmol KOH was mixed with 5 mL methanol in a vial. When both mixtures were clear, the KOH mixture was added dropwise (approximately 1 drop per second) to the Erlenmeyer flask. After the addition of KOH, the heat source was removed after one additional minute. The ZnO QDs were purified by the addition of hexane and isolated by centrifugation at 2000 rpm for 1 minute. The QDs were redissolved in ethanol and stored at -20 °C to avoid further growth by Ostwald ripening. The ZnO QDs were drop casted either on an ITO or on a home-made interdigitated gold electrode and annealed at 60 °C for an hour. The diameter of synthesized QDs was calculated as 3.6 nm by using the empirical correlation from Meulenkamp.<sup>39</sup>

**Electrochemical measurements.** All electrochemical measurements were performed in a N<sub>2</sub> filled glovebox with an Autolab PGSTAT128N potentiostat. A 3-electrode electrochemical cuvette cell was used, where the sample was deposited on the working electrode (WE). The WE was either an ITO or IDE, and was immersed into 0.1 M LiClO<sub>4</sub> acetonitrile or succinonitrile solution. The solution also contains a Ag wire as a pseudo reference electrode (PRE) and a Pt sheet as a counter electrode (CE). The PRE was calibrated with a ferrocene/ferrocenium couple and its potential was found to be constant at -4.76 eV vs. vacuum.

**Cyclic voltammetry measurements (CVs).** Every CV was performed at 0.05 V/s. The measurements were performed between 0 V and -1.0 V and reversed.

**Fermi-level stability measurements.** Fermi-level stability measurements were performed after charge injection into the conduction band of the QDs took place. When the system had reached an equilibrium, the CE was disconnected from the RE and the WE. By doing so, no more electrons could be injected into the QDs. The change in potential between the WE and the RE was measured vs. time. This potential is connected to the Fermi-level of the WE vs. the Fermi-level of the RE. If electrons leave the conduction band of the QDs the Fermi-level will drop, which leads to an increase in the measured potential.

**Conductance measurements.** Conductance measurements were performed on an IDE after electron injection into the conduction band of the QDs took place. When the system had reached an equilibrium the potentiostat was disconnected and the conductance was measured with a Keithly 2400 source meter. After the sample is disconnected from the potentiostat, no electrons can be injected into the conduction band of the QDs. The source-drain potential difference used was 10 mV.

## References

1. Boehme, S. C.; Azpiroz, J. M.; Aulin, Y. V.; Grozema, F. C.; Vanmaekelbergh, D.; Siebbeles, L. D.; Infante, I.; Houtepen, A. J., Density of Trap States and Auger-mediated Electron Trapping in CdTe Quantum-Dot Solids. *Nano Lett.* 2015, 15 (5), 3056-66.
2. Guyot-Sionnest, P., Charging colloidal quantum dots by electrochemistry. *Microchim. Acta* 2008, 160 (3), 309-314.
3. Hoyer, P.; Eichberger, R.; Weller, H., Spectroelectrochemical Investigations of Nanocrystalline ZnO Films. *Ber. Bunsenges. Phys. Chem* 1993, 97, 630-635.
4. Boehme, S. C.; Vanmaekelbergh, D.; Evers, W. H.; Siebbeles, L. D. A.; Houtepen, A. J., In Situ Spectroelectrochemical Determination of Energy Levels and Energy Level Offsets in Quantum-Dot Heterojunctions. *J. Phys. Chem. C* 2016, 120 (9), 5164-5173.
5. van der Stam, W.; Gudjonsdottir, S.; Evers, W. H.; Houtepen, A. J., Switching between Plasmonic and Fluorescent Copper Sulfide Nanocrystals. *J. Am. Chem. Soc.* 2017, 139 (37), 13208-13217.
6. van der Stam, W.; de Graaf, M.; Gudjonsdottir, S.; Geuchies, J. J.; Dijkema, J. J.; Kirkwood, N.; Evers, W. H.; Longo, A.; Houtepen, A. J., Tuning and Probing the Distribution of Cu(+) and Cu(2+) Trap States Responsible for Broad-Band Photoluminescence in CuInS<sub>2</sub> Nanocrystals. *ACS Nano* 2018, 12 (11), 11244-11253.
7. ECHEGOYEN, L.; ECHEGOYEN, L. E., Electrochemistry of Fullerenes and Their Derivatives. *Acc. Chem. Res.* 1998, 31, 593-601.
8. Braunger, M. L.; Barros, A.; Ferreira, M.; Olivati, C. A., Electrical and electrochemical measurements in nanostructured films of polythiophene derivatives. *Electrochim. Acta* 2015, 165.
9. Shim, M.; Wang, C.; Norris, D. J.; Guyot-Sionnest, P., Doping and Charging in Colloidal Semiconductor Nanocrystals. *MRS Bull.* 2001, 26 (12), 1005-1008.
10. Pei, Q.; Yu, G.; Zhang, C.; Yang, Y.; Heeger, A. J., Polymer Light-Emitting Electrochemical Cells. *Science* 1995, 269, 1086-1088.
11. Matyba, P.; Maturova, K.; Kemerink, M.; Robinson, N. D.; Edman, L., The dynamic organic p-n junction. *Nat. Mater.* 2009, 8 (8), 672-6.
12. Pei, Q.; Yang, Y.; Yu, G.; Zhang, C.; Heeger, A. J., Polymer Light-Emitting Electrochemical Cells: In Situ Formation of a Light-Emitting p-n Junction. *J. Am. Chem. Soc.* 1996, 118 (16), 3922-9.
13. Yu, D.; Wang, C.; Wehrenberg, B. L.; Guyot-Sionnest, P., Variable range hopping conduction in semiconductor nanocrystal solids. *Phys. Rev. Lett.* 2004, 92 (21), 216802.
14. Houtepen, A. J.; Kockmann, D.; Vanmaekelbergh, D., Reappraisal of Variable-Range Hopping in Quantum-Dot Solids. 2008, Vol. 8 (10), 3516-3520.
15. Boehme, S. C.; Wang, H.; Siebbeles, L. D. A.; Vanmaekelbergh, D.; Houtepen, A. J., Electrochemical charging of CdSe quantum dot films: Dependence on voids size and counterion proximity. *ACS Nano* 2013, 7 (3), 2500-2508.
16. Jehoulet, C.; Bard, A. J., Electrochemical Reduction and Oxidation of C<sub>60</sub> Films. *J. Am. Chem. Soc.* 1991, 113, 5457-5459.
17. Gooding, J. J., Nanostructuring electrodes with carbon nanotubes: A review on

- electrochemistry and applications for sensing. *Electrochim. Acta* 2005, 50 (15), 3049-3060.
18. Gao, J.; Yu, G.; Heeger, A. J., Polymer light-emitting electrochemical cells with frozen p-i-n junction. *Appl. Phys. Lett.* 1997, 71 (10), 1293-1295.
  19. Gooding, A. K.; Gómez, D. E.; Mulvaney, P., The Effects of Electron and Hole Injection on the Photoluminescence of CdSe:CdS:ZnS Nanocrystal Monolayers. *ACS Nano* 2008, 2 (4), 669-676.
  20. van der Stam, W.; du Fosse, I.; Grimaldi, G.; Monchen, J. O. V.; Kirkwood, N.; Houtepen, A. J., Spectroelectrochemical Signatures of Surface Trap Passivation on CdTe Nanocrystals. *Chem. Mater.* 2018, 30 (21), 8052-8061.
  21. Gao, J.; Li, Y.; Yu, G.; Heeger, A. J., Polymer light-emitting electrochemical cells with frozen junctions. *J. Appl. Phys.* 1999, 86 (8), 4594-4599.
  22. Niu, J.; Conway, B. E.; Pell, W. G., Comparative studies of self-discharge by potential decay and float-current measurements at C double-layer capacitor and battery electrodes. *J. Power Sources* 2004, 135 (1-2), 332-343.
  23. Jacobs, I. E.; Moule, A. J., Controlling Molecular Doping in Organic Semiconductors. *Adv. Mater.* 2017, 29 (42).
  24. Lakhwani, G.; Roijmans, R. F. H.; Kronemeijer, A. J.; Gilot, J.; Janssen, R. A. J.; Meskers, a. S. C. J., Probing Charge Carrier Density in a Layer of Photodoped ZnO Nanoparticles by Spectroscopic Ellipsometry. *J. Phys. Chem. C* 2010, 114, 14804-14810.
  25. Schimpf, A. M.; Gunthardt, C. E.; Rinehart, J. D.; Mayer, J. M.; Gamelin, D. R., Controlling carrier densities in photochemically reduced colloidal ZnO nanocrystals: size dependence and role of the hole quencher. *J. Am. Chem. Soc.* 2013, 135 (44), 16569-77.
  26. Rinehart, J. D.; Schimpf, A. M.; Weaver, A. L.; Cohn, A. W.; Gamelin, D. R., Photochemical electronic doping of colloidal CdSe nanocrystals. *J. Am. Chem. Soc.* 2013, 135 (50), 18782-5.
  27. Barrosse-Antle, L. E.; Bond, A. M.; Compton, R. G.; O'Mahony, A. M.; Rogers, E. I.; Silvester, D. S., Voltammetry in room temperature ionic liquids: comparisons and contrasts with conventional electrochemical solvents. *Chem.--Asian J.* 2010, 5 (2), 202-30.
  28. Coetzee, J. F., Recommended Methods for Purification of Solvents and Tests for Impurities. Pergamon Press: Great Britain, 1982.
  29. Zoski, C. G., Handbook of Electrochemistry. 1st ed.; Elsevier B.V.: Netherlands, 2007.
  30. Gudjonsdottir, S.; van der Stam, W.; Kirkwood, N.; Evers, W. H.; Houtepen, A. J., The Role of Dopant Ions on Charge Injection and Transport in Electrochemically Doped Quantum Dot Films. *J. Am. Chem. Soc.* 2018, 140 (21), 6582-6590.
  31. Gudjonsdottir, S.; Stam, W. v. d.; Koopman, C.; Kwakkenbos, B.; Evers, W. H.; Houtepen, A. J., On the Stability of Permanent Electrochemical Doping of Quantum Dot, Fullerene, and Conductive Polymer Films in Frozen Electrolytes for Use in Semiconductor Devices. *ACS Applied Nano Materials* 2019.
  32. Zhao, J.; A, M.; Holmes; Osterloh, F. E., Quantum Confinement Controls Photocatalysis- A Free Energy Analysis for Photocatalytic Proton Reduction at CdSe Nanocrystals. *ACS Nano* 2013, 7 (5), 4316-4325.

33. Tsui, E. Y.; Carroll, G. M.; Miller, B.; Marchioro, A.; Gamelin, D. R., Extremely Slow Spontaneous Electron Trapping in Photodoped n-Type CdSe Nanocrystals. *Chem. Mater.* 2017, 29 (8), 3754-3762.
34. Tsui, E. Y.; Hartstein, K. H.; Gamelin, D. R., Selenium Redox Reactivity on Colloidal CdSe Quantum Dot Surfaces. *J. Am. Chem. Soc.* 2016, 138 (35), 11105-8.
35. du Fossé, I.; ten Brinck, S.; Infante, I.; Houtepen, A. J., Role of Surface Reduction in the Formation of Traps in n-Doped II–VI Semiconductor Nanocrystals: How to Charge without Reducing the Surface. *Chem. Mater.* 2019.
36. Wu, K.; Lim, J.; Klimov, V. I., Superposition Principle in Auger Recombination of Charged and Neutral Multicarrier States in Semiconductor Quantum Dots. *ACS Nano* 2017, 11 (8), 8437-8447.
37. Brown, H. C.; Kim, S. C.; Krishnamurthy, S., Selective Reductions. 26. Lithium Triethylborohydride as an Exceptionally Powerful and Selective Reducing Agent in Organic Synthesis. Exploration of the Reactions with Selected Organic Compounds Containing Representative Functional Groups. *J. Org. Chem.* 1980, 45 (1), 1-12.
38. Bard, A. J.; Faulkner, L. R., *Electrochemical methods. Fundamentals and applications*. 2nd ed.; John Wiley & sons, INC.: New York, United states of America, 2001.
39. Meulenkamp, E. A., Synthesis and Growth of ZnO Nanoparticles. *J. Phys. Chem. B* 1998, 102 (29), 5566–5572.

## Appendix

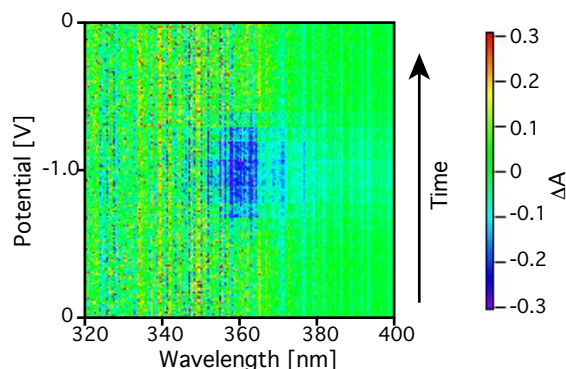


**Figure A4.1** Spectro-electrochemical measurement for a ZnO QD film in 0.1 M  $\text{LiClO}_4$  acetonitrile solution. The 2D plot shows the differential absorbance during a CV scan. The potential was scanned at 50 mV/s from 0 V to -1.0 V and reversed.

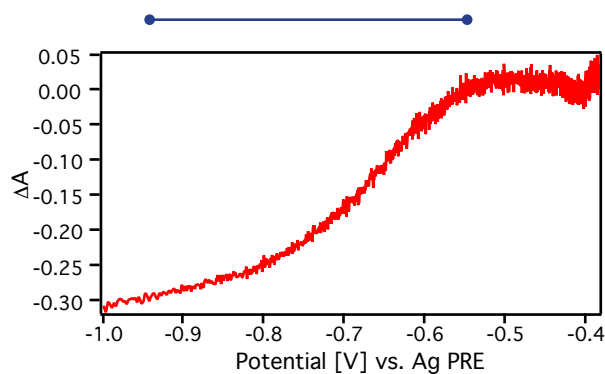


**Figure A4.2** Differential absorbance measurements during a Fermi-level stability measurements on a ZnO QD film. The graph shows the differential absorbance ( $\Delta A$ ) vs. potential. As the potential increases the bleach decreases which means that electrons are leaving the conduction band of the ZnO QDs.

### Profilometry measurements

Profilometry measurements were performed with a Veeco DekTak 8 stylus profiler. As the films are made by drop casting, they are not very smooth so the error in the measurement is high. Therefore each sample was measured 5 times and the average is shown in Table A4.1. Additionally, the thicker films have a higher error.

**Table A4.1** Average thickness in nm of the 5 films.

	1	3	5	7	9
Thickness	1867.56	4431.50	6362.56	6798.30	14268.19

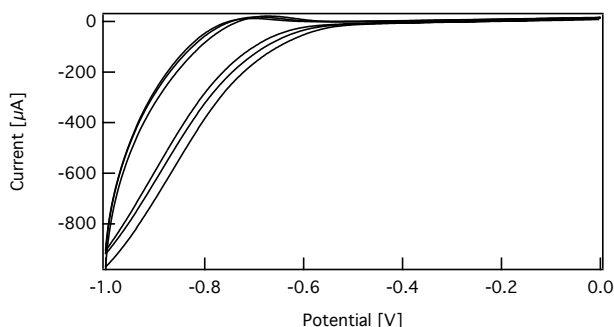


**Figure A4.3** CVs performed on a ZnO QD film measured in 0.1 M LiClO<sub>4</sub> acetonitrile solution in air. The CV was measured at a scan rate of 50 mV/s and includes three scans.

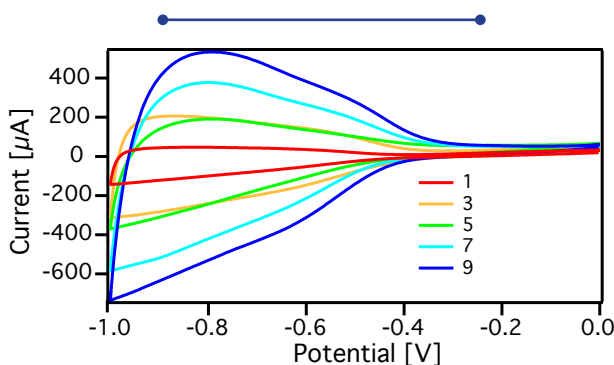


**Figure A4.4** CVs performed on ZnO QD films with different thicknesses in 0.1 M LiClO<sub>4</sub> acetonitrile solution. The numbers in legend indicate the number of QD drop casting steps used in making the films. As the film thickness increases, the current increases due to higher amount of injected electrons (the area of the films is the same).

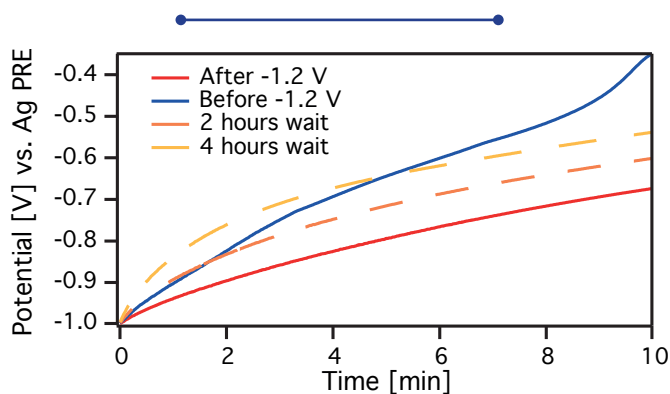


**Figure A4.5** Fermi-level stability measurements for a ZnO QD film on an ITO before, after a potential of -1.2 V was applied to the electrolyte solution (with a bare ITO for two hours) and after no potential has been applied for 2 and 4 hours (dashed lines). The measurements were performed in 0.1 M LiClO<sub>4</sub> acetonitrile solution. By applying a potential, the doping stability increases, but it returns close to its original value if no potential is applied to the solution for four hours.

**Table A4.2** The open circuit potential ( $V_{oc}$ ) for a ZnO QD film by addition of different concentration of super hydride ( $LiEt_3BH$ )

	ACN	$10^{-6}$ M	$10^{-5}$ M	$10^{-4}$ M
$V_{oc}$	-0.18	-0.18	-0.22	-0.05

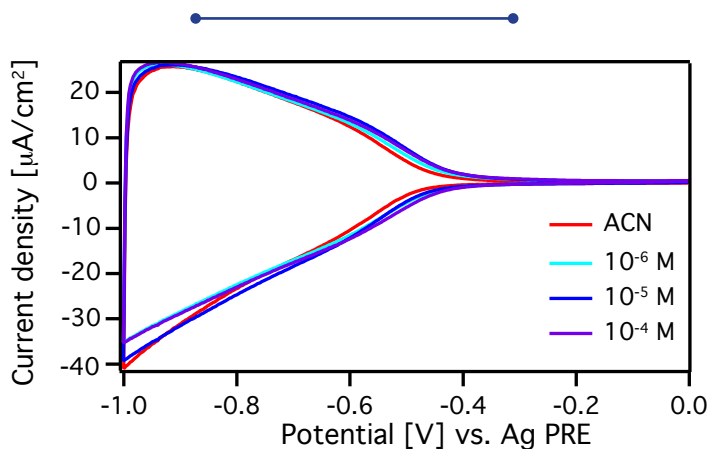


**Figure A4.6** CVs on a ZnO QD film performed in 0.1 M  $LiClO_4$  acetonitrile solution containing different concentration of  $Li[Et_3BH]$ .

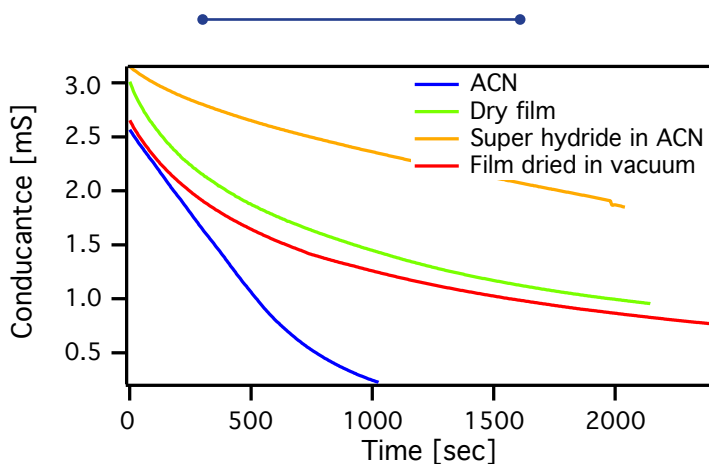


**Figure A4.7** Conductance measurements measured on the same ZnO QD film. Measurements in 0.1 M  $LiClO_4$  acetonitrile (ACN) solution (blue), acetonitrile solution containing super hydride (yellow), film taken out of the solution (dry film, green) and a film dried under vacuum for one minute (red).

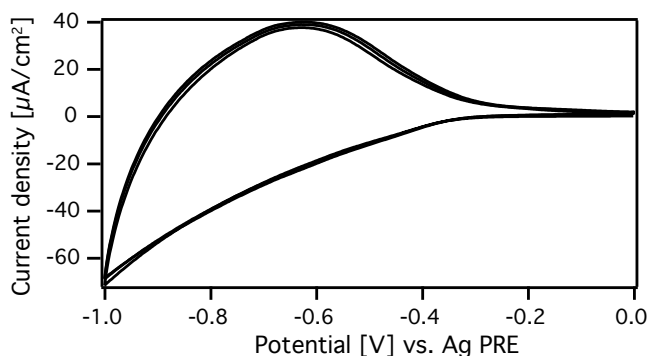


**Figure A4.8** CV of a ZnO QD film measured in 0.1 M LiClO<sub>4</sub> in succinonitrile at 70 °C. The scan rate is 50 mV/s and the scan is repeated three times.

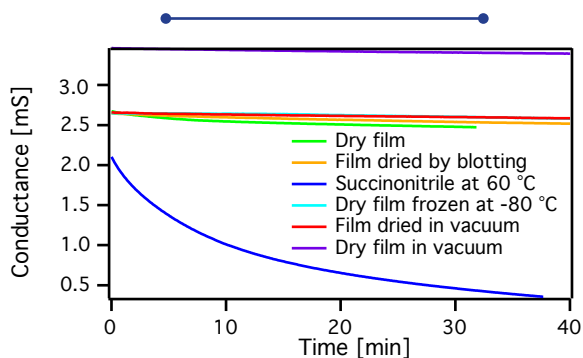


**Figure A4.9** Conductance measurements for a ZnO QD film. Measurements in 0.1 M LiClO<sub>4</sub> succinonitrile solution at 60 °C (blue), film taken out of the solution (dry film, green), a film dried under vacuum for one minute (red), a film dried by blotting (yellow), a film plunged into THF at -80 °C (cyan) and a film measured in vacuum (purple).

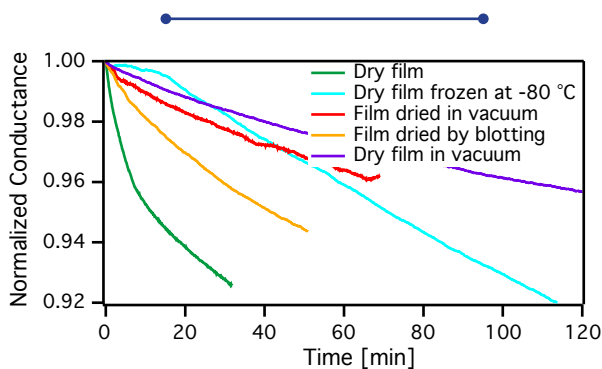


**Figure A4.10** Conductance measurements on a ZnO QD film. Dry film (green), after the sample was blotted with a filter paper (yellow), after the sample was stored under vacuum for one minute (red), after the sample was plunged into THF at -80 °C (cyan) and film measured in vacuum (purple).





# 5



## Permanent electrochemical doping of semiconductor films using frozen electrolyte solvents at room temperature

---

In Chapter 3 we showed stable electrochemically doping at  $-75\text{ }^{\circ}\text{C}$  by the use of succinonitrile (mp:  $57\text{ }^{\circ}\text{C}$ ) as the electrolyte solvent. Unfortunately, the doping was not stable at room temperature. Therefore, a solvent with a higher melting point is needed. In this chapter, we investigate stabilizing the doping density using four different nitrile based electrolyte solvents that have higher melting point than succinonitrile: trans-3-hexenedinitrile, cyanoacetamide, 1,2-dicyanobenzene and 1,3-dicyanobenzene. Using ZnO Quantum Dot (QD) films as test case, we show that no electrochemical charging/discharging takes place at room temperature in solvents with melting point over  $100\text{ }^{\circ}\text{C}$ . This implies that electrolyte ions are fully immobilized in frozen solvents. Of the investigated solvents, cyanoacetamide showed the best stability of the doping density at RT, in line with its superior cathodic stability. Therefore this solvent was chosen for a more in-depth analysis of the RT doping stability in ZnO QD films. By performing cyclic voltammetry measurements, we show that ion transport is entirely halted at room temperature. After electrochemical n-doping in liquid cyanoacetamide and cooling to RT, the electrical conductivity is fully stable for over 20 hours. On much longer time scales there is a slow but noticeable decrease in the conductivity, but after 10 days, 80% of the initial conductivity is retained, if the sample is stored in an inert atmosphere glovebox. When a doped film is exposed to ambient air, the conductivity drops rapidly, highlighting that oxidation by molecular oxygen is the dominant reason for the loss of electrons. This can be further prevented by the use of additional oxygen blocking layers. Finally, we show that this method is general and also works for films of PbS QDs and the conductive polymer P3DT. Furthermore, the conductivity of p-doped P3DT films drops only by 2% over the course of 76 days, and is not affected by ambient air at all. This is most likely because the stability of p-doped films is not affected by oxygen, but typically by water.

This chapter is based on: S.Gudjonsdottir and A. J. Houtepen. "Permanent Electrochemical Doping of Quantum Dots and Semiconducting Polymers". Advanced Functional Materials. Accepted.

## 5.1 Introduction

Over the last decades, various promising semiconductor materials have emerged, including colloidal quantum dots (QDs) and organic semiconductors. These semiconductors are known for their facile and cheap solution synthesis and their tunable optoelectronic properties.<sup>1,2-7</sup> Therefore, they are promising for, and indeed already used in, various semiconductor devices such as LEDs, light emitting electrochemical cells (LECs), lasers and solar cells.<sup>5, 8-18</sup> In order to use semiconductors in various devices, control over the charge carrier density is critical. There are, in principle, various ways to dope the abovementioned semiconductors, e.g. via impurity doping,<sup>19</sup> or photodoping,<sup>20-21</sup> although these methods are often faced with difficulties in controlling the charge density and the stability of the charge density.<sup>22-25</sup>

Arguably, the most controllable way of doping films of semiconductor QDs or organic semiconductors is via electrochemical doping. In this approach a semiconductor film is deposited on the working electrode (WE), and a potential is applied vs. the reference electrode (RE) in an electrochemical cell. By changing the potential of the WE toward more negative potentials, electrons can be injected into the conduction band of the material. In contrast, by applying more positive potentials, electrons can be extracted from the valence band. Therefore, the desired charge carrier density can be obtained by controlling the applied potential.<sup>26-29</sup> Essential for efficient electrochemical doping is that counterions are able to permeate the semiconductor films to provide charge neutrality. For films of QDs, fullerenes and organic semiconductors this is typically the case, so that electrochemical doping is a practical and generic method for all of them.

Unfortunately, it is usually observed that the injected charge density is not stable: when the electrochemical cell is disconnected from the potentiostat the semiconductor film discharges spontaneously.<sup>26, 30-31</sup> The main reasons for this self-discharge are intrinsic electrochemical reactions and redox reactions with impurities, typically oxygen or water.<sup>32-33</sup> Thus, in order to stabilize the doping density, the diffusion of the electrolyte ions and impurities should be minimized.

Electrochemically injected charges can be stabilized by freezing the electrolyte solvent. Guyot-Sionnest et al. and Houtepen et al. showed stable electrochemically doped semiconductor films at cryogenic temperatures.<sup>34-36</sup> These films were stable for days, but as soon as the temperature was increased the injected charge left the films. The same trend was observed by Heeger et al. for light emitting electrochemical cells (LECs), where the LECs were only stable at 200 K or lower.<sup>13, 37</sup> Clearly, it is not suitable to keep the films at cryogenic temperatures if they are to be used as semiconductor devices. Lately, extensive research has been going on to stabilize LECs at room temperature. While these measures increased the doping stability, unfortunately, none of them produced stable LECs at room temperature.<sup>38-40</sup>

In a previous study, we investigated electrolyte solvents with melting points above room temperature.<sup>33</sup> Various semiconductor films were charged at elevated temperature where the electrolyte solvent was liquid, and their doping stability was measured at lower temperatures. Surprisingly, the solvent with the highest melting point (mp), dimethyl

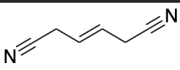
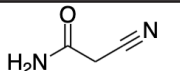
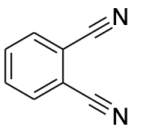
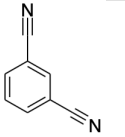
sulfone (mp: 109 °C), did not show the best stability at room temperature. A probable explanation for this is that other factors than the melting point play a role. For example the impurity concentration, the electrochemical stability of the solvent and how well it can crystallize at room temperature inside and on top of a semiconductor film.

Although the room temperature stability was increased greatly in our previous study, no solvent showed a truly stable electrochemical doped film at room temperature. However, by using succinonitrile (mp: 57 °C) as the electrolyte solvent, a fully stable electrochemically doped ZnO QD film was achieved at -75 °C. This suggests that a high melting point reduction occurs inside the semiconductor films, and only at -75 °C electrolyte ions and impurities have become immobile. It appears that succinonitrile is a suitable solvent for electrochemical doping, with low impurities content and high intrinsic electrochemical stability, however its melting point is too low for stable doping at room temperature. Taking inspiration from these results we have searched for chemically similar nitrile solvents with higher melting points.

In most cases the melting point of a molecule can be increased by increasing the molecular weight, adding aromaticity (to enhance the crystallinity in the solid state) or hydrogen bond forming groups such as alcohols.<sup>41-42</sup> In this chapter we investigate four different nitriles with high melting points: trans-3-hexenedinitrile (mp: 76 °C), cyanoacetamide (mp: 120 °C), 1,2-dicyanobenzene (mp: 138 °C) and 1,3-dicyanobenzene (mp: 164 °C). We start by determining the electrochemical stability window of the solvents. Thereafter, we perform electrochemical doping and stability measurements on ZnO QD films. All

5

**Table 5.1. Melting points and electrochemical potential windows for different nitriles.** Either  $\text{LiClO}_4$  or  $\text{TBAPF}_6$  was used as supporting electrolyte.  $20 \mu\text{A}/\text{cm}^2$  was chosen as the cutoff current density for the potential window.

Solvent	Melting point [°C]	Chemical structure	Cathodic limit, $\text{LiClO}_4$ [V vs. $\text{Fc}/\text{Fc}^+$ ]	Anodic limit, $\text{LiClO}_4$ [V vs. $\text{Fc}/\text{Fc}^+$ ]	Cathodic limit, $\text{TBAPF}_6$ [V vs. $\text{Fc}/\text{Fc}^+$ ]
Trans-3-hexenedinitrile	74-79		-1.39	1.16	--
Cyanoacetamide	119-121		-1.07	0.26	-1.03
1,2-dicyanoabene	137-139		-0.92	0.44	-0.67
1,3-dicyanobenzene	163-165		-0.29	1.00	--

solvents except trans-3-hexenedinitrile, show no charge injection at room temperature, which means that ion diffusion essentially does not happen. At temperatures above the mp, all solvents can be used to charge the ZnO QD films with electrons. When cooling down after charging, the n-doping of the films is retained. However, we observe a clear correlation between the stability of the electron density and the cathodic stability limit of the solvent. This shows that reduction of the solvent is an important factor in the charge stability of electrochemically doped films. Additionally, if the melting point of the solvent is not high enough, as is the case for trans-3-hexenedinitrile, the electron density gradually decreases. Of the solvents used, the stability of the doping density at RT was best for cyanoacetamide, in line with its superior cathodic stability. Therefore this solvent was chosen for a more in-depth analysis of the RT doping stability in ZnO QD films.

From an electrochemical analysis it is determined that at 140 °C, when cyanoacetamide is liquid, the diffusion coefficient of the  $\text{Li}^+$  ions is found to be  $\sim 10^{-9} \text{ cm}^2/\text{s}$ , while it drops to  $\sim 10^{-21} \text{ cm}^2/\text{s}$  at RT. This means that it would take a cation more than 300.000 years to diffuse through the 1  $\mu\text{m}$  thick ZnO QD film. Clearly, from an ion diffusion perspective the doping should be stable. Long-term conductivity measurements on doped ZnO QD films show that the electron density is fully stable over 20 hours. On much longer time scales there is a slow but noticeable decrease in the conductivity; after 10 days, 80% of the initial conductivity is retained, if the sample is stored in an inert atmosphere glovebox.

Given the very low diffusion coefficient of the ions, the observed drop in conductivity is likely caused by electrochemically active impurities (most likely oxygen). As solid cyanoacetamide is amorphous, it is possible for oxygen to penetrate the cyanoacetamide layer and react with injected electrons in the ZnO QD film. Indeed, taking a doped ZnO QD film out of the glovebox and exposing it to air causes the conductivity to drop to almost zero in about two hours. However, by placing a blocking layer such as PMMA on the film, the doping stability in air is increased greatly. At last, we show that this method does not only work for ZnO QDs but also for PbS QD films and poly(3-decylthiophene-2,5-diyl) (P3DT) films. For n-doped PbS QD films, the RT conductivity is entirely stable for over 5 days. However, as for the ZnO QD film the electrons gradually leave the film and after 40 days almost 10% of the injected charge has left the film. Interestingly, for p-doped P3DT films the conductivity decays only by 2% over the span of over 76 days. Additionally, when the film is taken out of the glovebox, the conductivity is not affected at all. This is most likely because oxygen is the main impurity responsible for the instability of n-doped films, whereas the stability of p-doped films is not affected by oxygen, but typically by water.

## 5.2 Results and Discussions

### 5.2.1 Electrochemical potential window

Our previous results showed that succinonitrile, despite a melting point of the pure solvent of 57°C, was not fully crystallized at RT when used as an electrolyte solvent to dope ZnO QD films. Table 5.1 shows the four different nitrile solvents investigated in this work with their melting points. Compared to succinonitrile, trans-3-hexenedinitrile has a longer carbon chain, cyanoacetamide can form hydrogen bonds and both 1,2-dicyanobenzene and 1,3-dicyanobenzene are aromatic molecules which are expected to demonstrate

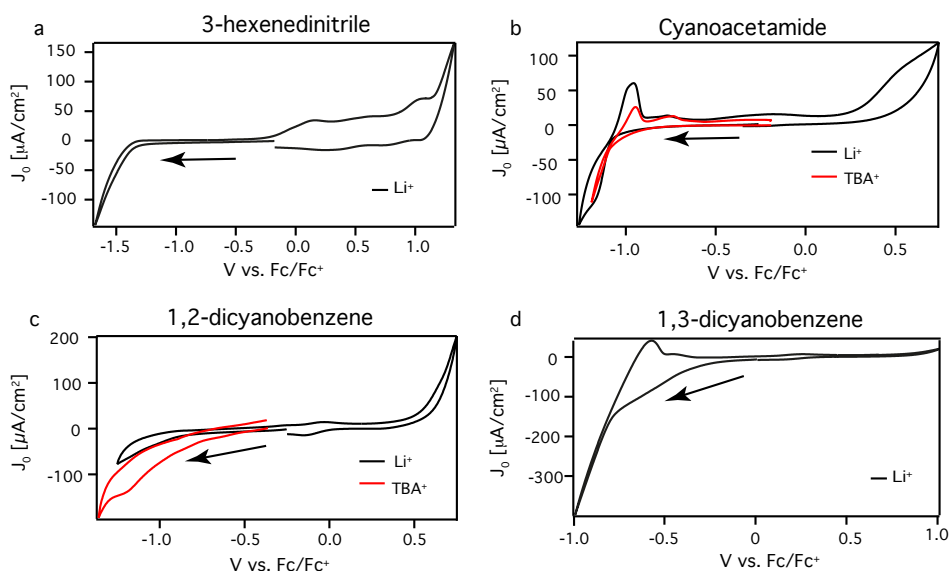


**Figure 5.1. Electrochemical potential window measurements in different electrolyte solvents.** The CVs are performed with blank Au electrodes in a) trans-3-hexenedinitrile, b) cyanoacetamide, c) 1,2-dicyanobenzene, d) 1,3-dicyanobenzene. The solvents contain 0.1 M of either  $\text{LiClO}_4$  (black trace) or  $\text{TBAPF}_6$  (red trace) and the scan rate is 50 mV/s. The scan is started around -0.3 V vs.  $\text{Fc/Fc}^+$  and is initially scanned in the cathodic direction (indicated by arrows in the Figure).

increased crystallinity when solid. The melting points of these solvents range from 74 to 165 °C.

In addition to having a high melting point the solvents need to be electrochemically stable at the potentials used for electrochemical doping. By adding functional groups such as a benzene or an amine group, the electrochemical stability of the solvent might differ greatly. The electrochemical potential window of the four high melting point nitriles has been determined by cyclic voltammetry (CV) on blank Au electrodes with a scan rate of 50 mV/s, as illustrated in Figure 5.1. Both  $\text{LiClO}_4$  and  $\text{TBAPF}_6$  were used as supporting electrolyte. We use a, somewhat arbitrary, cutoff current density of 20  $\mu\text{A}/\text{cm}^2$  to determine the cathodic and anodic stability limits. The resulting limits are shown in Table 5.1. We find that trans-3-hexenedinitrile is most stable both cathodically and anodically (-1.39 and +1.16 V vs.  $\text{Fc/Fc}^+$ ). In Figure 5.1a the oxidation peaks on the reverse scan between 0 and 0.5 V vs.  $\text{Fc/Fc}^+$  are connected to the reduction of the solvent at around -1.5 V vs.  $\text{Fc/Fc}^+$ . Therefore, the anodic limit is determined from Figure A5.1 in Appendix, where a smaller cathodic range was scanned so that no solvent reduction occurred. The electrochemical potential window of the other three solvents is considerably narrower. Of these solvents cyanoacetamide and 1,2-dicyanobenzene are more stable at negative potentials (vs.  $\text{Fc/Fc}^+$ ), while 1,3-dicyanobenzene is more stable at positive potentials (vs.  $\text{Fc/Fc}^+$ ). At last, the effect of different electrolyte salts is small, although  $\text{LiClO}_4$  seems to yield a somewhat better stability than  $\text{TBAPF}_6$ .

### 5.2.2 Doping of ZnO QD films

To see if these solvents are suitable for electrochemical doping, we performed electrochemical measurements with ZnO QD films. This material is selected as it exhibits stable and reversible electron injection, and furthermore allows multiple measurements to be performed on the same sample.<sup>30, 44</sup> Figure 5.2 shows CVs and Fermi-level stability measurements for ZnO QD films in 0.1 M LiClO<sub>4</sub> nitrile solutions. The measurements were performed at two different temperatures, above the melting point and at room temperature (20 °C).

Figure 5.2a shows CVs performed in trans-3-hexenedinitrile at both 100 °C and RT. In the first case, the CV shows clear charging and discharging of the ZnO QD film similar to CVs on such films using e.g. acetonitrile at RT.<sup>29-30</sup> However, upon lowering the temperature the current density decreases drastically. A zoom-in of a CV at room temperature in trans-3-hexenedinitrile is shown in Figure A5.2 in Appendix. It exhibits a minor, but detectable difference in current density on the forward and backward scan. This shows that the movement of electrolyte ions has been decreased immensely, but that some charging/discharging still takes place.

Figure 5.2b shows CVs in cyanoacetamide at both 140 °C and RT. As for trans-3-hexenedinitrile the current decreases drastically by lowering the temperature. However, a zoom-in of the CV at room temperature (Figure A5.3 in Appendix) shows no sign of charging/discharging for this solvent. In fact the CV looks very similar to what is measured when the potentiostat is disconnected (Appendix, Figure A5.4). This means that the electrolyte ions are effectively immobilized in the frozen solvent. Figures 5.2e,f show the same trend for both 1,2-dicyanobenzene and 1,3-dicyanobenzene. The magnified versions of the CVs at room temperature are in the Appendix, Figures A5.5 and A5.6, and again no charging currents are seen.

From the measured current in the CVs at high temperature, it is possible to calculate the charging ratio between injected and extracted electrons by the use of equation 5.1:

$$\frac{n_{extr}}{n_{inj}} = \frac{\sum(I * dE)}{\sum(I * dE)} \quad 5.1$$

Where  $n_{extr}$  is the number of extracted electrons,  $n_{inj}$  is the number of injected electrons,  $I$  is the measured current and  $dE$  is the potential step. We find that in trans-3-hexenedinitrile 88% of injected electrons are extracted. This number is slightly lower for cyanoacetamide (72%). On the other hand, it drops to 6% and 0% for 1,2-dicyanobenzene and 1,3-dicyanobenzene, respectively. These numbers can be related to the electrochemical (in) stability of the solvents shown in Figure 5.1. At potentials where electron charging occurs (roughly negative of -0.6 V vs. Fc/Fc<sup>+</sup>) 1,2-dicyanobenzene and 1,3-dicyanobenzene show non-negligible cathodic currents. This implies that the solvent can react with the electrons injected into the ZnO QDs and explains why they are not extracted.

Figures 5.2c,d,g,h show Fermi-level stability measurements for ZnO QD films in the different nitriles: the films are charged when the solvent is liquid, then the counter electrode

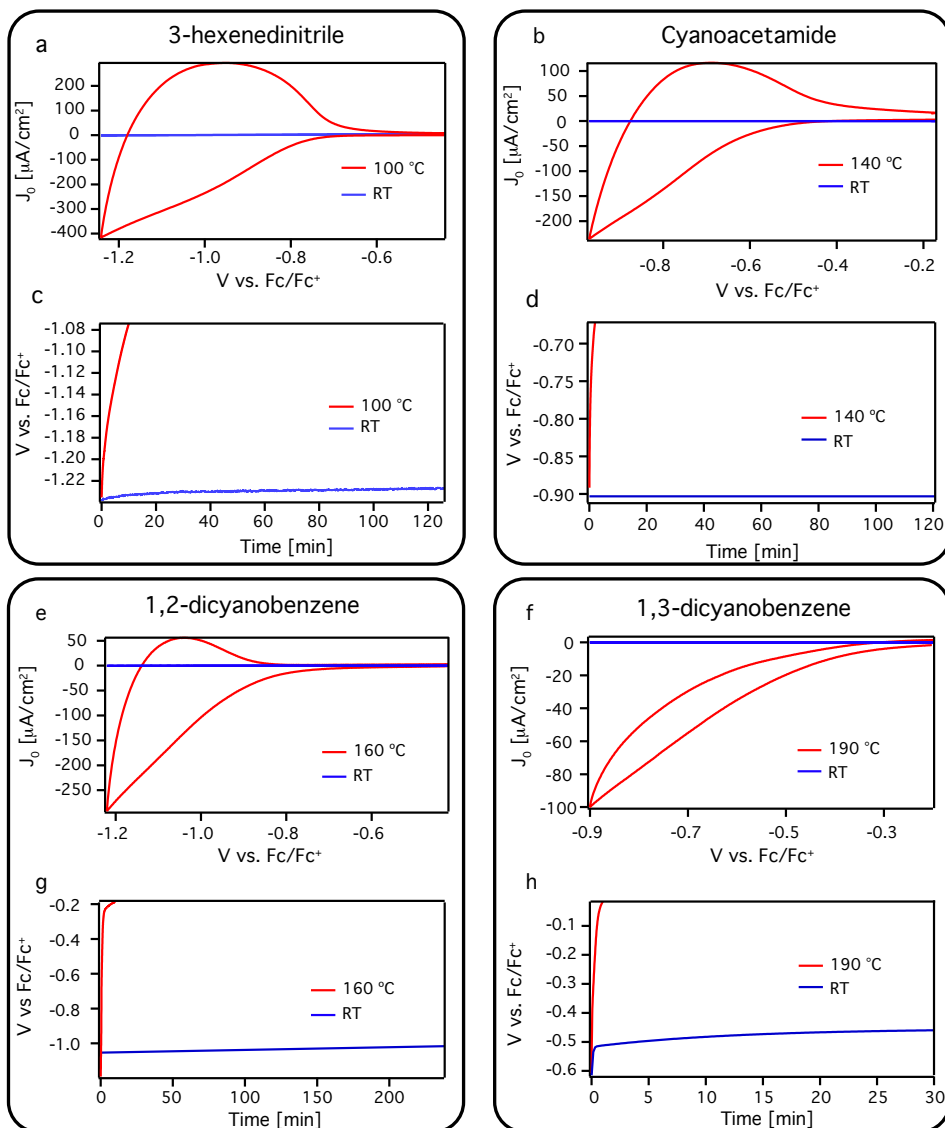


**Figure 5.2. Electrochemical measurements performed with ZnO QD films in different nitrile solvents.** CVs are performed with a scan rate of 50 mV/s performed in a 0.1 M  $LiClO_4$  a) trans-3-hexenedinitrile solution, b) cyanoacetamide solution, e) 1,2-dicyanobenzene solution, and f) 1,3-dicyanobenzene solution. Fermi-level stability measurements performed in a 0.1 M  $LiClO_4$  c) trans-3-hexenedinitrile solution, d) cyanoacetamide solution, g) 1,2-dicyanobenzene solution, h) 1,3-dicyanobenzene solution. The red traces show measurements performed when the solvent is liquid, while the blue traces show measurements performed at room temperature.

(CE) is disconnected so that no more charging or discharging is possible via the external circuit. If electrons disappear from the ZnO QD film, the measured potential will decay

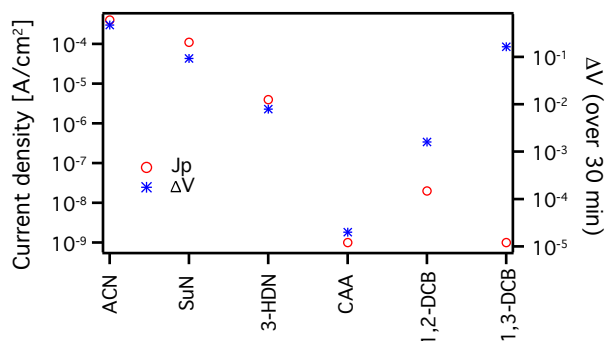


**Figure 5.3.** Current peak densities ( $J_p$ , red circles) and potential decay over 30 minutes in Fermi-level stability measurements ( $\Delta V$ , blue stars) for different nitrile solvents at room temperature. Used solvents are: acetonitrile (ACN, mp:  $-45^\circ\text{C}$ ), succinonitrile (SuN, mp:  $57^\circ\text{C}$ ), trans-3-hexenedinitrile (3-HDN, mp:  $76^\circ\text{C}$ ), cyanoacetamide (CAA, mp:  $120^\circ\text{C}$ ), 1,2-dicyanobenzene (1,2-DCB, mp:  $138^\circ\text{C}$ ) and 1,3-dicyanobenzene (1,3-DCB, mp:  $164^\circ\text{C}$ ). The peak current density for both cyanoacetamide and 1,3-dicyanobenzene is within the noise of the measurements ( $\sim 1\text{ nA}$ ).

5

towards its original open circuit potential before the film was charged. If no electrons leave the QDs, the measured potential is stable. For the measurements at room temperature, the CE was disconnected after room temperature was reached. From these measurements it is clear that the measured potential decays drastically faster at high temperatures than at RT. As shown in Figure 5.2c, a small drop in potential is seen for trans-3-hexenedinitrile over the course of two hours at RT. This potential decay can be related to the slight charging and discharging current in the CV at room temperature. This charging current suggests that the solvent is not entirely frozen. We conjecture that this also allows some diffusion of impurities such as molecular oxygen, which can react with the injected electrons and lower the potential. On the other hand, the potential in cyanoacetamide at RT does not decay at all during the two hours shown (Fig. 5.2d). For 1,2-dicyanobenzene a small drop in the potential is seen at RT (Fig. 5.2g) while a much faster drop in potential is seen for 1,3-dicyanobenzene (Fig. 5.2h). As this is in line with the ratio of the extracted and injected electrons in the CVs, this potential decay can be related to the limited cathodic stability of these solvents.

From these experiments it is clear that the solvent stability plays an equally important role as the melting point in producing stable electrochemically doped films at room temperature. To see this even clearer, Figure 5.3 shows a comparison of 6 different nitriles that were used in our previous study and this study.<sup>30</sup> The nitriles are: acetonitrile (ACN, mp:  $-45^\circ\text{C}$ ), succinonitrile (SuN, mp:  $57^\circ\text{C}$ ), trans-3-hexenedinitrile (3-HDN, mp:  $76^\circ\text{C}$ ), cyanoacetamide (CAA, mp:  $120^\circ\text{C}$ ), 1,2-dicyanobenzene (1,2-DCB, mp:  $138^\circ\text{C}$ ) and 1,3-dicyanobenzene (1,3-DCB, mp:  $164^\circ\text{C}$ ). In Figure 5.3 the peak current density at RT and the change in the potential,  $\Delta V$ , observed in Fermi-level stability measurements over 30 minutes at RT are shown for the different solvents. The RT current density and drop in Fermi-level generally decrease with increasing melting point. However, we do not observe that the solvents with the highest melting points have the best Fermi-level stability, since the two solvents with the highest melting point show (minor) cathodic

decomposition at the potentials used. By taking all these results into account we conclude that cyanoacetamide is the most promising solvent for obtaining a stable electrochemically n-doped semiconductor film at room temperature. Therefore, further measurements were performed with cyanoacetamide.

### 5.2.3 Cyanoacetamide as the electrolyte solvent

Figure 5.4a shows CVs performed on ZnO QD films in 0.1 M LiClO<sub>4</sub> cyanoacetamide solution at temperatures between 140 °C and 0 °C with a 10 degree interval. Figure 5.4b shows the peak current density as a function of temperature. A decrease of 6 orders of magnitude is observed. We have previously shown that the charging current is limited by cation diffusion.<sup>29</sup> Thus the decreasing current density results from a decreasing diffusion coefficient of the electrolyte cations.

Differential scanning calorimetry measurements indicate that the electrolyte salt causes a melting point reduction of at most 9 °C. For 0.1 M LiClO<sub>4</sub> in cyanoacetamide a recrystallization temperature of 75.6 °C was measured (see Appendix, Figure A5.7, A5.8, A5.9). Interestingly, no clear phase transition is seen in Figure 5.4b at 75 °C. This suggests that the crystallization inside the pores of the QD film is hindered and occurs over a wide temperature range. Full crystallization requires temperatures well below the melting point of the pure solvent.

We calculate the diffusion coefficient from the peak current density with the Randles-Sevcik equation:

$$j_p = 0.4463nFC^* \left( \frac{nFvD}{RT} \right)^{1/2} \quad 5.2$$

where  $j_p$  is the peak current density,  $n$  is the number of electrons,  $F$  is the Faradaic constant,  $C^*$  is the concentration of the electrolyte,  $v$  is the scan rate,  $D$  is the diffusion coefficient,  $R$  is the gas constant and  $T$  is the temperature. The diffusion coefficient is plotted on the right axis in Figure 5.4b. Values below 80 °C are an approximation of the diffusion coefficient as no clear charging maxima are seen in these CVs (see Appendix, Figure A5.10). Instead we used the lowest measured current (at around -1 V vs. Fc/Fc<sup>+</sup>). At 140 °C the diffusion coefficient of Li<sup>+</sup> in cyanoacetamide is ~10<sup>-9</sup> cm<sup>2</sup>/s, whereas at RT, it is 12 orders of magnitude lower, or around 10<sup>-21</sup> cm<sup>2</sup>/s. Considering the latter value, we can estimate that it would take a Li<sup>+</sup> ion ~10<sup>13</sup> seconds (>300,000 years) to diffuse out of a 1 μm thick ZnO QD film.

So far, in all the measurements the ZnO QD film has been submerged in the electrolyte solvent. That is, the film was inside a metal cell with a block of frozen solvent around it. Clearly, this configuration is not suitable for use in semiconductor devices. Therefore we also performed experiments where the film is removed from the electrolyte solution after electrochemical doping. The film is charged at 140 °C when the solvent is liquid, the potentiostat is disconnected and the film is quickly removed from the cell, causing the temperature to drop and the cyanoacetamide to solidify. Since in this case we cannot measure the potential vs. a reference electrode we now use source-drain electronic conductivity

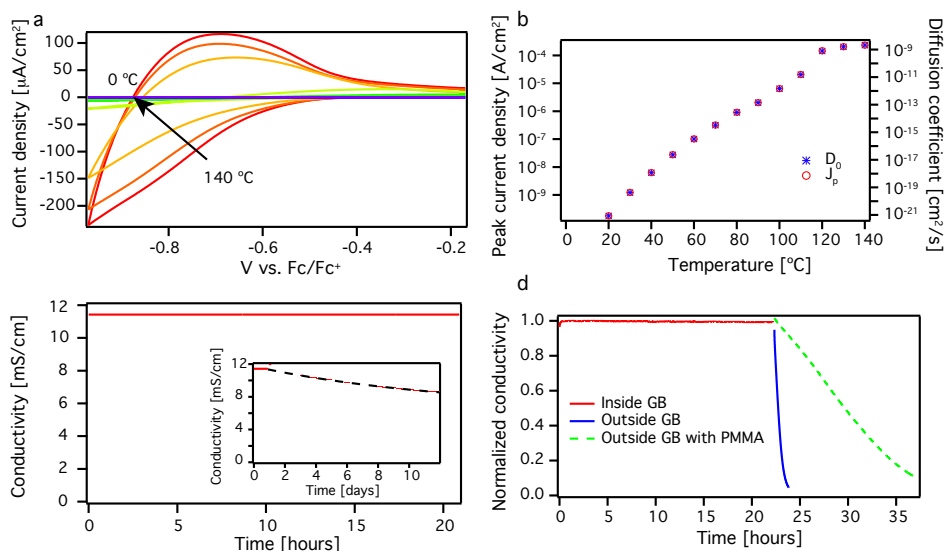


**Figure 5.4. Electrochemical measurements for a ZnO QD film in 0.1 M  $\text{LiClO}_4$  cyanoacetamide solution.** a) CVs performed between 140 °C and 0 °C with 10 degrees interval. The scan rate is 50 mV/s. b) The peak current density obtained from the CVs (red circles) and the calculated diffusion coefficient (blue stars). c) Source-drain electronic conductivity measurements for the ZnO QD film after it has been taken out of the cyanoacetamide solution. The measurement is carried out at room temperature, so the solution has solidified. The panel includes an inset that shows the measurements on a longer time scale, the black trace is a guide to the eyes for the decay of the conductivity. d) Electronic conductivity measurements performed both inside (red trace) and outside (blue trace) of the glovebox on a ZnO QD film measured outside of the electrochemical cell. The panel also shows conductivity measurements outside of the glovebox where a PMMA layer was added on top of the solid cyanoacetamide (green trace).

measurements to test the doping stability, employing a home-built interdigitated electrode (IDE) (Figure 5.4c, see an image of the film in the Appendix, Figure A5.11). The advantage of such conductivity measurements is that they do not require additional electrodes and can be performed on the doped film directly. Since the conductivity  $\sigma$  is linearly related to the charge density  $n$  via  $\sigma = ne\mu$ , where  $\mu$  is the electron mobility, the charge stability can be probed sensitively by measuring the conductivity. In comparison, the potential in Fermi-level stability measurements decays logarithmically with the charge carrier density, as expressed by the Nernst law.

Figure 5.4c shows that for the first 20 hours the conductivity does not decrease at all (see a magnified version in the Appendix, Figure A5.12), in line with the enhanced Fermi-level stability shown in Figure 5.2d. However, on much longer time scales the conductivity starts to gradually decrease (see inset in Figure 5.4c): after 10 days around 20% of injected charge has left the ZnO QD film (see a normalized graph in Appendix, Figure A5.13).

Since the conductivity did not decrease in the beginning of the measurement, we speculate that this gradual decrease on longer time scales might be due to molecular oxygen. We have

shown in a previous study the great impact of impurities, such as oxygen, on the doping stability of ZnO QD films.<sup>33</sup> Even the controlled atmosphere of a nitrogen filled glovebox contains impurities, most notably oxygen, in very low concentrations (the oxygen level of the glovebox used is typically <1 ppm). Therefore, if the solid cyanoacetamide film does not protect the ZnO QD film against diffusion of oxygen, given long enough time oxygen molecules will reach and oxidize the QDs. The diffusion of oxygen in cyanoacetamide is likely influenced by the fact that cyanoacetamide does not form a smooth consistent layer when it solidifies. Molecular oxygen has a standard reduction potential of  $\sim -1.2$  V vs Fc/Fc<sup>+</sup>.<sup>45</sup> However, this reaction is often irreversible, meaning that even electrons at less negative potentials (such as the electrons in the ZnO QDs which have a potential between -0.6 and -1.2 V vs Fc/Fc<sup>+</sup> in this experiment, set by the potential used during charging), will react with oxygen given long enough time.

In order to see if this is the case, we performed source-drain electronic conductivity measurements on a ZnO QD film both inside and outside of the nitrogen filled glove box (Figure 5.4d). Inside the glovebox the conductivity is stable in the first 20 hours. When the film is brought outside of the glovebox, the conductivity drops to intrinsic values in less than two hours. This shows that even if the cyanoacetamide solvent is frozen and immobilizes the electrolyte cations, it does not fully protect the film against oxygen.

One way of protecting the ZnO QD film against oxygen is to apply a protective layer on top of the cyanoacetamide solid layer. Figure 5.4d shows a measurement for a ZnO QD film in 0.1 M LiClO<sub>4</sub> cyanoacetamide solution with a poly(methyl methacrylate) (PMMA) layer on top of it, measured outside of the glove box. In this case it takes over 15 hours for the electronic conductivity to drop, compared to two hours when no PMMA is used. Since the protection of the film with PMMA has not at all been optimized, this gives hope that much higher stabilities could be reached. One notable interesting approach would be to use a thin alumina coating, which can for instance be deposited using ambient temperature Atomic Layer Deposition.<sup>46</sup>

#### 5.2.4 Stable doping of semiconductor materials

Since cyanoacetamide as a frozen electrolyte solvent works well to increase the stability of electrochemically doped ZnO QD films, it is of interest to see if this method can also be applied to other semiconducting materials. Figure 5.5 shows results for both films of PbS QDs and the conductive polymer P3DT. Films of PbS QDs can be n-doped,<sup>47</sup> while films of P3DT are easily p-doped electrochemically.<sup>30, 48</sup>

Figure 5.5a shows CVs for a PbS QD film in cyanoacetamide at 140 °C and at room temperature. At 140 °C there is a large current density, corresponding to charging and discharging of the PbS QDs with electrons. The clear separation between the reduction peak around -1.0 V and the oxidation peak around -0.8 V vs. Fc/Fc<sup>+</sup> is only observed when LiClO<sub>4</sub> is used as an electrolyte, but not when TBAPF<sub>6</sub> is used (see Appendix, Figure A5.14) and is probably an indication that Li<sup>+</sup> intercalation takes place.<sup>49</sup> As expected, at room temperature the current density in the CV has decreased drastically (a magnified version is shown in the Appendix, Figure A5.15), as a result of the freezing of the solvent. A similar trend is seen for P3DT in Figure 5.5b. At RT only negligible charging/discharging

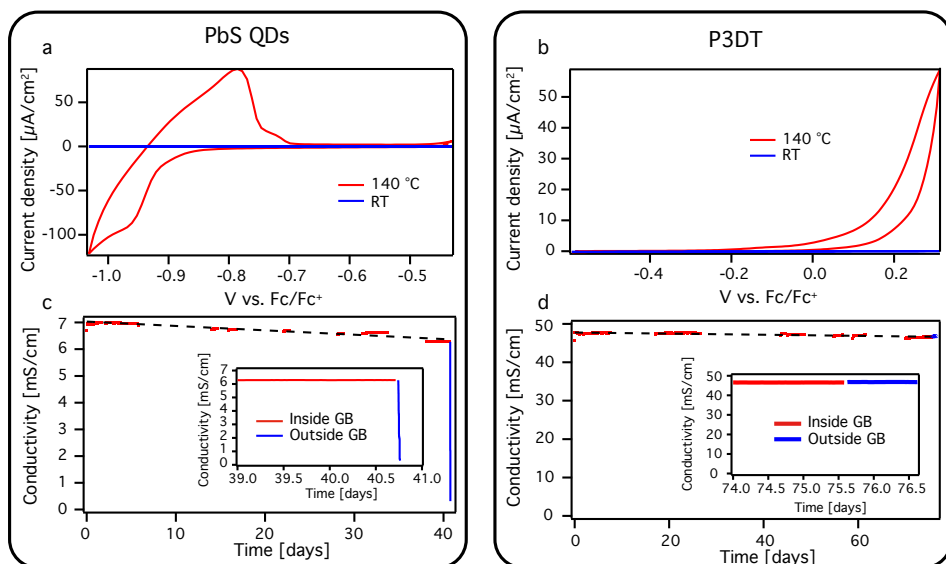


**Figure 5.5. Doping other semiconducting materials in 0.1 M LiClO<sub>4</sub> cyanoacetamide.** a) CVs for a PbS QD film at 140 °C (red trace) and RT (blue trace), the scan rate is 50 mV/s. b) CVs for a P3DT film at 140 °C (red trace) and RT (blue trace), the scan rate is 50 mV/s. c) Conductivity for a PbS QD film measured outside the electrochemical cell at room temperature both before and after it is taken out of the nitrogen filled glovebox. The black trace is a guide to the eye for the decay of the conductivity. The panel includes an inset which shows the conductivity in approximately the last two days of measurements. d) Conductivity for a P3DT film measured outside of the electrochemical cell at room temperature, both inside and outside of the glovebox. The panel includes an inset which shows the conductivity in approximately the last two days of measurements. The black trace is a guide to the eye for the decay of the conductivity. When the film is brought out of the cell, cyanoacetamide solidifies on top of the film.

is observed (see SI Figure S16 for a zoom in). At 140 °C the CV for P3DT shows clear hole injection at positive potentials, although no negative current is obtained in the reverse scan, indicating the holes are not extracted. If we look at Table 5.1 the anodic limit for cyanoacetamide is 0.262 V vs. Fc/Fc<sup>+</sup> and we are scanning to 0.3 V vs. Fc/Fc<sup>+</sup>. Therefore, we assume that cyanoacetamide partially oxidizes at this positive potential by reacting with the holes in the P3DT. 1,3-dicyanobenzene might be a better choice as electrolyte solvent for P3DT. On the other hand, it simplifies the doping process of semiconductor films if both p and n-type doping can be performed in the same electrolyte solvent.

For both PbS QDs and P3DT we performed source-drain electronic conductivity measurements in cyanoacetamide at RT after electrochemical doping at 140 °C. The conductivity is plotted for the PbS QD film in Figure 5.5c and for the P3DT film in Figure 5.5d. Figure 5.5c, shows that for the PbS QD film, the conductivity is constant for over 5 days (see also Appendix, Figure A5.17), before it starts to gradually decrease. After 40 days the conductivity has decreased by 9.6%. If the film is taken out of the glovebox it is seen that the rest of the charge leaves the PbS QD film within 2 hours (inset in Fig 5.5c). This

shows that oxidation by molecular oxygen is responsible for the drop in electron density. As for the ZnO QD film an additional oxygen blocking layer is needed.

Figure 5.5d show the conductivity for a P3DT film. Interestingly, after 76 days of measurements the conductivity has only dropped by 2% (see Appendix, Figure A5.18 for a magnification). Furthermore, when the film is taken out of the glovebox, the conductivity is not affected at all (inset in Fig 5.5d). This shows, that even if the doping takes place at the edge of the anodic limit for cyanoacetamide, the frozen solvent is still stable enough to maintain p-doping of the P3DT film. Additionally, the conductivity doesn't decrease gradually over time as for ZnO and PbS QD films. The main difference between these materials is that PbS and ZnO QD films are doped n-type while the P3DT film is doped p-type. Oxidation by molecular oxygen will not occur at the Fermi-level of the p-doped P3DT, and would not decrease the hole density even if it did. Rather, the risk is in reduction by other impurities such as water. As the conductivity does not decrease when the film is taken out of the glovebox, it shows that cyanoacetamide is a great diffusion barrier against impurities that oxidize at these potentials (such as water).

These measurements show that it is possible to obtain stable electrochemically doped semiconductor films made of both QDs (PbS and ZnO) and conductive polymers (P3DT) by the use of cyanoacetamide at room temperature. Unfortunately, the cyanoacetamide doesn't protect the films against oxygen in the case for n-type doping, while the p-type doping is stable. Therefore, it is important to find a solvent which recrystallizes in such a way that it protects the doped films against oxygen. Additionally, the electrochemical potential window of cyanoacetamide is too limited for doping of various semiconductors. For example, potentials of  $\sim -1.7$  V vs.  $\text{Fc}/\text{Fc}^+$  are needed to n-dope CdSe QDs, and many organic semiconductors need more positive potentials for p-doping compared to P3DT.<sup>30</sup> At last, this new solvent needs a melting point in the range of 100-200 °C to ensure stable doping at room temperature and that the films survive. If a solvent will fulfill these three requirements, it would be ideal for use to gain stable electrochemical doping at room temperature.

### 5.3 Conclusions

In summary, we have investigated different nitriles with high melting points as electrochemical solvents, to obtain stable electrochemically doped semiconductor films at room temperature. We showed that the stability of n-doping in ZnO QD films is related to both the electrochemical stability windows and the melting point of the solvents. In the end both the melting point and the solvent stability determine the suitability of the solvent for a stable doping by room temperature freezing. The best results for ZnO QD films were obtained with cyanoacetamide, as the electrolyte ions are completely immobilized at room temperature. Conductivity measurements of ZnO QD films charged in cyanoacetamide showed that the doping density is completely stable over 20 hours at room temperature. At longer timescales the conductivity starts to gradually decrease, and after 10 days around 20% of the injected electrons have left the ZnO QD film. This decrease is likely due to oxidation by molecular oxygen that penetrates the frozen cyanoacetamide.

At last, we performed electrochemical measurements in cyanoacetamide for two other

semiconductors, PbS QDs and the conductive polymer P3DT. The n-doped PbS QD film was stable for over 5 days, but after 40 days, around 10% of the injected electrons had disappeared. On the other hand, the p-doped P3DT film was stable over the full 76 days of the measurement (conductivity decreased by only 2%). These results show that electrochemical doping combined with room temperature freezing of the solvent is a promising method to prepare permanently doped semiconductor thin films, composed of for instance colloidal QDs or organic semiconductors. Therefore, by successful protecting of the doped film against impurities such as oxygen, the doped films can be implemented into devices as stable electrochemically doped films at room temperature.

## 5.4 Methods

**Materials.** Zinc acetate dihydrate ( $\text{Zn}(\text{CH}_3\text{COO})_2 \cdot 2\text{H}_2\text{O}$  reagent grade), potassium hydroxide (KOH pellets), cadmium oxide (CdO, 99.999%), oleic acid (OA, 90%), 1-octadecene (ODE, 90%), sulfur powder (S, 99.99%), oleylamine (OLA, 70%), lead chloride ( $\text{PbCl}_2$ , 99.999%), P3DT (poly(3-decylthiophene-2,5-diyl)), indium-doped tin oxide substrates (ITO, PGO Germany), lithium perchlorate ( $\text{LiClO}_4$ , 99.99%), tetrabutylammonium hexafluorophosphate ( $\text{TBAPF}_6$ , 98%), poly(methyl methacrylate) (PMMA), ferrocene (Fc, 98%), trans-3-hexendinitrile (97%), cyanoacetamide (99%), 1,2-dicyanobenzene (98%), 1,3-dicyanobenzene (98%), anhydrous solvents (acetonitrile, 99.99%, methanol, 99.8%, ethanol (maximum 0.01%  $\text{H}_2\text{O}$ ), hexane, 95%, chloroform, 99+%) were all purchased from Sigma-Aldrich unless stated otherwise. Acetonitrile was dried before use in an Innovative Technology PureSolv Micro column. All other chemicals were used as received.

**ZnO synthesis.** ZnO synthesis was performed in air as previously described.<sup>29</sup> 3.425 mmol of Zinc acetate dihydrate are dissolved in 50 mL ethanol at 60 °C in an Erlenmeyer flask. In a separate vial, 6.25 mmol of KOH are dissolved in 5 mL of methanol, and added dropwise to the stirred Zinc mixture. After a wait of 1 to 2 minutes the ZnO QDs were removed from the heat source and washed by addition of toluene. The flocculates are isolated by centrifugation at 2000 rpm for 1 minute and redissolved in ethanol. The mixture was kept in a freezer at -20 °C to avoid further growth.

**PbS synthesis.** PbS QDs were synthesized following the procedure of Zhang et. al<sup>43</sup> where CdS QDs are initially synthesized and PbS QDs are formed by Pb for Cd cation exchange.

CdS QDs were synthesized by initially heating a mixture of 1 mmol (0.128 g) CdO, 3 mmol (0.942 g) OA and 15 g of ODE for 20 minutes at 260 °C, then the temperature was set to 250 °C. The sulfur precursor was made by dissolving S powder in ODE (0.5 M) at 130 °C. 1 mL of the sulfur precursor was injected into the Cd precursor at 250 °C, the solution was maintained at 240 °C. After about 13 minutes additional sulfur precursor was added to the solution drop wise until the desired size was reached. The CdS QD solution was washed twice with hexane and ethanol and centrifuged at 7500 rpm for 5 minutes. The CdS QDs were redissolved in ODE.

For the PbS QDs,  $\text{PbCl}_2$  (1.5 mmol) was dissolved in OLA (5 mL) at 140 °C for 30 minutes until a white turbid solution was formed. The solution was heated to 190 °C and 1 mL of the CdS QDs was injected swiftly. The solution was quenched with a water bath 20 seconds later. At 70 °C 5 mL of hexane were added and at 40 °C 4 mL of OA were added. The solution was washed 3 times with hexane and ethanol and centrifuged at 7500 rpm for 5 minutes. The PbS QDs were redissolved in hexane.

**Film preparation.** All films were deposited on two different working electrodes (WE). The former one is an ITO electrode while the second one is a home-built interdigitated gold electrode (IDE). The ZnO quantum dot films were drop-casted on top of the substrate in air and annealed at 60 °C for an hour.

The PbS quantum dot films were made by dip-coating. Initially the substrate is dipped in the quantum dot solution, followed by dipping the substrate in methanol containing TBAI (11 mg/mL). The substrate was kept in the solution for around 30 seconds before being washed in a methanol solution for about 10 seconds.

For the P3DT films, 10 mg/mL of P3DT were dissolved in 1,2-dichlorobenzene. The solution was spin coated on the substrate for 60 seconds at 3000 RPM, with a ramp of 1000 RPM/s.

When PMMA was used as a protective layer, the PMMA solution (5 w% in chloroform) is drop casted on top of the film. This process was repeated several times.

**Electrochemical measurements.** All electrochemical measurements were performed in a nitrogen filled glovebox (moisture < 0.05 ppm and O<sub>2</sub> level < 0.1 ppm) unless stated otherwise. The measurements were performed either with an Autolab PGSTAT128N or Autolab PGSTAT204 potentiostat in a three electrode electrochemical cell. The working electrode (WE) was either ITO or a gold IDE, the counter electrode (CE) was a platinum sheet and the reference electrode (RE) was a Ag pseudoreference electrode. The reference electrode was calibrated with the ferrocene/ferrocenium (Fc/Fc<sup>+</sup>) couple before every measurement, and all potentials are given versus the Fc/Fc<sup>+</sup> couple.

**Source-drain electronic conductivity measurements.** The source-drain electronic conductivity measurements were performed as previously described with the homemade IDE.<sup>33</sup> Initially, the semiconductor film was charged by the use of a potentiostat. After a desired doping density was reached, the sample was disconnected from the potentiostat and the source-drain electronic conductance was measured with a Keithly 2400 source meter. After the potentiostat was disconnected, charges could no longer be injected into the semiconductor. The used source-drain potential was 10 mV.

From the measured conductance, the conductivity,  $\sigma$ , can be calculated with Equation 5.3:

$$\sigma = (G \times w) / (l \times h) \quad 5.3$$

where G is the conductance, w is the source-drain width, l is the gap length and h is the height of the sample.

For calculation of the conductivity for ZnO QD films, a common thickness of 1  $\mu\text{m}$  is used.<sup>33</sup>

For calculation of the conductivity for both PbS QD films and P3DT films, thickness measurements proved complicated due to the solid cyanoacetamide layer on top of the film. Therefore, the thickness of a PbS QD film and a P3DT film made in the same way are used. By using Dektak profilometer, the thickness for the PbS QD film was measured as approximately 90 nm, while it was approximately 30 nm for the P3DT film.

**Fermi-level stability measurements.** Fermi-level stability measurements were performed as

previously described.<sup>30, 33</sup> The sample was charged with a potentiostat, and when a desired doping density was reached and the system had reached an equilibrium, the CE was disconnected from the cell. This means that electrons could no longer be injected or extracted from the semiconductor film, while the potential of the WE vs. the RE was monitored. The measured potential is connected to the Fermi-level of the film. If injected charges left the film, the Fermi-level decayed into the band gap of the semiconductor. This means that the potential would decay to its original value (the open circuit potential) before charge injection took place.

## References

1. Talapin, D. V.; Lee, J.-S.; Kovalenko, M. V.; Shevchenko, E. V., Prospects of colloidal nanocrystals for electronic and optoelectronic applications. *Chem. Rev.* 2009, 110 (1), 389-458.
2. Bailey, R. E.; Nie, S., Alloyed semiconductor quantum dots: Tuning the optical properties without changing the particle size. *J. Am. Chem. Soc.* 2003, 125 (23), 7100-7106.
3. A.I.Ekimov; A.L.Efros; A.A.Onushchenko, Quantum Size Effect in Semiconductor Microcrystals. *Solid State Commun.* 1985, 56 (11).
4. Ekimov, A. I.; Hache, F.; Schanne-Klein, M. C.; Ricard, D.; Flytzanis, C., Absorption and Intensity-Dependent Photoluminescence Measurements on CdSe Quantum Dots- Assignment of the First Electronic Transitions. *J. Opt. Soc. Am. B* 1993, 10 (1).
5. Geffroy, B.; le Roy, P.; Prat, C., Organic light-emitting diode (OLED) technology: materials, devices and display technologies. *Polym. Int.* 2006, 55 (6), 572-582.
6. Coropceanu, V.; Cornil, J. r.; Filho, D. A. d. S.; Olivier, Y.; Silbey, R.; Bredas, J.-L., Charge Transport in Organic Semiconductors. *Chem. Rev.* 2007, 107, 926-952.
7. Würthner, F., Bay-substituted perylene bisimides: Twisted fluorophores for supramolecular chemistry. *Pure Appl. Chem.* 2006, 78 (12), 2341-2349.
8. Boehme, S. C.; Azpiroz, J. M.; Aulin, Y. V.; Grozema, F. C.; Vanmaekelbergh, D.; Siebbeles, L. D.; Infante, I.; Houtepen, A. J., Density of Trap States and Auger-mediated Electron Trapping in CdTe Quantum-Dot Solids. *Nano Lett.* 2015, 15 (5), 3056-66.
9. Lan, X.; Voznyy, O.; Garcia de Arquer, F. P.; Liu, M.; Xu, J.; Proppe, A. H.; Walters, G.; Fan, F.; Tan, H.; Liu, M.; Yang, Z.; Hoogland, S.; Sargent, E. H., 10.6% Certified Colloidal Quantum Dot Solar Cells via Solvent-Polarity-Engineered Halide Passivation. *Nano Lett.* 2016, 16 (7), 4630-4.
10. Wang, H.; Wang, Y.; He, B.; Li, W.; Sulaman, M.; Xu, J.; Yang, S.; Tang, Y.; Zou, B., Charge Carrier Conduction Mechanism in PbS Quantum Dot Solar Cells: Electrochemical Impedance Spectroscopy Study. *ACS Appl. Mater. Interfaces* 2016, 8 (28), 18526-33.
11. Shirasaki, Y.; Supran, G. J.; Bawendi, M. G.; Bulović, V., Emergence of colloidal quantum-dot light-emitting technologies. *Nat. Photonics* 2012, 7 (1), 13-23.
12. Fan, F.; Voznyy, O.; Sabatini, R. P.; Bicanic, K. T.; Adachi, M. M.; McBride, J. R.; Reid, K. R.; Park, Y. S.; Li, X.; Jain, A.; Quintero-Bermudez, R.; Saravanapavanantham, M.; Liu, M.; Korkusinski, M.; Hawrylak, P.; Klimov, V. I.; Rosenthal, S. J.;

- Hoogland, S.; Sargent, E. H., Continuous-wave lasing in colloidal quantum dot solids enabled by facet-selective epitaxy. *Nature* 2017, 544 (7648), 75-79.
13. Gao, J.; Yu, G.; Heeger, A. J., Polymer light-emitting electrochemical cells with frozen p-i-n junction. *Appl. Phys. Lett.* 1997, 71 (10), 1293-1295.
14. Qian, G.; Lin, Y.; Wantz, G.; Davis, A. R.; Carter, K. R.; Watkins, J. J., Saturated and Multi-Colored Electroluminescence from Quantum Dots Based Light Emitting Electrochemical Cells. *Adv. Funct. Mater.* 2014, 24 (28), 4484-4490.
15. Murphy, A. R.; Frechet, J. M. J., Organic Semiconducting Oligomers for Use in Thin Film Transistors. *Chem. Rev.* 2007, 107, 1066-1096.
16. Pei, Q.; Yu, G.; Zhang, C.; Yang, Y.; Heeger, A. J., Polymer Light-Emitting Electrochemical Cells. *Science* 1995, 269, 1086-1088.
17. Matyba, P.; Maturova, K.; Kemerink, M.; Robinson, N. D.; Edman, L., The dynamic organic p-n junction. *Nat. Mater.* 2009, 8 (8), 672-6.
18. Servaites, J. D.; Ratner, M. A.; Marks, T. J., Organic solar cells: A new look at traditional models. *Energy Environ. Sci* 2011, 4, 4410-4422.
19. Norris, D. J.; Efros, A. L.; Erwin, S. C., Doped Nanocrystals. *Science* 2008, 319, 1776-1779.
20. Schimpf, A. M.; Gunthardt, C. E.; Rinehart, J. D.; Mayer, J. M.; Gamelin, D. R., Controlling carrier densities in photochemically reduced colloidal ZnO nanocrystals: size dependence and role of the hole quencher. *J. Am. Chem. Soc.* 2013, 135 (44), 16569-77.
21. Rinehart, J. D.; Schimpf, A. M.; Weaver, A. L.; Cohn, A. W.; Gamelin, D. R., Photochemical electronic doping of colloidal CdSe nanocrystals. *J. Am. Chem. Soc.* 2013, 135 (50), 18782-5.
22. Fair, R. B., Impurity doping processes in silicon. North-Holland Publishing Company: New York, 1981; Vol. 2.
23. Schimpf, A. M.; Knowles, K. E.; Carroll, G. M.; Gamelin, D. R., Electronic doping and redox-potential tuning in colloidal semiconductor nanocrystals. *Acc. Chem. Res.* 2015, 48 (7), 1929-37.
24. Shim, M.; Wang, C.; Norris, D. J.; Guyot-Sionnest, P., Doping and Charging in Colloidal Semiconductor Nanocrystals. *MRS Bull.* 2001, 26 (12), 1005-1008.
25. Salzmann, I.; Heimel, G.; Oehzelt, M.; Winkler, S.; Koch, N., Molecular Electrical Doping of Organic Semiconductors: Fundamental Mechanisms and Emerging Dopant Design Rules. *Acc. Chem. Res.* 2016, 49 (3), 370-8.
26. Guyot-Sionnest, P., Charging colloidal quantum dots by electrochemistry. *Microchim. Acta* 2008, 160 (3), 309-314.
27. Vanmaekelbergh, D.; Houtepen, A. J.; Kelly, J. J., Electrochemical gating: A method to tune and monitor the (opto)electronic properties of functional materials. *Electrochim. Acta* 2007, 53 (3), 1140-1149.
28. Boehme, S. C.; Wang, H.; Siebbeles, L. D. A.; Vanmaekelbergh, D.; Houtepen, A. J., Electrochemical charging of CdSe quantum dot films: Dependence on voids size and counterion proximity. *ACS Nano* 2013, 7 (3), 2500-2508.
29. Gudjonsdottir, S.; van der Stam, W.; Kirkwood, N.; Evers, W. H.; Houtepen, A. J., The Role of Dopant Ions on Charge Injection and Transport in Electrochemically Doped Quantum Dot Films. *J. Am. Chem. Soc.* 2018, 140 (21), 6582-6590.
30. Gudjonsdottir, S.; Stam, W. v. d.; Koopman, C.; Kwakkenbos, B.; Evers, W. H.;

- Houtepen, A. J., On the Stability of Permanent Electrochemical Doping of Quantum Dot, Fullerene, and Conductive Polymer Films in Frozen Electrolytes for Use in Semiconductor Devices. *ACS Applied Nano Materials* 2019.
31. Pei, Q.; Yang, Y.; Yu, G.; Zhang, C.; Heeger, A. J., Polymer Light-Emitting Electrochemical Cells: In Situ Formation of a Light-Emitting p-n Junction. *J. Am. Chem. Soc.* 1996, 118 (16), 3922-9.
  32. du Fossé, I.; ten Brinck, S.; Infante, I.; Houtepen, A. J., Role of Surface Reduction in the Formation of Traps in n-Doped II–VI Semiconductor Nanocrystals: How to Charge without Reducing the Surface. *Chem. Mater.* 2019.
  33. Gudjonsdottir, S.; Koopman, C.; Houtepen, A. J., Enhancing the stability of the electron density in electrochemically doped ZnO quantum dots. *J. Chem. Phys.* 2019, 151 (14), 144708.
  34. Houtepen, A. J. Charge injection and transport in quantum confined and disordered systems. Utrecht University, 2007.
  35. Houtepen, A. J.; Kockmann, D.; Vanmaekelbergh, D., Reappraisal of Variable-Range Hopping in Quantum-Dot Solids. 2008, Vol. 8 (10), 3516-3520.
  36. Yu, D.; Wang, C.; Wehrenberg, B. L.; Guyot-Sionnest, P., Variable range hopping conduction in semiconductor nanocrystal solids. *Phys. Rev. Lett.* 2004, 92 (21), 216802.
  37. Gao, J.; Li, Y.; Yu, G.; Heeger, A. J., Polymer light-emitting electrochemical cells with frozen junctions. *J. Appl. Phys.* 1999, 86 (8), 4594-4599.
  38. Wantz, G.; Gautier, B.; Dumur, F.; Phan, T. N. T.; Gimes, D.; Hirsch, L.; Gao, J., Towards frozen organic PN junctions at room temperature using high-Tg polymeric electrolytes. *Organic Electronics* 2012, 13 (10), 1859-1864.
  39. Hoven, C. V.; Wang, H.; Elbing, M.; Garner, L.; Winkelhaus, D.; Bazan, G. C., Chemically fixed p–n heterojunctions for polymer electronics by means of covalent B–F bond formation. *Nat. Mater.* 2010, 9, 249-252.
  40. Tang, S.; Irgum, K.; Edman, L., Chemical stabilization of doping in conjugated polymers. *Organic Electronics* 2010, 11 (6), 1079-1087.
  41. Rao, S. P.; Sunkada, S., Making Sense of Boiling Points and Melting Points. *Resonance* 2007, 43-57.
  42. Stauffer, E.; A.Dolan, J.; RetaNewman, CHAPTER 4 - Chemistry and Physics of Fire and Liquid Fuels. In *Fire Debris Analysis*, 1st ed.; Elsevier: USA, 2008; p 672.
  43. Zhang, J.; Chernomordik, B. D.; Crisp, R. W.; Kroupa, D. M.; Luther, J. M.; Miller, E. M.; Gao, J.; Beard, M. C., Preparation of Cd/Pb Chalcogenide Heterostructured Janus Particles via Controllable Cation Exchange. *ACS Nano* 2015, 9 (7), 7151-7163.
  44. Shim, M.; Guyot-Sionnest, P., n-type colloidal semiconductor nanocrystals. *Letters to nature* 2000, 407, 981-983.
  45. Bard, A. J.; Faulkner, L. R., *Electrochemical methods. Fundamentals and applications*. 2nd ed.; John Wiley & sons, INC.: New York, United states of America, 2001.
  46. Valdesueiro, D.; Prabhu, M. K.; Guerra-Nunez, C.; Sandeep, C. S. S.; Kinge, S.; Siebbeles, L. D. A.; de Smet, L. C. P. M.; Meesters, G. M. H.; Kreutzer, M. T.; Houtepen, A. J.; van Ommen, J. R., Deposition Mechanism of Aluminum Oxide on Quantum Dot Films at Atmospheric Pressure and Room Temperature. *J. Phys.*

- Chem. C 2016, 120 (8), 4266-4275.
47. Koh, W. K.; Koposov, A. Y.; Stewart, J. T.; Pal, B. N.; Robel, I.; Pietryga, J. M.; Klimov, V. I., Heavily doped n-type PbSe and PbS nanocrystals using ground-state charge transfer from cobaltocene. *Sci. Rep.* 2013, 3, 2004.
  48. Braunger, M. L.; Barros, A.; Ferreira, M.; Olivati, C. A., Electrical and electrochemical measurements in nanostructured films of polythiophene derivatives. *Electrochim. Acta* 2015, 165.
  49. Augustyn, V.; Come, J.; Lowe, M. A.; Kim, J. W.; Taberna, P. L.; Tolbert, S. H.; Abruña, H. D.; Simon, P.; Dunn, B., High-rate electrochemical energy storage through Li<sup>+</sup> intercalation pseudocapacitance. *Nat. Mater.* 2013, 12 (6), 518-22.
  50. Dandrade, B.; Datta, S.; Forrest, S.; Djurovich, P.; Polikarpov, E.; Thompson, M., Relationship between the ionization and oxidation potentials of molecular organic semiconductors. *Organic Electronics* 2005, 6 (1), 11-20.

## Appendix

### Calculations for current densities.

The current densities in the paper are given for two different electrodes, an IDE and an ITO. When a semiconductor film is measured, the area of the film is used. In electrochemical stability measurements a blank Au electrode is used. During the measurement the four gold contacts are shorted, therefore the area of the electrode that touches the solvent is used.

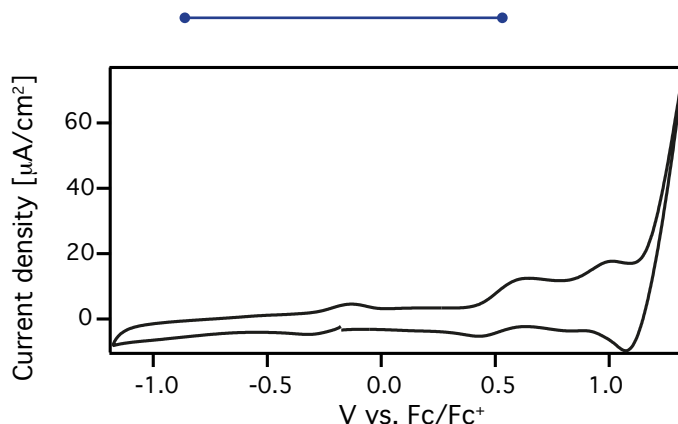


**Figure A5.1.** Electrochemical stability measurements in 0.1 M  $\text{LiClO}_4$  trans-3-hexendinitrile solution with a blank Au electrode. The CV is performed when the solvent is liquid (100 °C) The scan rate is 50 mV/s and is started around -0.2 V vs.  $\text{Fc}/\text{Fc}^+$  in the cathodic direction.

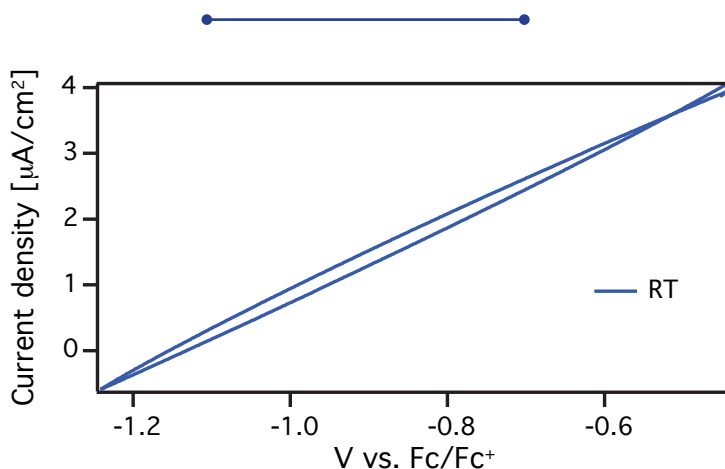


**Figure A5.2.** CV of a ZnO QD film in 0.1 M  $\text{LiClO}_4$  trans-3-hexendinitrile at room temperature. The scan rate is 50 mV/s.

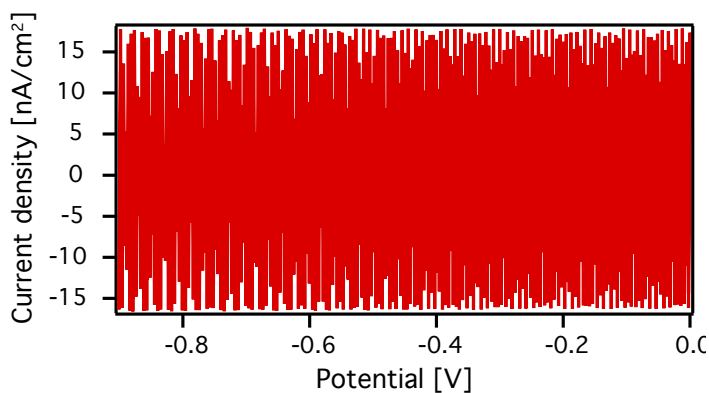


**Figure A5.3.** CV of a ZnO QD film in 0.1 M  $\text{LiClO}_4$  cyanoacetamide at room temperature. The scan rate is 50 mV/s.

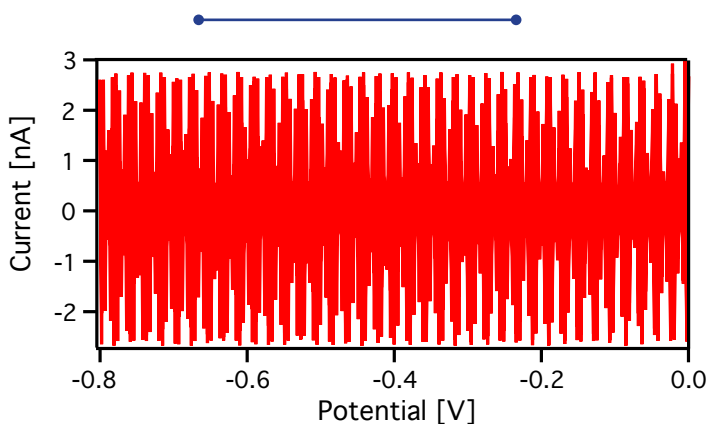


**Figure A5.4.** CV when the potentiostat is not connected to anything, that is the noise of the potentiostat. The scan rate is 50 mV/s.

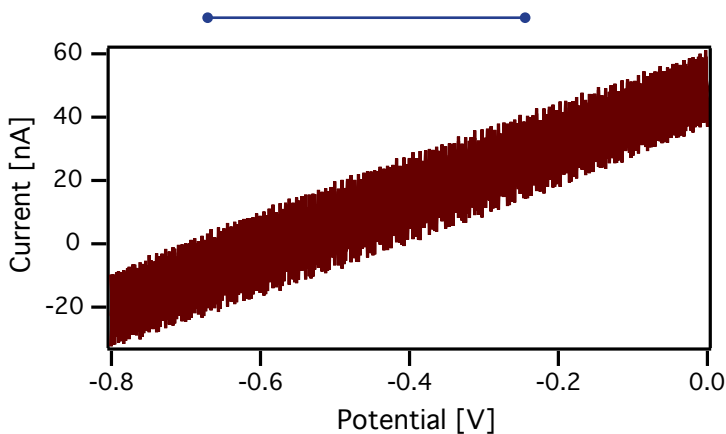


**Figure A5.5.** CV of a ZnO QD film in 0.1 M  $\text{LiClO}_4$  1,2-dicyanobenzene at room temperature. The scan rate is 50 mV/s.

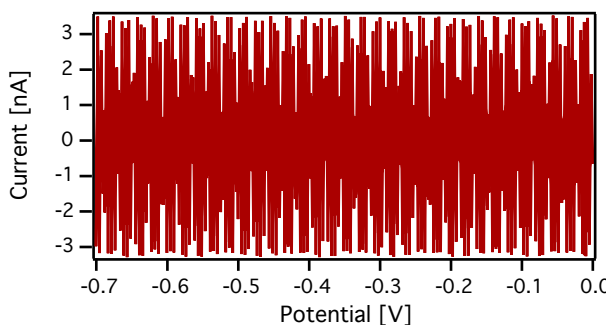


**Figure A5.6.** CV of a ZnO QD film in 0.1 M LiClO<sub>4</sub> 1,3-dicyanobenzene at room temperature. The scan rate is 50 mV/s.

## 5

### DSC measurements

DSC measurements were performed with Perkin Elmer Diamond DSC in nitrogen atmosphere at a scanning rate of 10 °C/s.

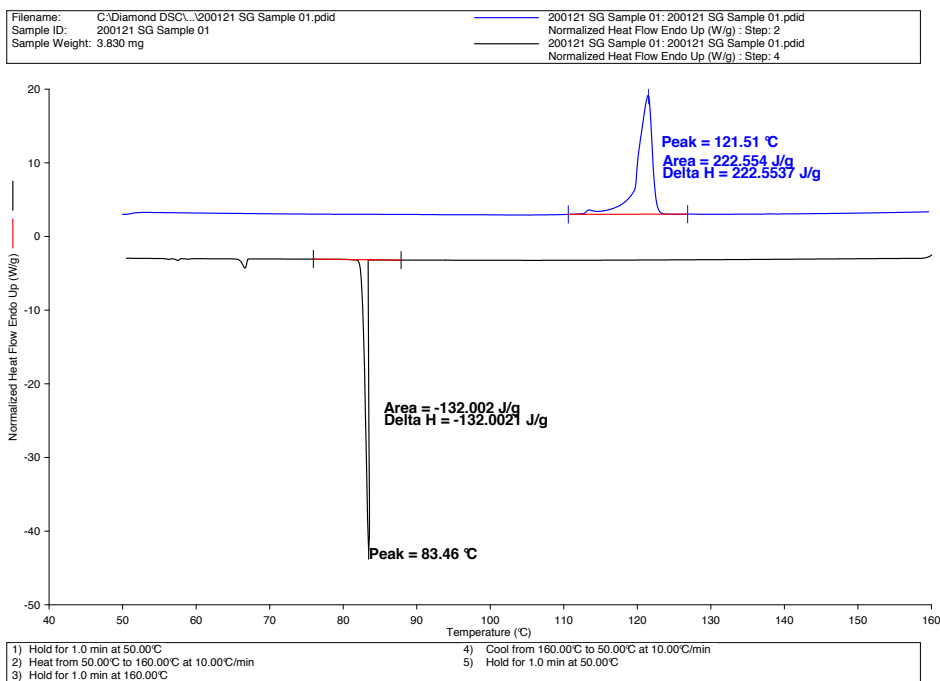


**Figure A5.7.** DSC measurements performed on cyanoacetamide.

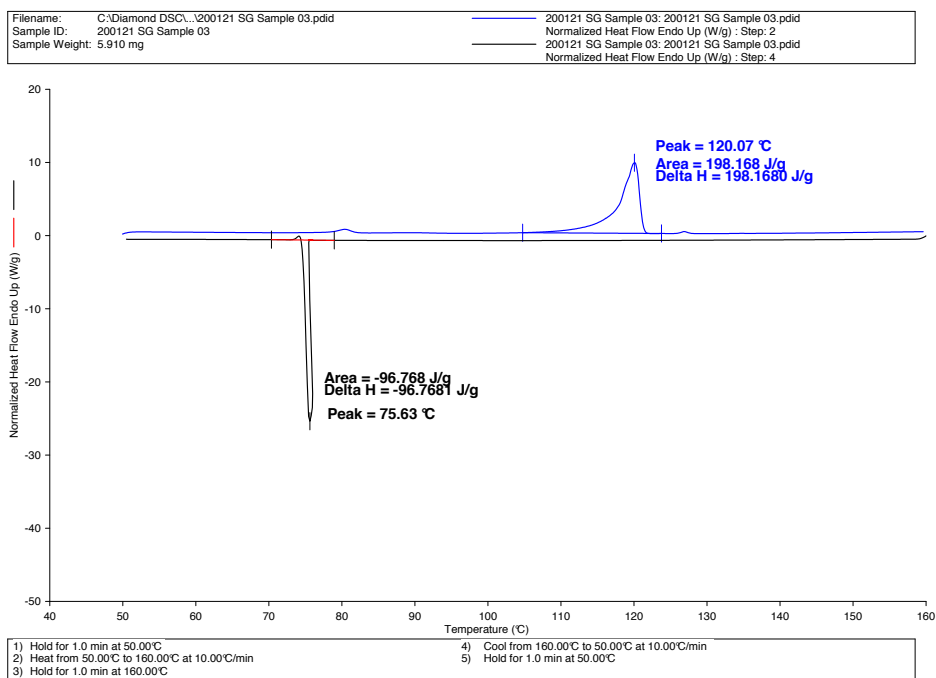


Figure A5.8. DSC measurements performed on 0.1 M LiClO<sub>4</sub> cyanoacetamide.

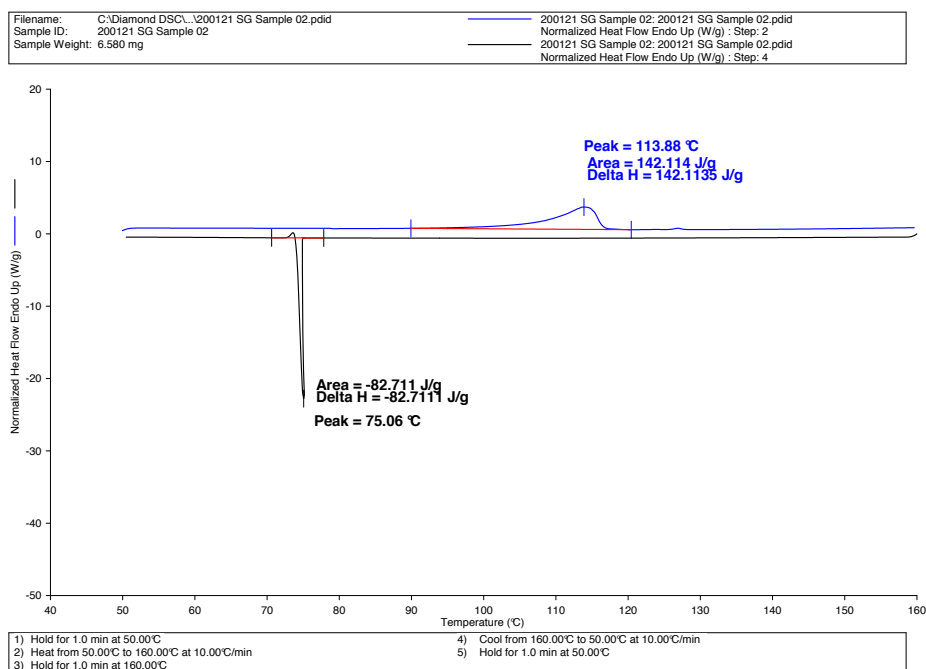
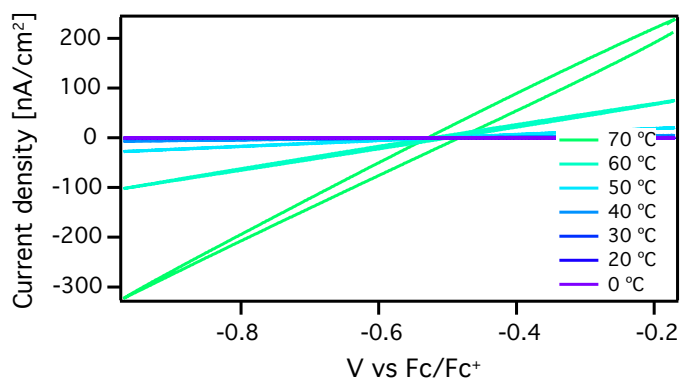
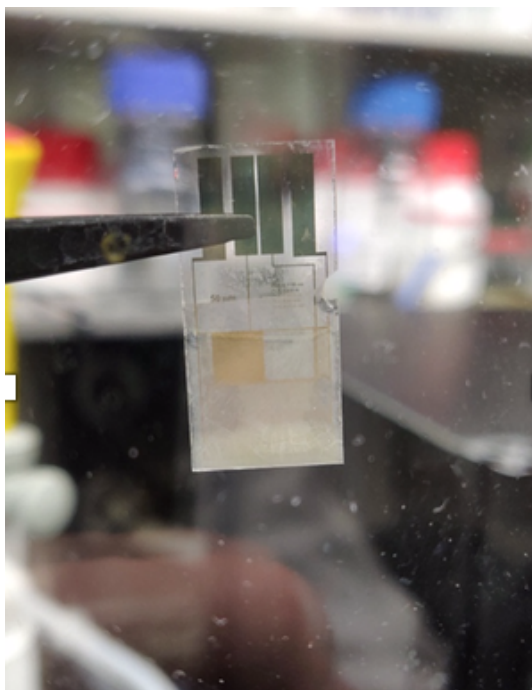


Figure A5.9. DSC measurements performed on 0.5 M LiClO<sub>4</sub> cyanoacetamide.



**Figure A5.10.** CVs performed in 0.1 M  $\text{LiClO}_4$  in cyanoacetamide for a ZnO QD film at different temperatures.



**Figure A5.11.** An image of a ZnO QD film with a thin layer of solid 0.1 M  $\text{LiClO}_4$  cyanoacetamide on top of the sample.

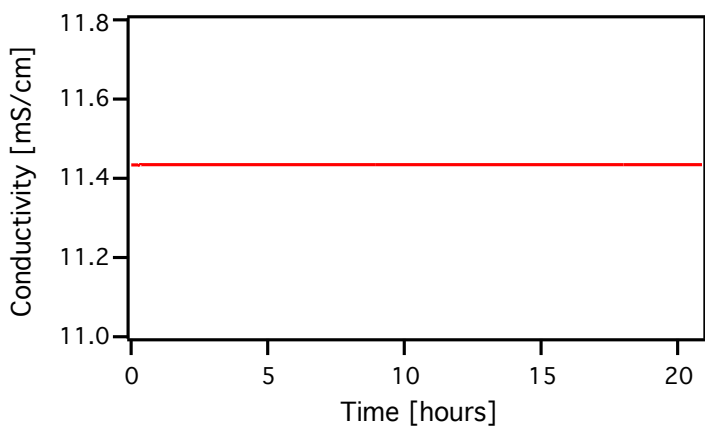


**Figure A5.12.** Conductivity measurements for a ZnO QD film with a thin layer of 0.1 M LiClO<sub>4</sub> cyanoacetamide solution on top of it. The source-drain difference is 10 mV.

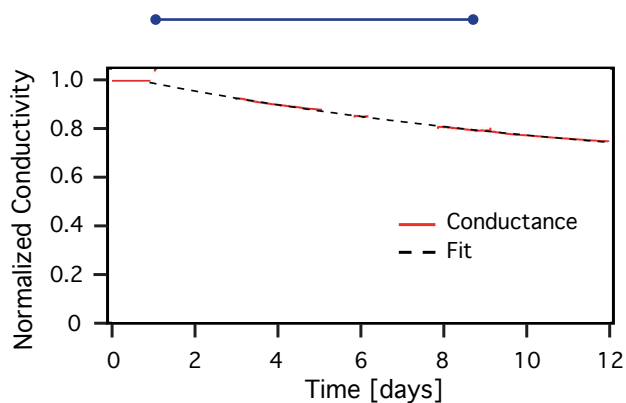


**Figure A5.13.** Normalized conductivity for a ZnO QD film with a thin cover of 0.1 M LiClO<sub>4</sub> cyanoacetamide solution on top of it. The source-drain difference is 10 mV.

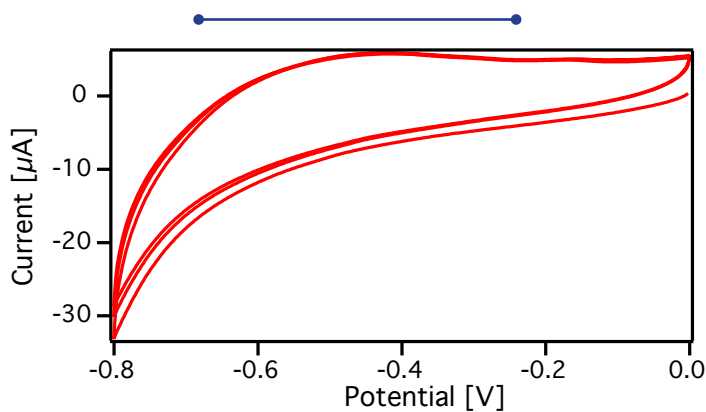


**Figure A5.14.** CV for PbS QD film measured in 0.1 M TBAPF<sub>6</sub> cyanoacetamide solution at 140 °C. The scan rate is 50 mV/s.

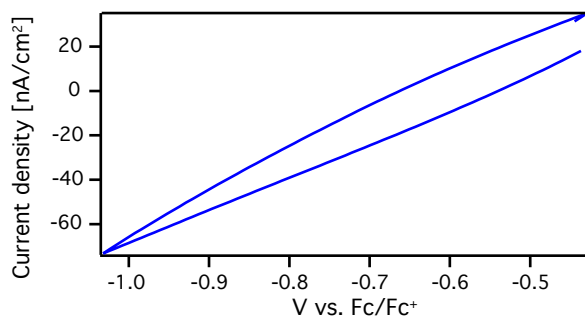


**Figure A5.15.** CV of a PbS QD film in 0.1 M  $\text{LiClO}_4$  cyanoacetamide at room temperature. The scan rate is 50 mV/s.

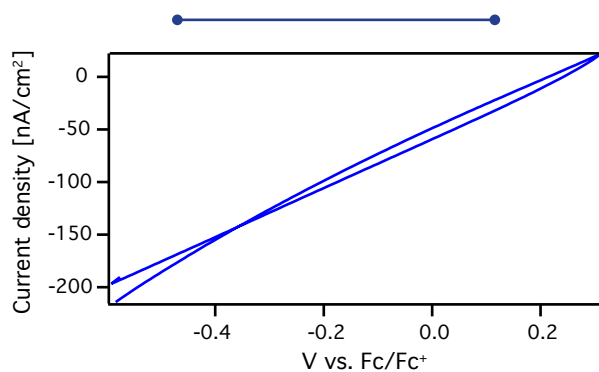


**Figure A5.16.** CV of a P3DT film in 0.1 M  $\text{LiClO}_4$  cyanoacetamide at room temperature. The scan rate is 50 mV/s.

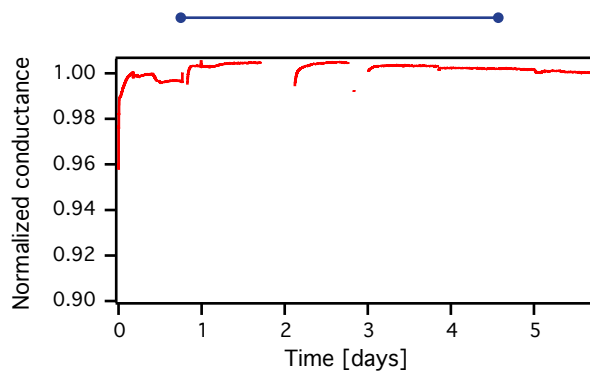


**Figure A5.17.** Normalized conductance for a PbS QD film with a thin layer of solid 0.1 M  $\text{LiClO}_4$  cyanoacetamide on top. The source-drain potential is 10 mV and the measurement is performed at room temperature.

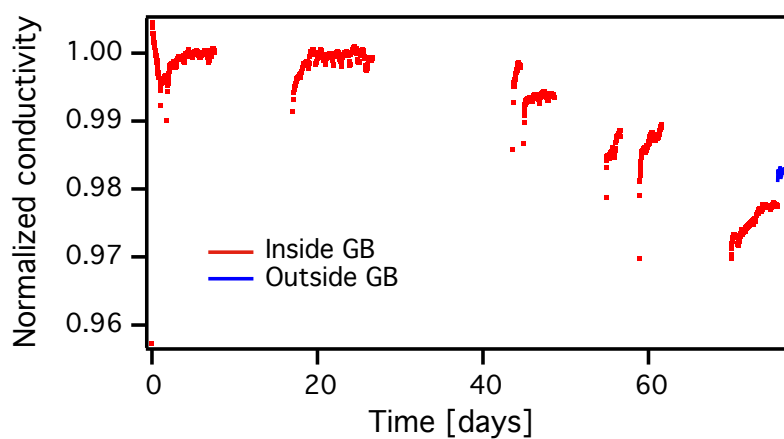


**Figure A5.18.** Normalized conductivity for a P3DT film with a solid 0.1 M LiClO<sub>4</sub> cyanoacetamide on top. The source-drain potential is 10 mV and the measurement is performed at room temperature.



# Summary and outlook

---

Control over the charge carrier density of semiconductor materials is essential for various electronic devices. Unfortunately, common electronic doping methods have not always been successful for new generations of semiconductors, such as organic semiconductors and colloidal quantum dots. Therefore, a new doping method that offers a great control over the charge carrier density is needed. Electrochemistry is a powerful way of doping porous semiconductor films, where the charge carrier density can be controlled by a button on a potentiostat. Unfortunately, when the semiconductor film is disconnected from the potentiostat, injected charges leave the film. The work performed in this thesis is aimed to understand electrochemical doping and the instability with the final goal of producing stable electrochemically doped semiconductor films at room temperature for the use in devices.

**Chapter 1** introduces the main concepts used in this thesis. The chapter starts by describing the electronic doping process in semiconductors in detail, and it is explained why we need doping of semiconductors for electronic devices. Two different doping methods are discussed, internal doping (impurity doping) and external doping; the latter can be split up into chemical and electrochemical doping. It is furthermore explained why the most common doping process, impurity doping, does not work well for both organic semiconductors and quantum dots. Finally, electrochemical doping is discussed as a promising way of doping porous semiconductor films. In electrochemical doping, charge is injected into either the conduction band or the valence band of a semiconductor. To neutralize the injected charge, electrolyte ions diffuse into the voids of the film. These electrolyte ions are external dopants. Unfortunately, the doping stability at room temperature is not good but at temperatures lower than 200 K the doped films are usually stable.

In order to provide stable electrochemically doped semiconductor films at room temperature, the doping process needs to be understood. In **Chapter 2** the role of the electrolyte ions in electrochemical doping is investigated. Spectro-electrochemical and electrochemical transistor measurements are used to investigate the effect of various electrolyte cations on electrochemical doping of ZnO QD films. It is observed that electron injection is limited by the diffusion of electrolyte cations into the voids of the film. Additionally, both the concentration and the size of the cation can affect the charge injection greatly. Strikingly, the onset of charge injection depends on the size of the cation, as it is at more positive potential for small ions such as  $\text{Li}^+$  and  $\text{Na}^+$ . This suggests that both  $\text{Li}^+$  and  $\text{Na}^+$  intercalate into the nanocrystals, while for the larger ions that is not possible due to steric hindrance. At last it is shown that the electrolyte cations do not affect the source-drain electronic conductivity.

In **Chapter 3** various electrolyte solvents are investigated to see if stable electrochemically

doped films can be made at room temperature. The used solvents are chemically similar to common electrolyte solvents, but have a higher melting point (ranging from 37-109 °C). Therefore, at room temperature the solvent should be frozen in the pores of the semiconductor film, and both impurities and electrolyte ions should be immobilized. By charging various porous semiconductor films at elevated temperature in different solvents, the charge stability at room temperature increases immensely, from seconds to days. Also at -75 °C by using succinonitrile (mp: 57 °C) as the electrolyte solvent, the injected charge becomes entirely stable on the time scale of our measurements. This shows that at such low temperature the solvent is frozen even inside the pores of the films. Unfortunately, the doped films are not completely stable at room temperature. This shows that the solvent is not completely frozen at room temperature, and that recrystallization occurs at much lower temperature in the nanopores of the film.

In order to gain stable doped films at room temperature, it is important to know the dominant process by which injected charges disappear. Therefore, in [Chapter 4](#) we perform electrochemical measurements on ZnO QD films of different thickness. We find that the doping stability increases with film thickness, which implies that impurities are the main reason for charge disappearance, rather than intrinsic electrochemical reactions of the ZnO QDs. In order to decrease the effects of impurities on the doping stability on ZnO QDs, we reduce these impurities. That is, we either apply a negative potentials or use reducing agents to reduce solvent impurities before doping of ZnO QD films takes place. After impurity reduction, the doping stability increases immensely. Unfortunately, this only lasts a limited amount of time as more redox active impurities will inevitably diffuse into the doped films on long timescales. To further minimize the effect of impurities from the solvent we have taken the films out of the electrolyte after charging and dried them in various way. In all cases this enhances the doping stability. The best results are obtained by using succinonitrile as solvent, charging just above its melting point and removing the film from the warm solution. In the best case this resulted in a drop of the charge density of only 4% in two hours.

As succinonitrile is the only solvent in Chapter 3 that showed stable electrochemically doped films, even if it was at -75 °C, nitrile solvents with higher melting points were investigated in [Chapter 5](#). As in chapter 3, the films are doped when the solvent is liquid, and the doping stability is measured at lower temperatures. Of the high melting point nitriles, cyanoacetamide gave the best results: at room temperature the estimated diffusion coefficient of electrolyte cations is only  $10^{-21}$  cm<sup>2</sup>/s. This means that it would take a Li<sup>+</sup> ion 300.000 years to diffuse through the ZnO QD film. Additionally, conductivity measurements were performed outside of the electrochemical cell. That is, the film is charged in liquid cyanoacetamide and then it is taken out of the solution where the cyanoacetamide solidifies around the film. We find that the conductivity of the n-doped ZnO QD film does not decrease at all for over 20 hours. Unfortunately, on longer time scales the injected charges gradually leave the film, causing the conductivity to decrease by 10% in 40 days. The same is seen for PbS QD films, where the conductivity was stable for over 5 days, but then started to gradually decrease. This is most likely due to molecular oxygen that can reach the QDs on long time scales. At last, p-type doping was performed for a P3DT film in cyanoacetamide, which gave a fully stable electrochemically doped

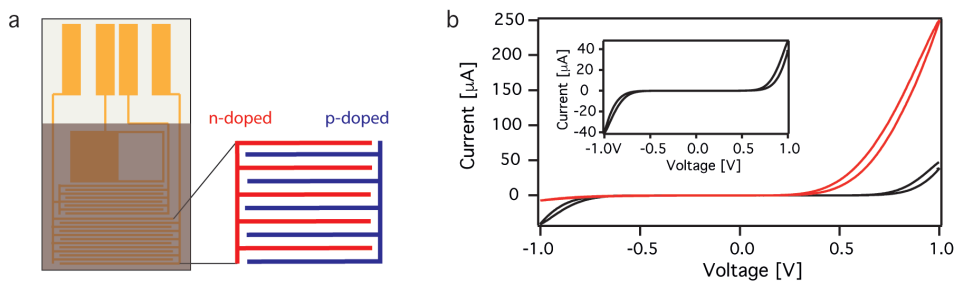


**Figure 1. PbS QD films diode measurements.** a) A schematic of a home-built interdigitated electrode (IDE) containing a PbS QD film. The interdigitated electrodes are used for the formation of a pn-junction diode by doping a part of the sample n-type with one working electrode and the rest of the sample p-type with second working electrode. b) Diode measurements for a PbS QD film with EDT as a cross-linking ligand in 0.1 M LiClO<sub>4</sub> cyanoacetamide at room temperature. The panel includes an uncharged film (0 V bias applied over the film, black trace) and a measurement where 1.4 V bias is applied between the two working electrodes (red trace). A magnification of the uncharged measurement is an inset.

film at room temperature both inside and outside of a nitrogen filled glovebox. The reason for the difference between the QD films and P3DT is most likely that in p-type doping other impurities (mostly water) play a role in charge disappearance than for n-type doping (mostly oxygen).

Overall the results of this thesis show that it is possible to use electrochemical doping on a very wide range of porous semiconductors and that the doping density can be stabilized by using solvents that are frozen at RT. It is expected that the application of a proper gas diffusion barrier, such as Al<sub>2</sub>O<sub>3</sub> could stabilize the charge density completely.

Future work includes making stable electrochemically doped films that survive in the oxygen rich atmosphere, and to use them in devices. Before designing a proper gas diffusion barrier it is possible to see if a stable pn junction diode can be made inside a glovebox. Promising preliminary measurements have been performed on PbS QD films in cyanoacetamide solution at room temperature. PbS QDs are used as they can be doped both n and p-type. By using a home-built interdigitated gold electrode, it is possible to use one working electrode to dope a part of the sample n-type, while another working electrode will dope another part of the sample p-type (Fig 1a). The doping process takes place at elevated temperature when the solvent is liquid. After the p-n junction has been made, the temperature is lowered to room temperature, so the cyanoacetamide solidifies.

Figure 1b shows two IV measurement for PbS QD films performed in 0.1 M LiClO<sub>4</sub> cyanoacetamide at room temperature. In the first measurement the sample is uncharged (no bias is applied between the two working electrodes), and a symmetric curve is seen, as expected. However, by applying a 1.4V bias (more than the 1 eV bandgap of the PbS QDs) between the two interdigitated electrodes a strongly asymmetric IV curve is obtained. This diode-like curve demonstrates that the pn junction is indeed formed. The application of a large bias does not destroy the pn junction since ions can no longer move in the frozen

solvent. The obtained ratio of the current at forward bias compared to reversed bias is between 10 and 40 for multiple samples. This shows that a diode is formed, although there is room for improvement.





# Samenvatting en vooruitzichten

---

Controle over de ladingsdichtheid van halfgeleidermaterialen is essentieel voor verschillende elektronische toepassingen. Gemeenschappelijke elektronische doteringsmethodes zijn helaas niet altijd succesvol geweest voor nieuwe generaties halfgeleiders, zoals organische halfgeleiders en colloïdale kwantum-stippen. Daarom is een nieuwe doteringsmethode nodig die goede controle geeft over de ladingsdichtheid. Elektrochemie is een methode waarmee poreuze halfgeleiderfilms te gedoteerd kunnen worden, waarbij de ladingsdichtheid kan worden geregeld met behulp van een potentiostaat. Wanneer halfgeleiderfilm wordt losgekoppeld van de potentiostaat, verlaten geïnjecteerde ladingen de film. Het werk in dit proefschrift is gericht op het begrijpen van elektrochemische dotering en de instabiliteit van de geïnjecteerde ladingen, met als uiteindelijk doel het produceren van stabiele elektrochemisch gedoteerde halfgeleiderfilms bij kamertemperatuur voor gebruik in apparaten.

**Hoofdstuk 1** introduceert de belangrijkste concepten die in dit proefschrift worden gebruikt. Het hoofdstuk begint met een gedetailleerde beschrijving van het elektronische doteringsproces in halfgeleiders en er wordt uitgelegd waarom we dotering van halfgeleiders voor elektronische apparaten nodig hebben. Er worden twee verschillende doteringsmethoden besproken, interne dotering (onzuiverheidsdotering) en externe dotering; deze laatste kan worden opgesplitst in chemische en elektrochemische dotering. Verder wordt uitgelegd waarom het meest voorkomende doteringsproces, onzuiverheidsdotering, niet goed werkt voor zowel organische halfgeleiders als kwantum-stippen. Ten slotte wordt elektrochemische dotering besproken als een veelbelovende manier om poreuze halfgeleiderfilms te doteren. Bij elektrochemische dotering wordt lading geïnjecteerd in de geleidingsband of de valentieband van een halfgeleider. Om de totale lading van een film neutraal te houden, diffunderen elektrolytionen in de holtes van de film. Deze elektrolytionen zijn externe doterings-deeltjes. Helaas is de stabiliteit van de dotering bij kamertemperatuur niet goed, maar bij temperaturen lager dan 200 K zijn de ladingen in de gedoteerde films meestal stabiel.

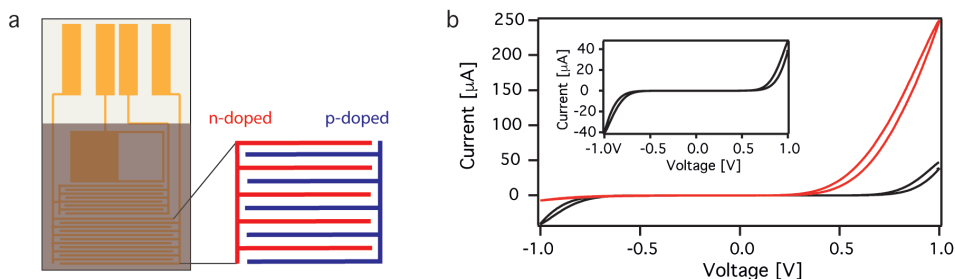
Om stabiele elektrochemisch gedoteerde halfgeleiderfilms bij kamertemperatuur te verkrijgen, moet het doteringsproces worden begrepen. In **Hoofdstuk 2** wordt de rol van de elektrolyt-ionen bij elektrochemische dotering onderzocht. Spectro-elektrochemische en elektrochemische transistormetingen worden gebruikt om het effect van verschillende elektrolytkationen op elektrochemische dotering van ZnO QD-films te onderzoeken. Wat we concluderen is dat elektroneninjectie wordt beperkt door de diffusie van elektrolytkationen in de holtes van de film. Bovendien kunnen zowel de concentratie als de grootte van het kation de ladinginjectie sterk beïnvloeden. Opvallend is dat het startpotentiaal van de ladinginjectie afhangt van de grootte van het kation, omdat het een positiever potentiaal heeft voor kleine ionen zoals  $\text{Li}^+$  en  $\text{Na}^+$ . Dit suggereert dat zowel  $\text{Li}^+$  als  $\text{Na}^+$  intercaleren in de nanokristallen, terwijl dat voor grotere ionen niet mogelijk

is vanwege sterische hindering. Er wordt ook aangetoond dat de elektrolytkationen de source-drain elektronische geleidbaarheid niet beïnvloeden.

In **Hoofdstuk 3** worden verschillende elektrolytoplosmiddelen onderzocht om te zien of stabiele elektrochemisch gedoteerde films gemaakt kunnen worden bij kamertemperatuur. De gebruikte oplosmiddelen zijn qua chemische structuur vergelijkbaar met reguliere elektrolytoplosmiddelen, maar hebben een hoger smeltpunt (variërend van 37-109 °C). Daardoor is het oplosmiddel bij kamertemperatuur bevroren in de poriën van de halfgeleiderfilm en kunnen zowel onzuiverheden als elektrolytionen worden geïmmobiliseerd. Door verschillende poreuze halfgeleiderfilms bij verhoogde temperatuur in verschillende oplosmiddelen op te laden, neemt de ladingsstabiliteit bij kamertemperatuur enorm toe, van enkele seconden tot dagen. Ook in succinonitril als elektrolyt oplosmiddel (mp: 57 °C) bij -75 °C wordt de geïnjecteerde lading volledig stabiel op de tijdschaal van onze metingen. Dit toont aan dat het oplosmiddel bij lage temperaturen zelfs in de poriën van de films wordt bevroren. Helaas zijn de gedoteerde films niet volledig stabiel bij kamertemperatuur. Dit toont aan dat het oplosmiddel niet volledig bevriest bij kamertemperatuur en dat herkristallisatie plaatsvindt bij veel lagere temperatuur in de nanoporiën van de film.

Om stabiele gedoteerde films bij kamertemperatuur te maken, is het belangrijk om het dominante proces te kennen waardoor geïnjecteerde ladingen verdwijnen. Daarom voeren we in **Hoofdstuk 4** elektrochemische metingen uit op ZnO QD-films van verschillende diktes. We vinden dat de doteringsstabiliteit toeneemt met filmdikte, wat impliceert dat onzuiverheden de belangrijkste reden zijn voor het verdwijnen van ladingen, in plaats van intrinsieke elektrochemische reacties van de ZnO kwantum-stippen. Om de effecten van onzuiverheden op de doteringsstabiliteit op ZnO kwantum-stippen te verminderen, verwijderen we deze onzuiverheden. Dat wil zeggen, we passen ofwel een negatieve potentiaal toe of gebruiken reductiemiddelen om de hoeveelheid onzuiverheden in de oplosmiddelen te verminderen voordat dotering van ZnO QD-films plaatsvindt. Na vermindering van onzuiverheid neemt de doteringsstabiliteit enorm toe. Helaas duurt dit slechts een beperkte hoeveelheid tijd, omdat meer redox-actieve onzuiverheden onvermijdelijk in de gedoteerde films op lange tijdschalen zullen diffunderen. Om het effect van onzuiverheden uit het oplosmiddel verder te minimaliseren, hebben we de films na het opladen uit het elektrolyt gehaald en op verschillende manieren gedroogd. Dit verhoogt in alle gevallen de doteringsstabiliteit. De beste resultaten worden verkregen door succinonitril als oplosmiddel te gebruiken, de film net boven het smeltpunt op te laden en de film uit de warme oplossing te verwijderen. In het beste geval resulteerde dit in een vermindering van de ladingsdichtheid van slechts 4% in twee uur.

Aangezien succinonitril het enige oplosmiddel in Hoofdstuk 3 was waarmee we stabiele elektrochemisch gedoteerde films verkregen, zelfs als het bij -75 °C was, werden nitriloplosmiddelen met hogere smeltpunten onderzocht in **Hoofdstuk 5**. Net als in hoofdstuk 3 worden de films gedoteerd wanneer het oplosmiddel is vloeibaar en wordt de doteringsstabiliteit gemeten bij lagere temperaturen. Van de nitrillen met een hoog smeltpunt gaf cyanoacetamide de beste resultaten: bij kamertemperatuur is de geschatte diffusiecoëfficiënt van elektrolytkationen slechts  $10^{-21}$  cm<sup>2</sup>/s. Dit betekent dat het 300.000



Figuur 1: a) Schematische weergave van de elektrode en de verdeling van potentiaal over de geïnterdigiteerde goud-‘vingers’. b) CVs uitgevoerd op een film van PbS kwantum-stippen in vaste 0.1 M  $\text{LiClO}_4$  in cyanoacetamide. Zwart: de onopgeladen film, waarbij voor de meting een 1.4 V source-drain spanning is aangelegd. Rood: de film die wel is opgeladen voor de metingen. We zien een factor 10-40 verhoging van de stroom die loopt bij

jaar zou duren om een  $\text{Li}^+$  ion te laten diffunderen door de ZnO QD-film. Daarnaast werden geleidbaarheidsmetingen uitgevoerd buiten de elektrochemische cel. De film wordt opgeladen in vloeibaar cyanoacetamide en vervolgens uit de oplossing gehaald waar het cyanoacetamide rond de film stolt. We vinden dat de geleidbaarheid van de n-gedoteerde ZnO QD-film gedurende meer dan 20 uur helemaal niet afneemt. Helaas verlaten de geïnjecteerde ladingen op langere tijdschalen de film geleidelijk, waardoor de geleidbaarheid in 40 dagen met 10% afneemt. Hetzelfde wordt gezien voor films van PbS kwantum-stippen, waar de geleidbaarheid meer dan vijf dagen stabiel was, maar daarna geleidelijk begon af te nemen. Dit komt waarschijnlijk door moleculaire zuurstof die de kwantum-stippen op lange tijdschalen kan bereiken. P-type dotering is uitgevoerd voor een P3DT-film in cyanoacetamide, wat een volledig stabiele elektrochemisch gedoteerde film bij kamertemperatuur opleverde. De reden voor het verschil tussen de films van kwantum-stippen en P3DT is hoogstwaarschijnlijk dat bij p-type dotering andere onzuiverheden (meestal water) een rol spelen bij het verdwijnen van ladingen dan bij n-type dotering (meestal zuurstof).

Al met al laten de resultaten van dit proefschrift zien dat het mogelijk is om elektrochemische dotering toe te passen op een zeer breed scala aan poreuze halfgeleiders en dat de doteringsdichtheid kan worden gestabiliseerd door oplosmiddelen te gebruiken die bij kamertemperatuur zijn bevroren. Verwacht wordt dat het gebruik van een goede gasdiffusiebarrière, zoals  $\text{Al}_2\text{O}_3$ , de ladingsdichtheid volledig zou kunnen stabiliseren.

Toekomstig werk omvat het maken van stabiele elektrochemisch gedoteerde films, waarbij de gedoteerde ladingen de zuurstofrijke atmosfeer overleven en waarbij de films in apparaten gebruikt kunnen worden. Voordat een goede gasdiffusiebarrière is ontworpen, is het mogelijk om te zien of een stabiele pn-junctiediode in een handschoenenkast kan worden gemaakt. Er zijn veelbelovende metingen uitgevoerd op film van PbS kwantum-stippen in cyanoacetamide-oplossingen bij kamertemperatuur. PbS kwantum-stippen worden gebruikt omdat ze zowel n als p-type kunnen worden gedoteerd. Door een zelfgebouwde, geïnterdigiteerde goud-elektrode te gebruiken, is het mogelijk om één

werk-elektrode te gebruiken om een deel van het monster n-type te dopen, terwijl een andere werk-elektrode een ander deel van het monster p-type zal dopen (Fig 1a). Het doteringsproces vindt plaats bij verhoogde temperatuur wanneer het oplosmiddel vloeibaar is. Nadat de p-n-overgang is gemaakt, wordt de temperatuur verlaagd tot kamertemperatuur, zodat het cyanoacetamide stolt.

Figuur 1b toont cyclisch voltammogrammen (CVs) uitgevoerd op dezelfde PbS film in een vaste 0.1 M  $\text{LiClO}_4$  cyanoacetamide-oplossing bij kamertemperatuur. De eerste meting wordt uitgevoerd wanneer het monster niet is opgeladen, terwijl de tweede meting wordt uitgevoerd wanneer het monster is opgeladen door een 1.4 V source-drain spanning. De spanning wordt aangelegd wanneer de oplossing vloeibaar is, de film wordt uit de oplossing gehaald (terwijl de spanning nog steeds wordt aangelegd). De CV wordt gemeten wanneer de cyanoacetamide-oplossing is gestold. De CV van het ongeladen monster vertoont, zoals verwacht, een symmetrische curve rond 0 V. In figuur 1b is de curve niet symmetrisch rond 0 en lijkt de het op een (niet ideale) diode.

Zoals hierboven vermeld, toont Figuur 1 voorlopige resultaten. Deze veelbelovende resultaten tonen aan dat elektrochemische dotering van verschillende halfgeleiderfilms voor gebruik in functionele apparaten (zoals diodes) nuttig kan zijn, maar laten ook zien dat dit verder geoptimaliseerd moet worden.





# List of publications

---

## **This thesis was based on the following publications:**

S. Gudjonsdottir, W. van der Stam, N. Kirkwood, W. H. Evers and A. J. Houtepen. "The Role of Dopant Ions on Charge Injection and Transport in Electrochemically Doped Quantum Dot Films". *Journal of the American Chemical Society*, 2018, 140 (21), 6582-6590.

S. Gudjonsdottir, W. van der Stam, C. Koopman, B. Kwakkenbos, W. H. Evers and A. J. Houtepen. "On the Stability of Permanent Electrochemical Doping of Quantum Dot, Fullerene, and Conductive Polymer Films in Frozen Electrolytes for Use in Semiconductor Devices". *ACS Applied Nano Materials*, 2019, 2 (8), 4900-4909.

S. Gudjonsdottir, C. Koopman and A. J. Houtepen. "Enhancing the Stability of the Electron Density in Electrochemically Doped ZnO Quantum Dots". *The Journal of Chemical Physics*, 2019, 151 (14), 144708.

S. Gudjonsdottir and A. J. Houtepen. "Permanent Electrochemical Doping of Quantum Dots and Semiconducting Polymers". *Advanced Functional Materials*. Accepted.

## **Other publications:**

W. van der Stam, S. Gudjonsdottir, W. H. Evers and A. J. Houtepen. "Switching Between Plasmonic and Fluorescent Copper Sulfide Nanocrystals". *Journal of the American Chemical Society*, 2017, 139 (37), 13208-13217.

W. van der Stam, M. de Graaf, S. Gudjonsdottir, J. J. Geuchies, J. J. Dijkema, N. Kirkwood, W. H. Evers, A. Longo and A. J. Houtepen. "Tuning and Probing the Distribution of Cu<sup>+</sup> and Cu<sup>2+</sup> Trap States Responsible for Broad-Band Photoluminescence in CuInS<sub>2</sub> Nanocrystals". *ACS Nano*, 2018, 12 (11), 11244-11253.

W. van der Stam, G. Grimaldi, J. J. Geuchies, S. Gudjonsdottir, P. T. van Uffelen, M. van Overeem, B. Brynjarsson, N. Kirkwood and A. J. Houtepen. "Electrochemical Modulations of the Photophysics of Surface-Localized Trap States in Core/Shell/(Shell) Quantum Dot Films". *Chemistry of Materials*, 2019, 31 (20), 8484-8493.

G. Grimaldi, M. J. van den Brom, I. du Fossé, R. W. Crisp, N. Kirkwood, S. Gudjonsdottir, J. J. Geuchies, S. Kinge, L. D. A. Siebbeles and A. J. Houtepen. "Engineering the Band Alignment in QD Heterojunction Films via Ligand Exchange". *The Journal of Physical Chemistry C*, 2019, 123 (49), 29599-29608.

J. Geuchies, B. Brynjarsson, G. Grimaldi, S. Gudjonsdottir, W. van der Stam, W. H. Evers and A. J. Houtepen. “Quantitative Electrochemical Control Over Optical Gain in Quantum-Dot Solids”. Submitted.





# Curriculum Vitae

---

Sólrún Guðjónsdóttir was born on the 8th of August 1991 in Reykjavík, Iceland. She obtained her Bachelor Degree in Chemistry from University of Iceland in 2014. The chosen track was Chemistry with Emphasis on Chemical Engineering. She entered a Master program the same year at Delft University of Technology in Chemical Engineering at the track Product Engineering. In 2016 she received her Master degree with a thesis entitled “Revealing the Charge Carrier Dynamics in Lead Free Perovskites for Photovoltaics”.

In September 2016 she started working on her project “Doping on Demand” in the Optoelectronic Materials section under the supervision of Arjan J. Houtepen at Delft University of Technology in the Chemical Engineering section.



Sólrún enjoys exercising and is particularly fond of hiking and skiing. She enjoys travelling, meeting new people and reading.

